Master's Degree Thesis

ISRN: BTH-AMT-EX--2009/D-01--SE

Finite Element Modeling to Verify Residual Stress in Orthogonal Machining

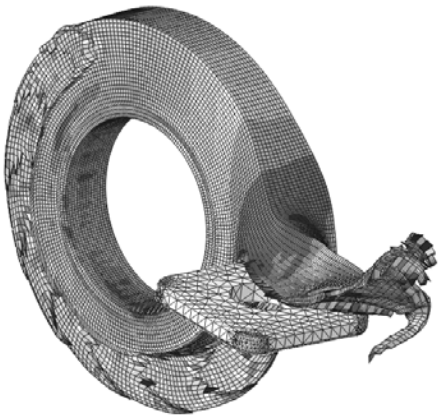

Chandra Shekhar Prasad

Department of Mechanical Engineering
Blekinge Institute of Technology
Karlskrona, Sweden
2009

Supervisors: Ansel Berghuvud, Ph.D Mech Eng, BTH
Prof Arne Melender (Swerea KIMAB), PhD Mech Eng
Dr Niclas Stenberg (Swerea KIMAB),PhD Mech Eng
Håkan Thoors (Swerea KIMAB) , M.Sc Mech Eng

FINITE ELEMENT MODELING TO VERIFY RESIDUAL STRESS IN ORTHOGONAL MACHINING

Chandra Shekhar Prasad

Department of Mechanical Engineering
Blekinge Institute of Technology
Karlskrona, Sweden
2009

Thesis submitted for completion of Master of Science in Mechanical Engineering with emphasis of Structural Mechanics at the Department of Mechanical Engineering, Blekinge Institute of Technology, Karlskrona Sweden.

Abstract

The aim of this thesis paper, to create a numerical model to examine the residual stresses induced by orthogonal machining in the finished work piece and the model is validated by comparing with experimental result.

The finite element method is used to simulate and analyze the residual stresses induced by a orthogonal metal cutting process.

A Dynamics explicit time integration technique with Arbitrary Lagrangian Eulerian (ALE) adaptive meshing Finite Element Method (FEM) is employed to simulate the model. The Johnson-Cook material model is used to describe the work material behaviour and fully coupled thermal-stress analysis are combined to realistically simulate high speed machining with an orthogonal cutting.

Finite Element modelling of Residual stresses and resultant surface properties induced by round edge cutting tools is performed as case studies for high speed orthogonal machining of 20NiCrMo5 steel.

As a conclusion we can say that results from 2D simulations are very close to the experimental results at the surface level, but there is bit difference when we go down in the material. In 3D simulation, results agree with the experimental values in all levels So we can say that it is possible to model residual stresses, induced by orthogonal machining with accepted amount of accuracy.

Keywords

Residual stress, FE-modelling, ALE formulation,3D.ABAQUS/CAE

Acknowledgements

This work has been done at Swerea KIMAB in metal forming and machining department ,Stockholm under the project group-22.This project is the sub part of Mera program and Supported by Scania AB and Sandvik coromant AB .This thesis work has been carried out under the supervision of Prof.Arne Melander,Dr. Niclas Stenberg and M.Sc Håkan Thoors at swerea KIMAB.This thesis work is final part of the master of science programme in Mechanical engineering emphasis on structural mechanics at Blekinge institute of technology , Karlskrona Sweden.

I would like to thank my supervisor at Swerea KIMAB Prof Arne melander,Dr.Niclas Stenberg and Msc. Håkan Thoors for their guidance and enthusiasm during the thesis work.I would like to thank Dr. Dr. Ansel Berghuvud at Blekinge institute of technology, department of mechanical engineering. Finally I would like to thank all the member of Swerea KIMAB for their valuable guidance and help during this thesis work.

Stockholm, January 2009

Chandra Shekhar Prasad

Table of Contents

Notation

A	Arbitrary constant
B	Arbitrary constant
C	arbitrary constant
E	Young’s modulus
F	Force
f	feed rate
a_p	depth of cut
G	Shear modulus
M	mass
$K_{\mathbf{t}}$	Stiffness matrix
l	Length
m	Mass
Sp	Specific heat
T	Temperature
T_{room}	Room temperature
T_{melt}	melting temperature
t	Time
V	Volume
v	Velocity
$\bar{\varepsilon}$	Equivalent plastic Strain
$\dot{\bar{\varepsilon}}$	Strain rate
μ	Co-efficient of friction
ρ	Density
σ	Normal Stress
τ	Shear stress
τ_{th}	threshold shear stress
τ_c	critical frictional shear stress

1. Introduction

The essence of this research work is to create a numerical model to simulate the machining induced residual stresses in the finished work material and try to have the better understanding about their behaviour and also the effect of cutting parameters on their trend. In order to achieve this FEM has been used to create the numerical model. First the simple 2D model has been studied and then 3D model has been developed.

Cutting is a common way of shaping metals. From a mechanical point of view it is very complex process and still the details are poorly understood.

In front of the tool the work piece material is undergoing very large strains at high strain-rates, which causes the temperature to rise considerably. Large strains and stresses cause a material deformation, where a chip is formed. The interaction between the chip and the tool may include high frictional forces and even undesired adhesion, under elevated temperature.
Possible problems arising in metal cutting operations are:

- Residual stresses in the finish work piece
- Irregularities in the cut surface finished work piece.
- Wear and fatigue of the tool.
- Too long chips.

In order to improve product quality and tool performance, a better understanding of the process is crucial.

Till now the development of cutting tools and the choice of appropriate cutting parameters have been based on experimental studies and on the experience of the tool designer. Some quantities, such as Residual stress and temperature distributions, are very difficult to measure in an experiment. Therefore computer simulations could be a valuable contribution, and cutting parameters can be effectively be evaluated to achieve an optimal process.

As significance for this research work we can say that this will be a great help for the manufacturer and cutting tool designer to understand the nature of machining induced residual stress and also to minimize their effect on the finished product.

1.1 Historical Background

The reliability of a mechanical component depends to a large extent on the physical state of its surface layers. This state includes the distribution of residual stresses induced by machining. Depending on their nature, compressive or tensile stresses, they could either enhance or impair the ability of a component to withstand severe loading conditions present in different services such as fatigue, creep, stress corrosion cracking, etc.

Furthermore, the residual stress distribution on a component may also cause dimensional instability i.e. distortion after machining. This poses enormous problems in engine/structural assembly and affects the structural integrity of the whole part. The direct influence of residual stresses on the functional behaviour like the static and dynamic strength, chemical and electrical properties, and fatigue, rust, etc. of the component is relatively well known. However, a number of questions still persist about the causes and the mechanisms of residual stress generation in machining and how these residual stresses could be controlled in order to achieve a desirable distribution.

Therefore, the understanding of residual stresses and proper control of these in machining is a prerequisite in order to enhance component performance and minimize risks of failure. The study of machining residual stresses is particularly important when critical structural components are machined, especially if the objective is to reach high reliability levels.

1.2 Literature Survey

Several studies on residual stresses induced by machining have been performed. Unfortunately, due to limitations in finite element (FE) modelling of the metal cutting process and the complex physical phenomenon involving the formation of machining residual stresses, most of these studies remain experimental in nature [1,2,3,4].

Although many studies on FE modelling of the orthogonal cutting process have been published until now, these were mainly applied to predict with reasonable accuracy of the strains, stress and temperatures during cutting [5, 6, 7, 8, 9, 10]. Only a few studies on FE modelling involving the prediction of the machining residual stresses with decent accuracy can be found in the literature, with special attention to the residual stresses in plain carbon steels and hardened steels [11,12].Concerning modelling of machining induced residual stresses in stainless steels, the available studies are even more restricted [7,8,9].Wiesner [10] studied the residual stresses generated after orthogonal cutting of AISI 304 steel using uncoated cemented carbide tools. Using the X-ray diffraction technique, Wiesner determined the influence of the cutting speed and cutting depth on in-depth distribution of the residual stresses in the direction of primary motion (the cutting speed direction). High tensile residual stresses (close to +700MPa) were found on the machined surface. In order to explain these high tensile residual stresses, a finite element method (FEM) was employed to analyse the influence of the thermal and mechanical effects on the residual stress state separately, although in the paper he presents the results for the thermal effect only. Wiesner concluded that the thermal effect is not the only reason for tensile residual stresses in machined components. The mechanical effect does not always produce compressive residual stresses, but can also contribute to tensile residual stresses.

Liu and Guo [13] proposed an FE model to investigate the effect of sequential cuts and tool-chip friction on residual stresses in a machined layer of AISI 304 steel. They reported a reduction in the superficial residual stresses when the second cut is performed. Moreover, the residual stresses can be compressive, depending on the uncut chip thickness of the second cut. They also found that residual stress on the machined surface is very sensitive to the friction condition of the tool–chip interface. Later, using the same work material, Liu and Guo [14] presented a similar study on the effect of sequential cuts on residual stresses. They showed that decreasing the uncut chip thickness below a critical value in the second cut may result in favourable compressive residual stress distribution.Thus, they conclude that it would be better to set an appropriate finishing cut condition in consideration of the effects of sequential cuts to control the residual stress distribution. Unfortunately, Liu and Guo[14] did not present any experimental evidence for the work material under investigation (AISI 304 steel) to validate their FE model.

Yang and Liu [15] performed a sensitivity study of the friction condition on the tool–chip contact, the cutting forces and the residual stresses in machining-affected layers of AISI 304 steel. In this study they proposed a new stress based polynomial model for modelling the tool–chip contact, which represents a simple curve fitting the experimentally obtained shear and normal stresses acting at the tool–chip interface. When comparing this new friction model with other friction models based on an average friction coefficient deduced from cutting forces or from stresses, they found significant differences among the predicted residual stresses. They concluded that the conventional force-based friction model is inadequate to predict the residual stresses induced by machining, and they showed the potential for improving the quality in predicting machining residual stress by adopting the stress based polynomial model. Although it is widely accepted that friction conditions will change along the tool–chip contact length, the authors did not present any experimental evidence to support their conclusions.

The prior investigations show that modelling residual stress in machining stainless steel was studied for a very limited range of cutting conditions and for specific analysis.Özel and Zeren [16,17] propose a model to simulate the effect of cutting edge radius on the induced stresses and Özel and Altan[18] also work in this area to simulated the flow of stress in the machined work piece and find the effect of tool-chip friction on the stress field,but they have simulated model with pre-define chip geometry to get the continuos chip formation using ALE adaptive meshing techniques which seems not very realistic.

Most of the FE-modelling have been performed with 2D models [7,15,16,17,18] & [5, 6, 7, 8, 9, 10] due to coplexsity of 3D model,where we need consider the translational motion of tool and the rotation motion of the workpiece for the orthogonal machining. These to mutually perpendicular motion makes the numerical model very complex to simulated for the researcher.But M. Vaz Jr. · D.R.J. Owen ,V. Kalhori · M. Lundblad and L.-E. Lindgren [19] , Özel and Zeren [7,16] have presented FE-models for the 3D case in their studies. Unfortunately they only considered the one dimensional motion of either tool or workpiece in their proposed 3D models of orthogonal machining simulation, which makes their models 3D turning operation instead of 3D orthogonal machining .Also it keep the model bit apart from the reality of orthogonal machining.

1.3 Research Goal

The main goal of this research is to experimentally and numerically verify the machining induced residual stresses in the 20NiCrMo5 steel for the different cutting parameters.

As a scope of this work we can say so far the work done in this field remains bit apart from the reality due not consideration of all motion involved in the orthogonal machining, Therefore, there is a need for a more fundamental model of the process, which takes into consideration work piece material behaviour, effects of cutting tool geometry and material, and cutting regime parameters concurrently to predict the residual stress profile in machining.

In the present investigation, a 2D and 3D numerical model of orthogonal cutting of AISI 316L steel is employed with the objective of predicting the in-depth residual stress profiles in the machined component for several cutting parameters, including: cutting speed, uncut chip thickness, tool geometry, cutting feed and cutting depth. This allows the effects of such cutting parameters in the surface and subsurface residual stress distributions to be investigated. This numerical model is validated by comparing the predicted results (such as chip morphology, cutting forces, temperatures and residual stresses induced by the operation) to the experimental evidence conducted in the laboratory.

In the 3D model presented in this research, considers both the motions involve in the orthogonal machining operation to simulate the real time 3D orthogonal machining. But due to high computational cost and time limitation it is not possible to check parameters by varying them in 3D model, Only one set of parameter have been verified with 3D model. To reduce the computational time and cost most of the results and verification is done for the 2D models.

2. Basic Aspect of Orthogonal Machining

A process of two different kind of Orthogonal-machining has been shown in Figure2.1 and Figure 2.1 [*Fundamentals Of Machining* And *Machine* Tools][20].The process consist of a rotating workpiece with a cutting tool having translational motion along the axis of rotation in Figure2.2 and cutting tool having translational motion towards the axis in Figure 2.1. When the tool is engaged with the rotating workpiece material starts to remove from the workpiece.The point where tool touches the material is called machining zone. The motion of the tool is perpendicular with the motion of the workpiece Figure 2.1,Figure 2.2.The rotation speed of the work piece is called *'cutting speed(V)'* expressed in 'rpm' in fig1a,b.The distance moved by the tool along the axis of rotation in Figure 2.2 and towards the axis in Figure 2.1, for each revolution of the workpiece in called *'feed(f)'* and expressed in 'mm/rev'. In the Figure 2.2, the distance between outer most surface to the finished machined surface in the measured in the radial direction, along y-axis in the Figure 2.2 is called *Depth of Cut*(a_p) expressed in mm.In the Figure 2.2 *Depth of Cut*(a_p) thickness of the circular thread measured in axial direction.

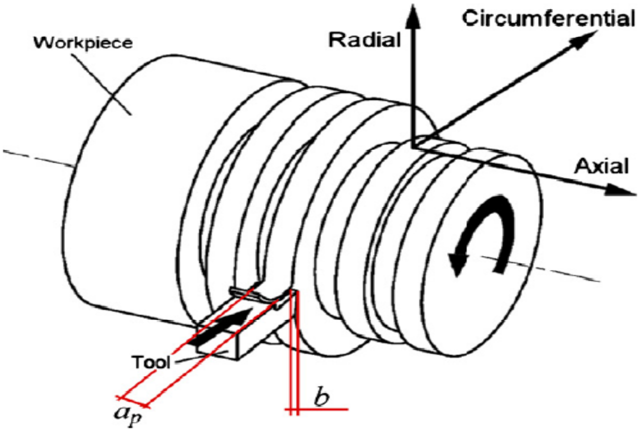

Figure 2.1 Configuration of Orthogonal Cutting process (motion of tool towards the axis of rotation)

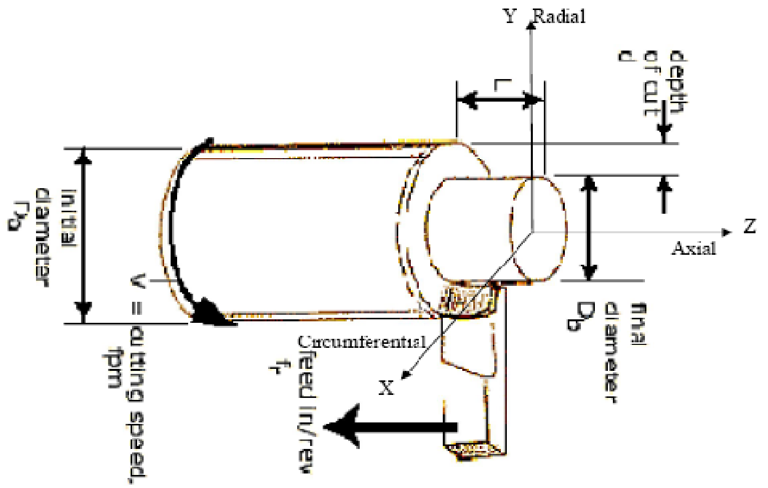

Figure 2.2 Configuration of Orthogonal Cutting process (motion of tool parallel to axis of rotation)

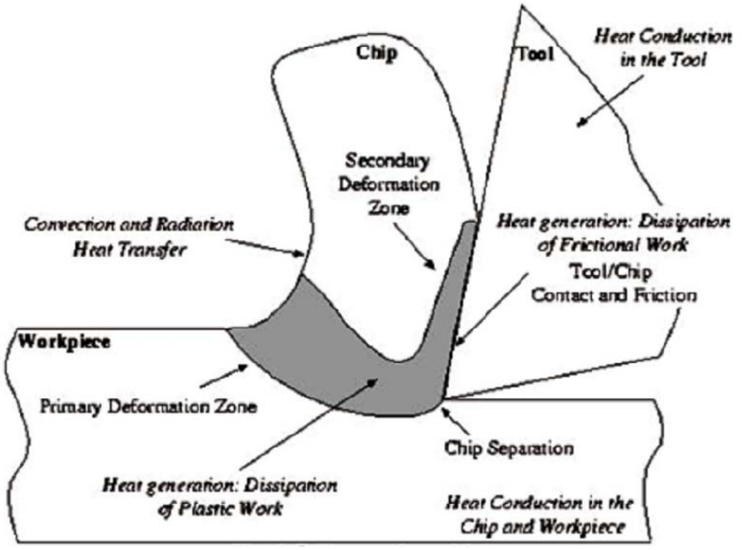

Figure 2.3 Terminology in metal orthogonal Cutting

A more idealized cutting process is shown in the Figure 2.3 This figure shows the enlarged view of the cutting zone where a tool is engaged with the work piece. The shear plane, the main region of plastic deformation, and the area of contact between the chip and the tool will be of particular interest.

2.1 The Shear Plane

Under a normal working condition the material undergoes large strains as it crosses a thin region around the shear plane. Some material, such as cast iron, cannot withstand any large plastic deformations. They fracture, resulting in a discontinuous chip. Lamellar chips get their shape from thermoplastic instabilities at the shear plane.

2.2 Contact Region

The friction forces at the tool interface affect the cutting forces and the chip geometry. High friction results in a thicker chip. The contact between tool and work material is further complicated by high temperatures and very large contact stresses.

2.3 Mechanism of Chip Formation

Cutting processes involve a wide range of physical phenomena. This section introduces the mechanical, thermal and tribological principles on which understanding of the process is based. In the Figure 2.4 the types of chips that can be formed, depending on the material and cutting conditions. Figure 2.6, Figure 2.7 describes the main regions of plastic flow and discusses how the dissipation of the inelastic work generates energy resulting in a subsequent temperature rise. The forces generated on a tool during cutting are described in Figure 2.7, Figure 2.8, and Figure 2.9

2.3.1 Chip Geometry and Influencing Factors

The type of chip produced can characterize the various cutting processes. Although there exist many individual types or combinations thereof, a general classification is widely accepted today. In general, the chips are classified as *discontinuous*, *continuous*, *continuous with built-up-edge* and *shear-localized*, as shown in Figure 2.4. The discontinuous chip is commonly observed when brittle materials are cut at low cutting speeds. The chip separation mechanisms have not been fully explained and several factors are said to affect the process. The phenomenon is frequently described through plastic shear strain, shear stress and shear instability models. The *continuous* chip is commonly produced when cutting ductile materials and the operation can be regarded as steady state. However, long continuous chips cause handling and removal problems in practical operations. Under conditions of low cutting speeds where the friction between the chip and the rake face of the tool is high the chip may weld onto the tool face. This accumulation of chip material is known as a *built-up edge* (BUE).

Finally, the last type of chips is macroscopically continuous chips consisting of narrow bands of heavily deformed material alternating with larger regions of relatively unreformed material. These *shear-localized* chips can be formed when the yield strength of the workpiece decreases with temperature Madhavan and Adibi-Sedeh (2005) [19]. Under the proper conditions, rapidly heated material in a narrow band in front of the tool can become much weaker than the surrounding material, leading to localized deformation. This type of chip is obtained when cutting hardened and stainless steels and titanium alloys at high cutting speeds. This is verified with 2D model and results are presented in the section 7.10 of this research work.

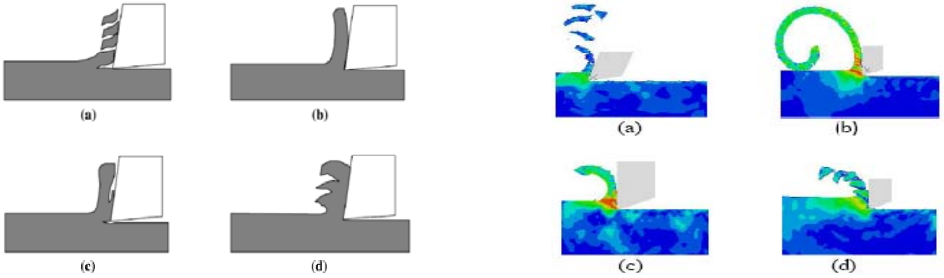

Theoretical *2D simulation*

Figure 2.4 Four basic types of chips: (a) discontinuous, (b) continuous, (c) continuous with built-up edge (BUE), (d) shear localized

The characteristics of crack formation have a significant influence on the chip formation pattern as the cutting process involves the separation of a chip from the workpiece. Further more, M. Vaz Jr. · D.R.J. Owen ,V. Kalhori · M. Lundblad (2005) [8] postulates that fracture is inherent in material removal processes, including continuous chip formation. When the cutting tool movement towards the workpiece starts, the stress concentration in front of the cutting edge is increased (see Figure 2.5(a)). When this stress reaches a certain maximum limit, the following may happen:

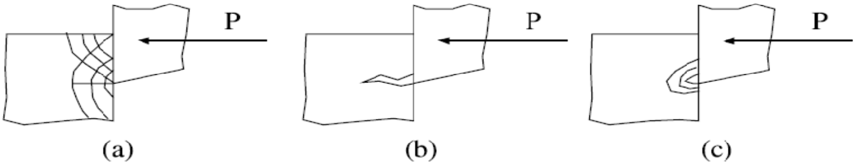

Figure 2.5 Cutting tool starting to advance into the workpiece

I. If the workpiece material is brittle, then a crack appears in front of the cutting edge, which finally causes fracture,Figure 2.5b.

II. If the workpiece material is ductile, then a certain elastoplastic zone forms in the workpiece, Figure 2.5c. The dimensions of the plastic and elastic parts of this zone depend on the ductility of the workpiece material.

2.3.2 Deformation Process Zones

The major deformations during the machining process are concentrated in two regions close to the cutting tool edge. These regions are usually called the primary and the secondary deformation zones, Figure. 5,6The *primary deformation region* extends from the tip of the cutting tool to the junction between the undeformed work material and the deformed chip. The workpiece is subjected to large deformation at a high strain rate in this region. The heating is due to energy dissipation from the plastic deformation. At the *secondary deformation zone*, heat is generated due to the plastic deformation and friction between the cutting tool and the chip.

The secondary deformation zone may be divided into two regions, the sticking region and the sliding region, Figure 2.6,Figure 2.7. In the sticking region, the workpiece material adheres to the tool and shear occurs within the chip. The heat generation per unit volume is large in this region due to the highly localized plastic deformation near the surface of the chip. The highest temperature usually occurs in the sliding region close to the sticking region.

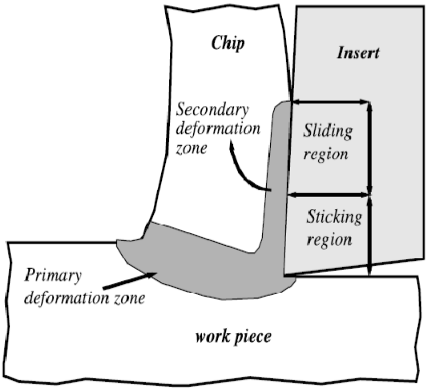

Figure 2.6 Locations of the primary and secondary deformation zones and the sliding and sticking regions

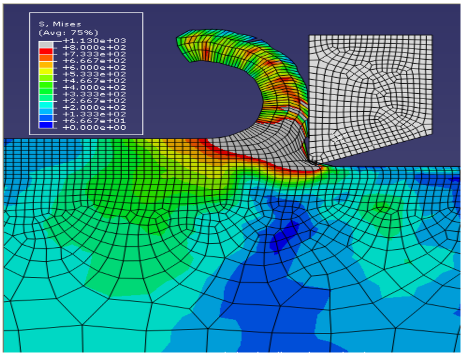

Figure 2.7 FEA-Model(Abaqus/Explicit)

2.3.3 Mechanical Effects in The Cutting Zone

The forces involved in chip formation, in orthogonal cutting, are depicted in Figure 2.8 The fracture in the chip formation occurs due to the combined bending stress, the component S,and the shearing stress due to compression Q. The presence of the bending stress in the deformation zone distinguishes the processes of metal cutting from other deforming and separating manufacturing process. The competition between deformation hardening and thermal softening in the deformation zone constitutes a cyclical character of the chip formation process. As a result, the parameters of the cutting system vary over each chip formation cycle. The cutting force depends on several parameters, such as the tool angles, feed and cutting speed.

Figure 2.8 the interaction between tool rake face and the chip. The penetration force *P* acts on the chip, causing the compressive force *Q* and the bending force *S* The more general three-dimensional case occurs, for instance, in lathe turning. In this case the resultant force has three components, Figure 2.9 The component of the force acting on the rake face of the tool, normal to the cutting edge, in the direction *OY* is called *cutting force* F_c. This is usually the largest force component, and acts in the direction of the cutting velocity. The force component acting on the tool in the direction *OX*, parallel with the direction of feed, is referred to as the *feed force* F_f . The third component, acting in the *OZ* direction, pushes the cutting tool away from the work in the radial direction. This is the smallest of the force components. The specific work done in cutting, W_c, depends mainly on two factors: the fracture shear strain and the temperature. The former changes because the shear stress at fracture of the work piece material depends on the strain. The latter combined with high strain rates that occur in cutting will affect the frictional shear stress τ_f and must therefore affect W_c. M. Vaz Jr. · D.R.J. Owen ,V. Kalhori · M. Lundblad [8]

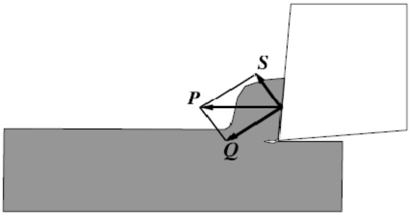

Figure 2.8 The interaction between tool rake face and the chip. The penetration force P acts on the chip, causing the compressive force Q and the bending force S

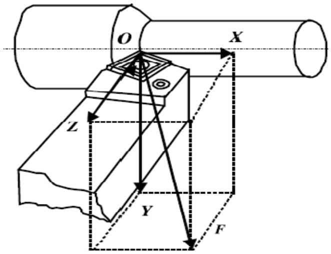

Figure 2.9 Cutting forces acting on the tool in a semi-orthogonal cutting

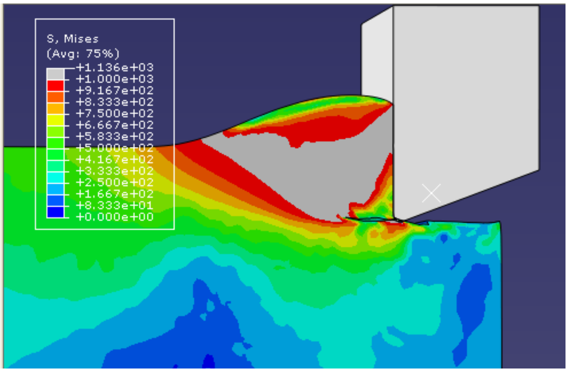

Figure 2.10 FEA-Model(Abaqus/Explicit)

3 Material and Models

3.1 Constitutive Material Model

In FEA, accurate flow stress models are considered highly necessary to represent work material constitutive behaviour under high strain-rate deformation conditions. The constitutive model proposed by Johnson and Cook [21] describes the flow stress of a material with the product of strain, strain rate and temperature effects as given in Equation (3.1). In this model, the constant A is the initial yield strength of the material at room temperature and a strain rate of 1/s and $\bar{\varepsilon}$ represents the plastic equivalent strain. The strain rate $\dot{\bar{\varepsilon}}$ is normalized with a reference strain rate $\dot{\bar{\varepsilon}}_0$. Temperature term in the J-C model reduces the flow stress to zero at the melting temperature of the work material, leaving the constitutive model with no temperature effect. In this study, FEA of machining of 20NiCrMo5 steel in annealed condition is investigated and its J-C material model constants are given in Table 3.1.The J-C material model constants used for this simulation are experimentally determined in SWEREA KIMAB lab by Dr. Chandrashekharn.

$$\bar{\sigma} = [A + B(\bar{\varepsilon})^n]\left[1 + Cln\left(\frac{\dot{\bar{\varepsilon}}}{\dot{\bar{\varepsilon}}_0}\right)\right]\left[1 - \frac{T - T_{room}}{T_{melt} - T_{room}}\right]^m \tag{3.1}$$

Table 3.1 Constants of the J-C constitutive model for the work materials.

Material	20NiCrMo5 steel
A (MPa)	490
B (MPa)	600
n	0.21
C	0.015
m	0.6
T_{melt}	1900

3.1.1 Material Physical Property

During this study all experiments and the FE-model is based for the 20NiCrMo5 steel material which is used for the pinion production for the heavy torque transmission in trucks. To minimize the difference between reality and the model we used the carbide material to define the tools physical properties in the beginning stage models. But as this study is not very much intended towards machining effect on cutting tool, we dropped the elastic tool concept and consider tool as a rigid body in later simulations. The Work material and the Tool material data is given in the Table 3.2.

Table 3.2 Work Material and Tool Material physical property

Property	Work Material(20NiCrMo5)	Tool material
Density(kg/cm3)	7.8	15
Poisson's ratio	0.3	0.3
Young's Modulus(GPa)	210	800
Thermal conductivity (W/m°C)	47.7	46
Specific heat(J/kg/°C)	556	203
Expansion (μm /m°C)	1.2	4.7

3.2 Tool-Chip Friction Model

Friction along the tool–chip contact interface, during the cutting process, is a very complex phenomenon [5,7,8,14,15,17]. It influences the chip geometry, built-up edge formation, cutting temperature and tool wear. Therefore, it is necessary to understand the friction mechanism across the faces and around the edge of the tool, in order to be able to develop accurate models for cutting forces and temperature. The most simple friction model is Coulomb friction,given by equation (3.2)

$$\tau=\mu\sigma \tag{3.2}$$

where τ is the frictional shear stress and σ is the normal stress to the surface. Usually the friction coefficient μ is assumed to be constant for a given interface [8]. There exist advanced models that are more relevant for the cutting process where rate, pressure and temperature dependency are accounted for. However, it is not possible to perform direct measurements of these for the extreme conditions that exist in the contact region. Therefore Modified Coulomb Friction Law is adopted to model the effect of contact friction along the tool-chip interface, it states that relative motion at a contact point will occur if the applied shear stress τ tangent to the contact interface reaches the critical frictional shear stress τ_c defined below equation (3.3)

$$\tau_c = \min(\mu p, \tau_{th}) \tag{3.3}$$

where p is the normal pressure at the contact point, μ is the coefficient of friction, and τ_{th} is a threshold shear stress value. It is noted that, when τ_{th} is set to infinity, the conventional Coulomb Friction Law is recovered. In this study, the work piece material is 20NiCrMo5 steel and τ_{th} is taken to be 210 MPa, which is equal to the material's yield stress in simple shear.

3.3 Damage Initiation Criterion

In metal cutting simulations, material start to deform and chips start to produce at the same time, when the stress and deformation states in a small region ahead of the tool tip satisfy a certain *Damage Initiation criterion*. In the present study *Ductile damage initiation criterion* is used, according to this if the shear strain value reaches to the certain critical plastic strain value, material start to deform. It is worth noting that the study by Huang and Black, [4] has shown that the geometry of the chip and the distribution of stress and strain fields are not very much influenced by the use of a particular Damage Initiation criterion. The critical plastic strain value used to govern the damage initiation is ε_p 1.5.

3.4 Contact Pair Modelling

Contact modelling is of great importance in metal machining due to the important effects associated with the tool–chip interface. The two most common algorithms for solving contact problems are the *penalty* approach and *Kinematic* approach. In this study *Kinematic predictor/corrector* Contact Algorithm [22] is used for the contact between tool and work material with high stiffness value of 210MPa.These special procedures have been developed for the explicit integration method, such as momentum-related techniques in which modifications are made to the acceleration, velocities and displacements. One of the aims of the latter is to avoid the penalizing effect on the time step of the explicit procedure, which can be introduced by the high stiffness, associated with penalty approaches. The contact condition is not fulfilled exactly in the *penalty* approach. *Kinematic predictor/corrector* Contact Algorithm [22] method has used by *Özel and Zeren* [7,16,17] in their study of FE Modelling of high speed marching. More details discussion and mathematical formulation of this approach is given in the section.5.5 and section.5.6.It has also been mention in section5.5 and 5.6, how Abaqus algorithm implements these methods for analysis.

3.5 Thermal Effect due High Speed Machining

The effect of temperature on the stress–strain relationship and fracture properties is well known but difficult to quantify.In general the strength of the material decreases and ductility increases as the temperature increases. In cutting operations the heat transfer is strongly dependent on the cutting velocity. At very low cutting speeds there may be adequate time for conduction to occur. At the other extreme, at very high cutting speeds there is nearly no time for heat conduction and adiabatic conditions may exist with high local temperatures in the chip. Zorev (1966) [23] and Shaw (1984) [24] assumed adiabatic conditions. This means that heat generated in the primary deformation zone and the average temperature T_{avg} in this region are proportional to the specific work for metal removal w_c. The increase of temperature in the chip is related to the increase of plastic deformation and thereby w_c. The average temperature can be estimated by equation (3.4)

$$T_{avg} = \frac{w_c}{\rho c} + T_0 \qquad (3.4)$$

where ρ is the density of workpiece material, c is the specific heat and T_0 is the temperature prior to deformation. The computed heat generation due to plastic dissipation and friction is confirmed in the numerical analysis shown in Figure 3.1

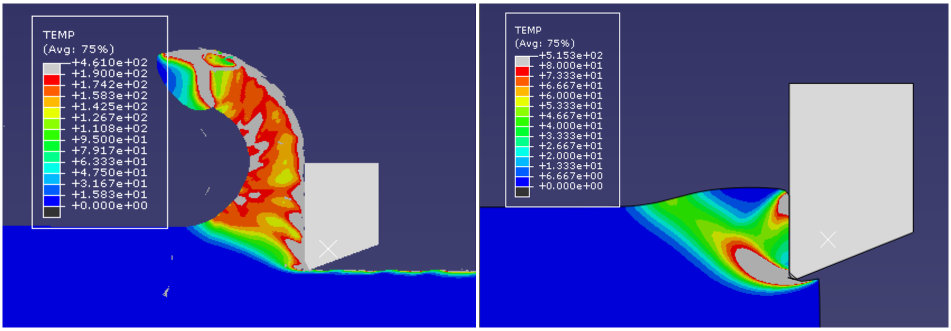

Figure 3.1 Avg. Temp in Deformation zone due to adiabatic condition

4. Finite Element Modelling

The great importance of the numerical modeling of the orthogonal maching is evinced by the increasing number of research works which have been published in the last thirty five years since the pioneering studies by *Usui and Shirakashi (1974, 1982) [25*] and *Klamecki (1973) [26]*. A review of modeling methods, including early numerical works, discussed by Ehmann et al. (1997) [27], and the extensive bibliography presented by Mackerle (1999,2003) further highlight the efforts being made to develop new problems.Also *V.Madhavan and A.H.Adibi-Sedeh[19]* works on understanding of finite Element Analysis machining based on Oxley's Machining approaches to solve this class of Model is reviewed very well to develop the Model. In this section, a discussion on the application of numerical models to metal machining in commercial software for FEM called ABAQUS/CAEV6.8, is presented, which includes mechanical and thermo-mechanical simulations. Individual aspects of simulation techniques and numerical strategies are presented, such as solution methods, constitutive models, thermo-mechanical coupling strategies, time integration schemes, chip morphology, friction models, element technology, mesh and re-meshing procedures, contact and fracture. The finite element model should incorporate some of these numerical strategies in order to accurately simulate the complex physical phenomena.

4.1 Choice of Formulation

The thermo-mechanical complexity of the cutting process makes analytical models incapable of capturing the all details needed for the satisfactory quantitative prediction of the mechanical and thermal stresses generated in the work piece and tool.

A model must be fairly general and flexible to correctly treat different geometries and material. FE-formulation seems, at the present time, to be the only reasonable choice.
Since the main aim of this study is to investigate the residual stress in the finish work piece due to different cutting condition, we are considering the tool as rigid body in the model to make the model simpler.

With an FE-formulation one has to choose between explicit and implicit time integration.Due to its simplicity, explicit time integration is normally used to solve transient problem where small time step sizes can be accepted. Implicit methods often have convergence problems, especially in the presence of contact and large deformations.The advantage of explicite method over implicit is also accepted by the other reasearcher like,Lars Olovsson[6], M. Vaz Jr. · D.R.J. Owen · V. Kalhori · M. Lundblad · L.-E. Lindgren [8],Özel and Zeren[7,16], *V.Madhavan and A.H.Adibi-Sedeh[19]*.Further on, one must choose between a Lagrangiian, an Eulerian and an ALE-formulation. brief description of the ALE-formulation is given in next section.

4.2 Lagrangian Formulation

A Lagrangian formulation of the problem might, at first, seem to be a good choice, because *Lagrangian* formulations assume that the finite element mesh is attached to material and follows its deformation, which brings the following advantages to machining simulation: the chip geometry is the result of the simulation and provides simpler schemes to simulate transient processes and discontinuous chip formation. However, element distortion has been a matter of concern and has restricted the analysis to incipient chip formation or machining ductile materials using larger rake angles and/or low-friction conditions. Pre-distorted meshes or re-meshing have been used to minimize the problem. An alternative approach to simulate steady state chip formation using a *Lagrangian* formulation was proposed by Usui and Shirakashi (1974, 1982) [25]. The strategy, known as “iteration convergence scheme, computes the chip final geometry and corresponding variables based on an initial assumption and on a combination of a small tool advance and an iterative evaluation of the stress field, velocity distribution and cutting forces Unfortunately a closer investigation reveals that the drawbacks dominate over the advantages.

Advantages

- The theory is easy to understand and the resulting is simple. Most available computer program are based are on a Lagrangian formulation.
- It possible to analyze cracking

Drawbacks

- As the material passes the shear plane, large strains distort the element geometry. the accuracy decrease and the critical time step size can drop significantly.
- It is impossible to simulate a flow zone with unlimited starin.The elements will be too distorted.
- If one wants to study the steady state situation, quite a long cut distance must be analysed.Many elements required and the computation time will be huge.

4.3 Eulerian Formulation

In *Eulerian* formulations, the mesh is fixed in space and material flows through the element faces allowing large strains without causing numerical problems. Moreover, this strategy is not affected by element distortion and allows steady state machining to be simulated. However, *Eulerian* approaches do not permit element separation or chip breakage and require a proper modeling of the convection terms associated with the material properties. In addition, such formulations also require the prior knowledge of the chip geometry and chip–tool contact length, thereby restricting the application range. In order to overcome this shortcoming, various authors have adopted iterative procedures to adjust the chip geometry and/or chip/tool contact length. However, just as for the Lagrangian formulation, there are some serious disadvantages that make the method less interesting.

Advantages

- Large strains will not cause numerical problem.
- Using flow boundary condition, only a small region around the tool needed to model.

Drawbacks

- The geometry of the chip must be known from the beginning. For good results one cannot accept a fixed geometry.
- Since the boundary is not allowed to move, cracking cannot be handled.

4.4 ALE- Formulation

In an attempt to combine advantages of both *Lagrangian* and *Eulerian* formulations, a mixed approach, known as *Arbitrary Lagrangian–Eulerian* formulation (ALE) has been proposed to model machining operations[6,7,8,16,17,19]. This method applies *Lagrangian* and *Eulerian* steps sequentially and uses the so-called operator split, illustrated in Figure 4.1.The first step assumes that the mesh follows the material flow, in which a *Lagrangian* problem is solved for displacements subsequently, the reference system is moved (the mesh is repositioned) and an advection problem is solved (*Eulerian* step) for velocities. Despite the fact that ALE methods reduce the element distortion problem typical of *Lagrangian* approaches, a careful numerical treatment of the advection terms is required. More elaborate discussions on use of ALE formulations in modelling metal machining are presented by Rakotomalala etal. (1993) [10],Olovsson etal. (1999) [6],Movahhedy et al. (2000) [28], and Madhavan and Adibi-Sedeh (2005) [19].

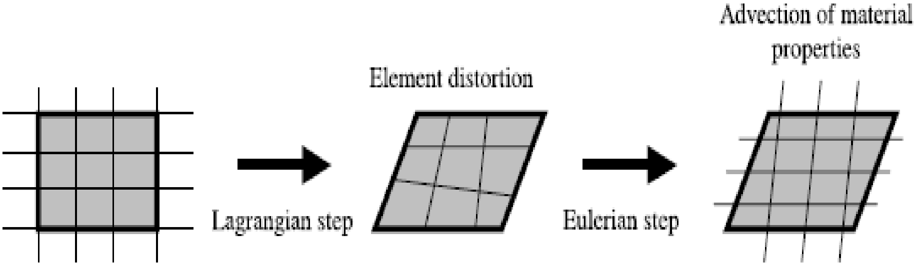

Figure 4.1 The ALE operator

4.4.1 Example of ALE-Procedure In Abaqus/Explicite V6.8

To illustrate the value of adaptive meshing, simple examples of transient and steady-state forming applications follow. For simplicity, two-dimensional cases are shown. In each case Abaqus/Explicit is used in the simulation. Example Axisymmetric forging [22].In this example a well-lubricated rigid die of sinusoidal shape moves down to deform Figure 4.2

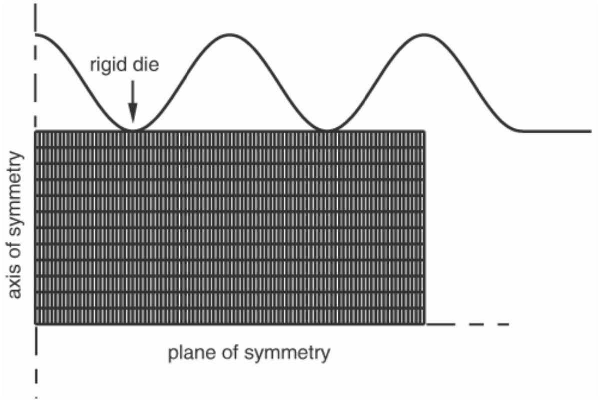

Figure 4.2 A blank of rectangular cross-section

The indentation depth is 80% of the original blank thickness. Material extrudes upward and outward (radially) as the blank is indented. The die is modeled with an analytical rigid surface, and the blank is modeled with axisymmetric continuum elements in a regular mesh configuration. The blank is assumed to have elastic-plastic material properties.

A pure Lagrangian analysis of this problem does not run to completion because of excessive distortion in several elements, as shown in Figure 4.3. The contact surface cannot be treated correctly because of the gross distortion of the elements at the troughs of the sinusoidal rigid surface.

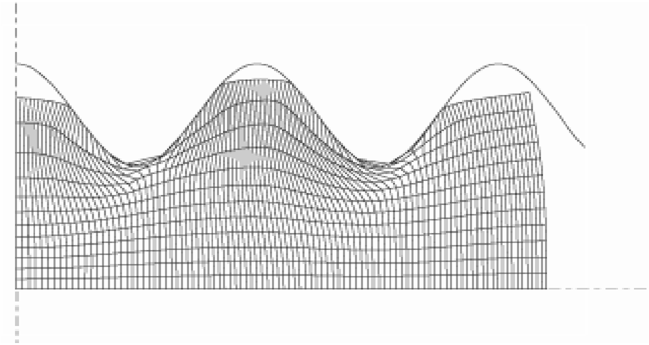

Figure 4.3 Eventually, the purely Lagrangian analysis will terminate because of excessive element distortion

Adaptive meshing allows the problem to run to completion. A Lagrangian adaptive mesh domain is created for the entire blank.

Figure 4.4 and Figure 4.5 show the deformed mesh at various stages of the forming analysis. Because the mesh refinement is maintained on the areas of the slave surface that contact the die troughs as the material flows radially, contact conditions are resolved correctly throughout the analysis.

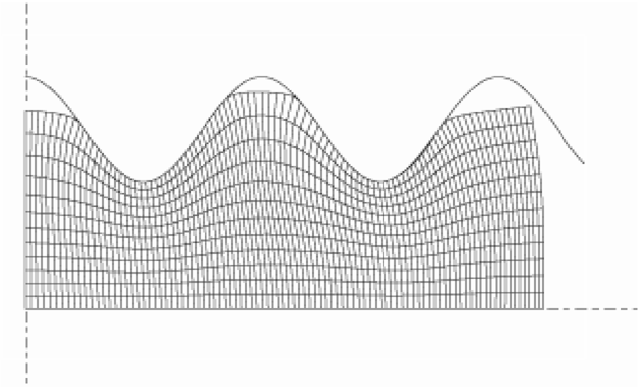

Figure 4.4 Deformed configurations at an intermediate stage of the analysis

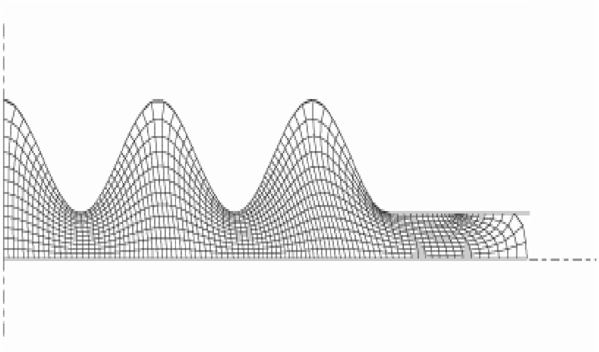

Figure 4.5 Deformed configurations upon completion of the analysis

So ALE-meshing controls the element distortion. This is more clearly illustrated in the Figure 4.6 below

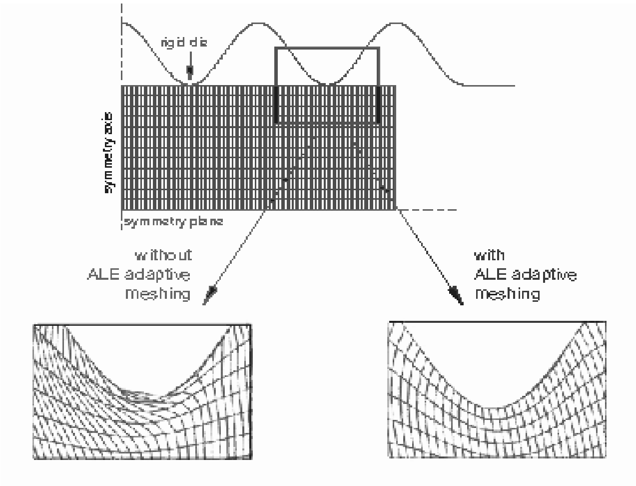

Figure 4.6 Use of ALE adaptive meshing to control element distortion.

Which omit the problems of convergence due large deformation, as we have in the purely Lagrangian formulation.

4.5 Choice of Element Type

Due to high complexity of the machining operation from the numerical modelling point of view, it is very necessary to select the right element for the FE-modeling, to handle this type of complex thermo-mechanical coupled problem, where large deformation are also the important factor. As we know elements with low order shape functions are known to perform poorly, showing the typical volumetric locking behavior which, in many circumstances, invalidates the finite element solution. In spite of such a major drawback, low order elements, often together with special formulations to avoid this locking problem, are preferred due to their inherent simplicity. This is particularly true in cutting simulations where a number of complex interacting phenomena, such as the ones discussed in the paper, may be present. Barge et al.(2005) [29], well aware of such difficulties, presented a discussion on the influence of the numerical parameters, in special the *hourglass* effect upon the equivalent stress, equivalent plastic strain and cutting forces.

Linear, plane strain, isoperimetric quadrilateral elements and structured meshes have been generally adopted throughout previous simulations. Quadrilateral, 8-node elements were employed by Joshi et al. (1994) [30], Mc-Clain et al. (2002) [31], whereas quadrilateral, 9-node elements were used by Eldridge et al. (1991) [32]. Linear, triangular elements have been used widely in the works of Usui and Shirakashi (1974, 1982) [25] and Lin and co-workers (1992,1993) [33], and Marusich and Ortiz (1995) [34] have used 6-nodded triangular elements and re-meshing strategies.

In the resent years research in this area Özel and Zeren [7] and V.Madhawan and A.H. Adibi-Sedeh[2005] [19], used 4 node quadrilateral Coupled temperature-displacement plan strain reduced integration elements CPE4RT,with ALE-formulation to handle thermo-mechanical coupled machining problems and they get fairly accurate and quit realistic results.

In this 4-node quadrilateral Coupled temperature-displacement plan strain reduced integration elements CPE4RT, with ALE-formulation. The details about the elements property given in the ABAQUS user manual [22].But in the preliminary stage 4 node quadrilateral plain strain reduced integration elements are also used CPE4R.

4.6 Thermo-Mechanical Coupling

In cutting processes, energy is generated due to the dissipation of both inelastic work and frictional work, being transferred through the work piece/chip and tool and lost to the surrounding environment by convection and radiation. Temperature rise causes thermal strains and affects the material properties. Most finite element approximations use the concept of the weak form of the governing equation, as equation (4.1)[8]

$$C_T\dot{T}_n + K_T T_n = Q(t_n) \tag{4.1}$$

in which T_n are the nodal temperatures at time t_n,C_T and K_T are, respectively, the heat capacity and heat conduction matrices and Q is the heat flux and heat generation due to inelastic deformation.

In *adiabatic* processes no heat transfer takes place (K_T is assumed very less value (0.047) in equation. (4.1), i.e., the heat generated due to inelastic deformation and friction is kept inside the element causing the temperature to rise [14,35,36].As seen in the Figure 4.7

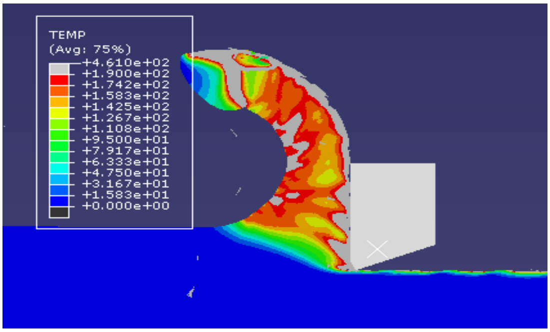

Figure 4.7 Rise of temperature due to adiabatic process

Due to very high speed machining the process is considered to partial adiabatic, chip has no time to radiate the heat, tool is consider to be a rigid body though out the simulation.

4.7 Time Integration Technique

Dynamic explicit time integration technique is adopted for the FE-modeling of machining operation which involves high nonlinearity, Complex friction-contact conditions, thermo-mechanical coupling and fragmentation. The finite element discretization can be derived from the weak form of the mechanical equilibrium equations (4.2) [8] given as

$$\mathrm{M}\ddot{\mathrm{u}}_{\mathrm{n}} + \mathrm{C}\dot{\mathrm{u}}_{\mathrm{n}} + \mathrm{F}_{\mathrm{n}}^{\mathrm{int}}(\mathrm{u}_{\mathrm{n}}) = \mathrm{F}_{\mathrm{n}}^{\mathrm{ext}}(\mathrm{t}_{\mathrm{n}}) \tag{4.2}$$

where $\ddot{\mathrm{u}}, \dot{\mathrm{u}}$ and u are the nodal acceleration, velocity and displacement at time t_n, M and C are mass and damping matrices (the latter is disregarded in some explicit formulations) and $\mathrm{F}^{\mathrm{int}}$ and $\mathrm{F}^{\mathrm{ext}}$ are internal and external forces, velocity and acceleration can be approximated in terms of the displacements integrating them using the explicit central-difference integration rule given by equation (4.3) and equation (4.4)

$$\dot{\mathrm{u}}_{\mathrm{i}+\frac{1}{2}}^{\mathrm{N}} = \dot{\mathrm{u}}_{\mathrm{i}-\frac{1}{2}}^{\mathrm{N}} + \frac{\Delta\mathrm{t}_{(\mathrm{i}+1)} + \Delta\mathrm{t}_{(\mathrm{i})}}{2}\ddot{\mathrm{u}}_{\mathrm{i}}^{\mathrm{N}}\ , \tag{4.3}$$

$$\mathrm{u}_{(\mathrm{i}+1)}^{\mathrm{N}} = \mathrm{u}_{(\mathrm{i})}^{\mathrm{N}} + \Delta\mathrm{t}_{(\mathrm{i}+1)}\dot{\mathrm{u}}_{\mathrm{i}+\frac{1}{2}}^{\mathrm{N}}\ , \tag{4.4}$$

where u^N is a degree of freedom (a displacement or rotation component) and the subscript i refers to the increment number in an explicit dynamics step. The central-difference integration operator is explicit in the sense that the kinematic state is advanced using known values of _ and from the previous increment.

The explicit integration rule is quite simple but by itself does not provide the computational efficiency associated with the explicit dynamics procedure. The key to the computational efficiency of the explicit procedure is the use of diagonal element mass matrices because the accelerations at the beginning of the increment are computed by equation (4.5) given below

(4.5)

where M^{NJ} is the mass matrix, P^{J} is the applied load vector, and I^{J} is the internal force vector. A lumped mass matrix is used because its inverse is simple to compute and because the vector multiplication of the mass inverse by the inertial force requires only *n* operations, where *n* is the number of degrees of freedom in the model. The explicit procedure requires no iterations and no tangent stiffness matrix. The internal force vector, I^{J}, is assembled from contributions from the individual elements such that a global stiffness matrix need not be formed. More details is given in Abaqusv6.8 user manual.[22]

5 Finite Element Modelling With Abaqus/Explicit

In this section the functions of FEA commercial code ABAQUS/CAE V6.8 are described. First the general information about the program is given. Subsequently the ALE formulation, mesh smoothing technique; thermo-mechanical coupling, Model geometry and boundary condition are also described.

5.1 General Information about Abaqus/Caev6.8

The Abaqus Unified FEA product suite offers powerful and complete solutions for both routine and sophisticated engineering problems covering a vast spectrum of industrial applications. In the automotive industry engineering work groups are able to consider full vehicle loads, dynamic vibration, multibody systems, impact/crash, nonlinear static, thermal coupling, and acoustic-structural coupling using a common model data structure and integrated solver technology. Best-in-class companies are taking advantage of Abaqus Unified FEA to consolidate their processes and tools, reduce costs and inefficiencies, and gain a competitive advantage.

Abaqus/CAE is divided into modules, where each module defines a logical aspect of the modeling process; for example, defining the geometry, defining material properties, and generating a mesh. As you move from module to module, you build up the model. When the model is complete, Abaqus/CAE generates an input file that you submit to the Abaqus analysis product. Abaqus/Standard or Abaqus/Explicit reads the input file generated by Abaqus/CAE, performs the analysis, sends information to Abaqus/CAE to allow you to monitor the progress of the job, and generates an output database. Finally, you use the Visualization module to read the output database and view the results of your analysis. As you interact with Abaqus/CAE, a replay file is generated that contains Abaqus/CAE commands for every modeling operation that you perform.[22].

5.2 Boundary Condition and Model Geometry

Many of the researcher, Özel and Zeren[7,16],V.Madhavan and A.H.Adibi-Sedeh[19],C.Shet and X.Deng[9] have used predefine chip geometry to simulalate the orthogonal machining using Eulerian,Lagrangian and ALE formulation. As it is quite unrealistic to use pre-define chip geometry in the model. So in this study Modelling is done using ALE-remeshing technique with purely Lagrangian boundary condition, in which mesh follows the work material. by doing this we can get rid from the pre-define chip geometry problem to make the model more realistic.

In the Figure 5.3 2D finte element simulation model for ALE formulation with purly lagrangian boundary conditions is given.Length in the x-direction is 5mm and y-direction is 2 mm,the uncut chip thickness is 0.2 mm.The nose radius of the tool is 0.02mm.The workpiece is modeled with Lagrangian boundries at the four ends,which is depicted by the thick perpel line around the workpiece.Mechanical constrains are applied at the bottom surface of the work materail i.e motion of the workpiece is resticted in the y-direction.Tool is fixed in and its motion is constarined in the all direction.The materials in flow and out flow velocity is same in the x-direction V_x= V_c

5.2.1 Transition Of Model Fron 3D To 2D

As mentioned the process is simplified to a plain strain model. The picture below Figure 5.1 illustrates the transition from reality to model, and the parts of the model.

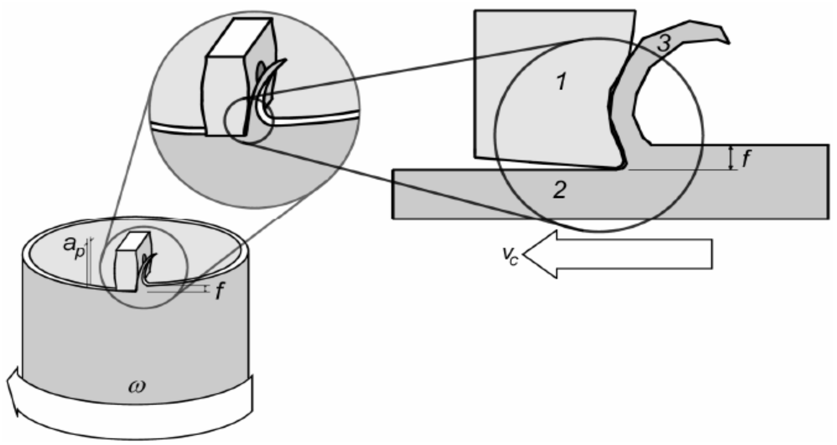

Figure 5.1 The simplification from reality to the plain strain model, where ap is depth of cut, f feed and velocity vc = ωx r. The numbers in the images indicate; 1) Tool, 2) Work-piece and 3) Chip.

5.2.2 Tool Geometry

Form the practical experience and the previous research [7,37]in this field has proved that the tool geometry has a great influence on the surface properties of the machined work piece, so it has been give a very keen importance in the model to design to tool geometry. It is very difficult to see the cutting tool's micro geometry with naked eye, So to look at the magnifying view of the tool's cutting edge geometry and measure the dimension *light optic microscope* have been used Figure 5.2 shows the geometry and dimension of the cutting edge of the tool measured under the microscope in the lab. The parameters are used in the simulation model.

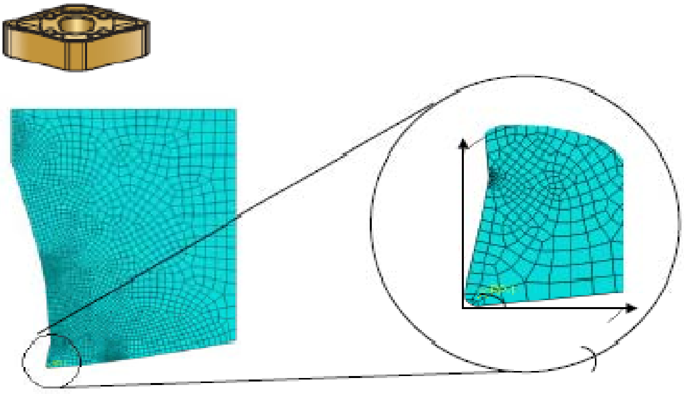

Figure 5.2 Tool geomerty

The nose radios of the tool is 0.02 mm and rake angle $6^{o.}$ clearence angle 6^{o}

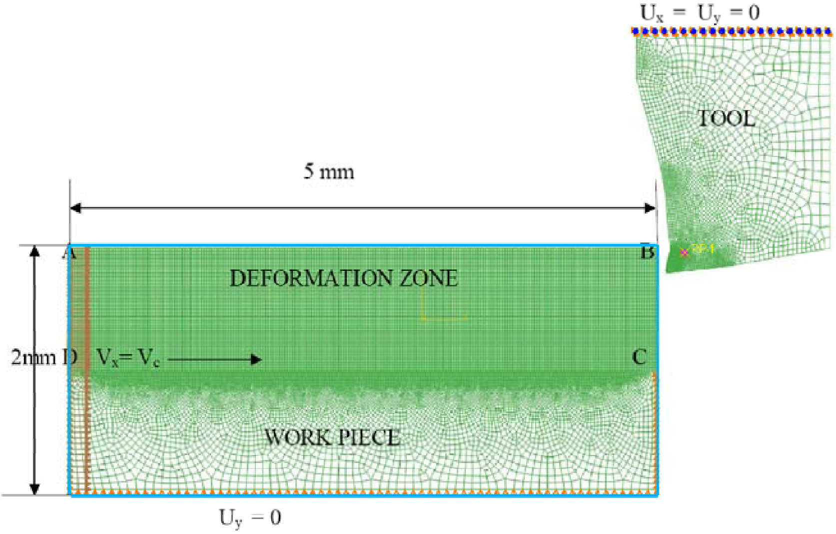

Figure 5.3 Finte Element simulation Model for ALE formulation with purely Lagrangian boundary condition ABAQUS/Explicit v6.8 with fine mesh

5.3 Finite Element Meshing

As shown in the Figure 5.3 the entire geometry is descriptive into very small finite element. The elements size of the tool geometry is constant and it is discredited into 489 CPE4RT elements. But the element size of the work material varies at the different part of the work piece, The element size in the deformation zone ABCD in the Figure 5.3 is very much smaller than the rest part as we move down from the top surface of the work piece. The entire geometry has 41503CPE4RT elements. the mesh density just below the cutting plane is very fine this is intentionally done to increase the accuracy of the result in this zone, but the mesh is kept coarse below this zone to reduce the computational time and its generally doesn't affect the result very much.

5.3.1 Meshing Type and Algorithms

In the model deformation zone is meshed with structured mesh technique. The structured meshing technique generates structured meshes using simple predefined mesh topologies. Abaqus/CAE transforms the mesh of a regularly shaped region, such as a square or a cube, onto the geometry of the region you want to mesh. For example, Figure 5.4 illustrates how simple mesh patterns for triangles, squares, and pentagons are applied to more complex shapes.

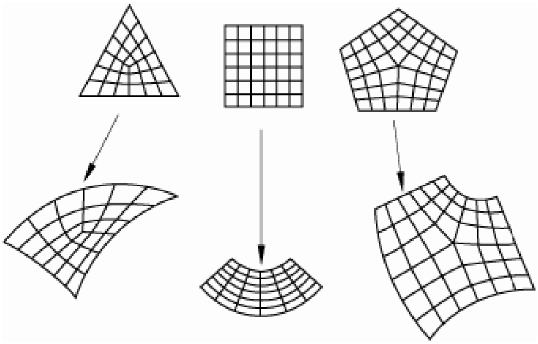

Figure 5.4 Two-dimensional structured mesh patterns.

One can apply the structured meshing technique to simple two-dimensional regions (planar or curved) or to simple three-dimensional regions that have been assigned the Hex or Hex-dominated element shape option. In general, structured meshing gives you the most control over the mesh that Abaqus/CAE generates. More details about assigning element shapes to a region is given in Abaqus user manual [22].

The Tool and the region below the deformation zone is meshed with the free meshed technique with Advancing front Algorithm. Free meshing with quadrilateral elements is the default meshing technique for two-dimensional regions. The free meshing technique with quadrilateral elements can be applied to any planar or curved surface. Free meshes are usually not symmetric, even if the part or part instance itself is symmetric. Abaqus/CAE allows choosing between two meshing algorithms when we create a quadrilateral or quadrilateral-dominated mesh.

- Medial Axis
- Advancing front

More information about the these algorithm are given in the [22]

The difference between both the algorithms can be shown in the Figure 5.5 and Figure 5.6

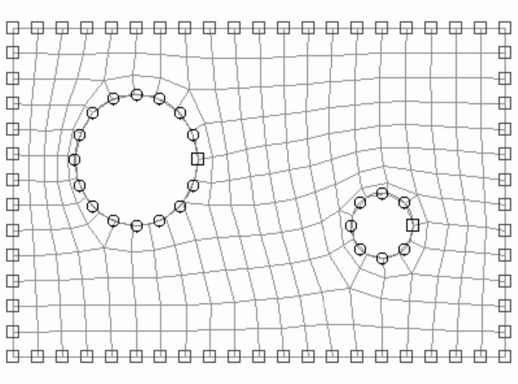

Figure 5.5 Medial Axis Algorithms

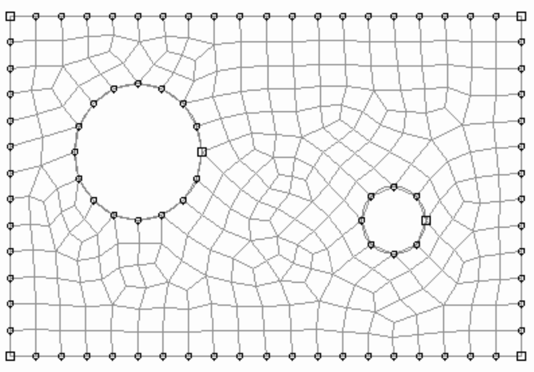

Figure 5.6 Advancing front Algorithm

The main advantage of the later is that it’s easy to mesh the complex boundary regions and corner .It also reduces the mesh transition compare to the medial axis algorithm.

5.3.2 Element Property

To model machining operation which in involves very complex thermo-mechanical coupling and large stain rate. It is very important to choose the right element to get the correct result from the simulation. In this simulation '4-node bilinear displacement and temperature, reduced integration with hourglass control' CPE4RT from the ABAQUS/CAE element library have been used, due to controlled *hourglass* these elements has very less effect upon the equivalent stress, equivalent plastic strain and cutting forces.

Hour glassing is a phenomenon that creates an artificial stress field on the top of the real field. Therefore you see geometric stress patterns that do not have any physical basis.
Hour glassing causes problem in accuracy. The way to check for hour glassing is to look at the artificial energy and compare it to strain energy. The ratio should not exceed 1%.Most of the researchers have used this element for their work. Özel and Zeren[7,16], V.Madhavan and A.H.Adibi.Sedeh [19].

5.4 ALE Adaptive Meshing and Remapping In Abaqus/Exlicit

Adaptive meshing in Abaqus/Explicit is designed to handle a large variety of problem classes, and employs a variety of smoothing methods, with controls that one can use to tailor the adaptivity to specific problems. The Abaqus/Explicit implementation allows us to do the following:

- can be used to analyze Lagrangian problems (in which no material leaves the mesh) and Eulerian problems (in which material flows through the mesh);
- can be used as a continuous adaptive meshing tool for transient analysis problems undergoing large deformations (such as dynamic impact, penetration, and forging problems);
- can be used as a solution technique to model steady-state processes (such as extrusion or rolling);
- can be used as a tool to analyze the transient phase in a steady-state process; and
- Can be used in explicit dynamics (including adiabatic thermal analysis) and fully coupled thermal-stress procedures.

- Initial mesh sweeps cannot be used to improve the quality of the initial mesh definition.
- The method is not intended to be used in general classes of large-deformation problems, such as bulk forming.

- Diagnostics capabilities are currently limited.

5.4.1 ALE Adaptive Mesh Domain

The ALE Adaptive mesh domain is created by selecting the whole work material i.e adaptive meshing is applied on the whole work piece. It defines the portions of a finite element model where mesh movement is independent of material deformation. The frequency for the remeshing is taken 100 here, which means remeshing will be done after 100 increments, large value of frequency may decrease the computational time but also reduces the accuracy. During each adaptive meshing increment, the new mesh is created by performing one or more mesh sweeps and then advecting the solution variables to the new mesh. The remeshing sweep per increment and the initial sweep value is taken 5 here, it means intensity of remeshing per incremental step in Abaqus will be 5. In an adaptive meshing increment, a new, smoother mesh is created by sweeping iteratively over the adaptive mesh domain. During each mesh sweep, nodes in the domain are relocated—based on the current positions of neighbouring nodes and elements—to reduce element distortion. In a typical sweep a node is moved a fraction of the characteristic length of any element surrounding the node. Increasing the number of sweeps increases the intensity of adaptive meshing in each adaptive meshing increment. The default number of mesh sweeps is 1. One should be very care full while choosing the sweep value because large sweep value increases the accuracy but also the computational time very much. So one should choose the optimal value. For more details [22]

5.4.2 ALE Adaptive Mesh Controls

The ALE adaptive mesh control is used to control the various aspects of the adaptive meshing and advection algorithms applied to an adaptive mesh domain. It can be used only in conjunction with the Adaptive Mesh option in Abaqus/Explicit.

5.4.2.1 Mesh Smoothing

For the mesh smoothing in the present model, *Enhanced algorithm based on evolving geometry* technique is used. This technique is used to mitigate the distortion of the elements. The conventional forms of the basic smoothing methods do not perform well in highly distorted domains, this algorithm is used with three basic smoothing methods: volume smoothing, Laplacian smoothing, and equipotential smoothing. The smoothing methods are applied at each node in the adaptive mesh domain to determine the new location of the node based on the locations of surrounding nodes or elements. Although all the smoothing methods tend to smooth the mesh and reduce element distortion, the resulting meshes will differ depending on the methods used. So it very important to determine the weight factor or combination factor for this three method, in the present model the optimize weight factors are taken as follows.

- Volume smoothing 0.8
- Laplacian smoothing 0.1
- Equipotential smoothing 0.1

For more details one can refer to [30]

The weight factor for the first method is choose very high compare to the others, because Volume smoothing relocates a node by computing a volume-weighted average of the element centers in the elements surrounding the node. In Figure 5.8 the new position of node M is determined by a volume-weighted average of the positions of the element centers, C, of the four surrounding elements. The volume weighting will tend to push the node away from element center C1 and toward element center C3, thus reducing element distortion.

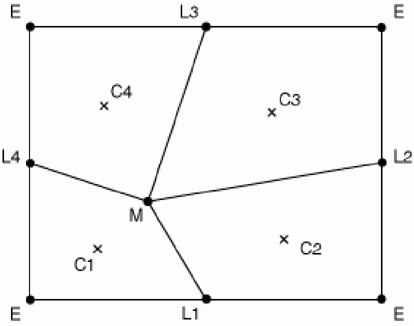

Figure 5.7 Relocation of a node during a mesh sweep.

So Volume smoothing is very robust compare to other two methods.

The *Improve aspect ratio* based adaptive mesh smoothing technique is choose in the model to minimizes element distortion and improves element aspect ratios at the expense of diffusing initial mesh gradation, it also handle the large deformation very well. That why it’s also recommended by large number of user as well.

Since the model has purely Lagrangian boundary condition and under goes very large deformation rate it is preferable to choose mesh sweeping based on *current nodal locations*, which account for material motion accumulated since the last adaptive mesh increment. For more details [22].

5.4.2.2 The Advection step

Element and material state variables must be transferred from the old mesh to the new mesh in each advection sweep. The number of variables to be advected depends on the material model and element formulation; however, stress, history variables, density, and internal energy are always solution variables. So t *second-order method* based on the work of Van Leer (Van Leer, 1977) has been choose for the remapping after adaptive mesh or for Advection step. For the momentum Advection *The element center projection method* because it requires only requires the fewest numerical operations and two variable in 2D case which makes it more economical compare to the *Half index-shift method*.More details [22].

The schematic flow chart for Adaptive meshing procedure by M.Vaz Jr,D.R.J, V.Kalhori [8] is given below in Figure 5.8

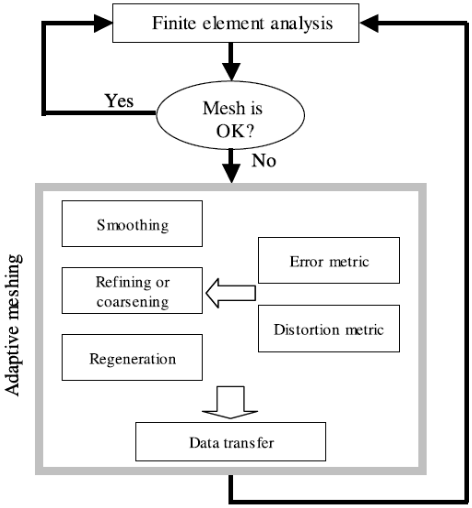

Figure 5.8 Adaptive meshing procedures

5.4.3 ALE Adaptive Mesh Constrains

Adaptive mesh constraints allow full control over the mesh movement and act independently of any boundary conditions or loads applied to the underlying material. Here adaptive mesh nodes are constrained to follow the underlying material, this ALE adaptive mesh constrain is called Lagrangian constrain because mesh motion follows the underlying material movement.

5.5 Definition of Contact-Pair

In the model surface-to-surface contact condition is used to define the Tool-chip as well as tool-work piece contact pair. Mechanical constrains are purely master-slave type Kinematic control. The main advantage of this type contact formulation is node of the slave surface, here work piece, can't penetrate the surface of the master surface, here Tool surface. Infinite sliding formula is adopted to dine the relative sliding between two surfaces, because,the finite-sliding formulation allows for arbitrary separation, sliding, and rotation of the surfaces.

5.6 Definition of Contact Properties

The mechanical contact properties between the two surfaces have a great impact on the result value and also for the continuous chip formation this should be handled very carefully.

To define the Tangential behavior of the contact surfaces Penalty-method with frictional co-efficient value $\mu=0.4$ is choosed, because it permits some relative motion of the surfaces (an "elastic slip") when they should be sticking.

While the surfaces are sticking (i.e $\bar{\tau} < \bar{\tau}_{crit}$) the magnitude of sliding is limited to this elastic slip. Abaqus will continually adjust the magnitude of the penalty constraint to enforce this condition. For more information [21].The Penalty-method is based on Coulomb friction model, the basic concept of the Coulomb friction model is to relate the maximum allowable frictional (shear) stress across an interface to the contact pressure between the contacting bodies. In the basic form of the Coulomb friction model, two contacting surfaces can carry shear stresses up to a certain magnitude across their interface before they start sliding relative to one another; this state is known as sticking. The Coulomb friction model defines this critical shear stress, τ_{crit} at which sliding of the surfaces starts as a fraction of the contact pressure, *p*, between the surfaces ($\tau_{crit} = \mu\rho$)the stick/slip calculations determine when a point transitions from sticking to slipping or from slipping to sticking. The fraction, μ, is known as the coefficient of friction,here critical or limiting shear stress value is taken 210MPa.After this value chip start to slip over tool front face.It is also possible to control the elastic slip by specifying the small fraction of sticking surface of here it's taken as slip tolerance= 0.005.The liming slip tolerance value is taken is 200MPa slightly lower than the normal stiffness value. Slip regions for the friction model with a limit on the critical shear stress given the Figure 5.9

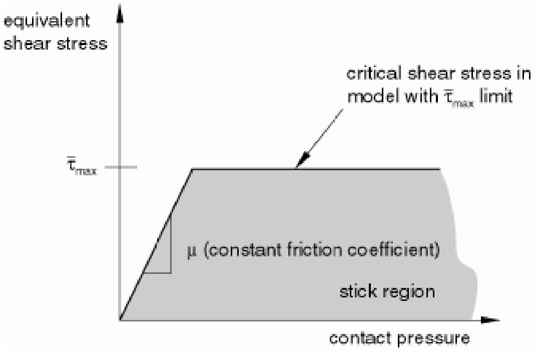

Figure 5.9 Slip regions for the friction model with a limit on the critical shear stress

The Normal behavior or contact pressure-over closure relationship that governs the motion of the surfaces in a mechanical contact analysis is chosen as Linear with positive value for the slope of the pressure-over closure curve, *k=210MPa.*

More details [22].

6. Experiment setup, Measurements and Simulation

6.1 Experiments and Cutting Conditions

Within the limited scope of this part of the project it was decided to make a parametric model of the influence of the cutting data on the residual stresses.

Residual stresses were measured tangentially and axially in the pinion production line for different combinations of feed and depth of cut. The tests were duplicated at the machining lab at KIMAB on ordinary round bars. One aim was to find out if lab tests would give the same residual stresses, making testing easier, not having to disturb production.

A parametric model has some advantages. Within the limitations of the range of cutting data, cutting geometry and work and tool material it is quite accurate. However, it will not be able to predict anything outside the scope of the tested parameters. The approach for the parametric study was adapted from work made by Mittal and Liu on hard machining [38].

The method resembles the statistical approach to design experiments with high (+), low (-) and middle (0) values for all parameters studied. The effect of each parameter and the effect of the combination of the parameters is then determined. The more parameters that are examined, the more experiments have to be carried out. Since the depth distribution of residual stresses is the result parameter and these measurements are time consuming and costly, it was decided to only vary feed, f, and depth of cut, a, and keep the cutting speed constant. For each set of parameters a residual stress distribution was measured axially and tangentially to a depth of 150 μm.

The experiments are done for the different cutting condition, same as used in the FE-models to get a check of the results. The tested cutting conditions are given the Table 6.1

Table 6.1 Cutting conditions

Parameter	Test 1	Test 2	Test 3	Test 4	Test 5	Test 5	Test 7	Test 8	Tes t9	Test 10
Cutting Speed, Vc m/mm	400	300	200	160	120	80	40	200	200	260
Feed mm/rev	0,2	0,2	0,2	0,2	0,2	0,2	0,2	0,1	0,3	0,45
Width of cut w(mm)	3	3	3	3	3	3	3	3	3	3
Tool rake angle α(degree)	+6	+6	+6	+6	+6	+6	+6	+6	+6	+6
Tool clearance angle(deg	+6	+6	+6	+6	+6	+6	+6	+6	+6	+6
Tool edge radius(m m)	0.02	0.02	0.02	0.02	0.02	0.02	0.02	0.02	.02	0.02

6.2 Experimental Setup and Measurements

Experiments are done at in house facility at Swerea KIMAB and also in the production line in SCANIA.The test result are given in the Table 6.2 & Table 6.3 below.

The schematic diagram of the experiment is given in the Figure 6.1 and the actual set up to measure the residual stresses is given in the Figure 6.2.In SWEREA KIMAB lab the experiment is performed on the simple rounded bar. The experimental result obtained is compared with the values measured during production in SCANIA.The comparison between two values are given in the Figure-6.3.Result are tabulated in the Table 6.2 and Table 6.3

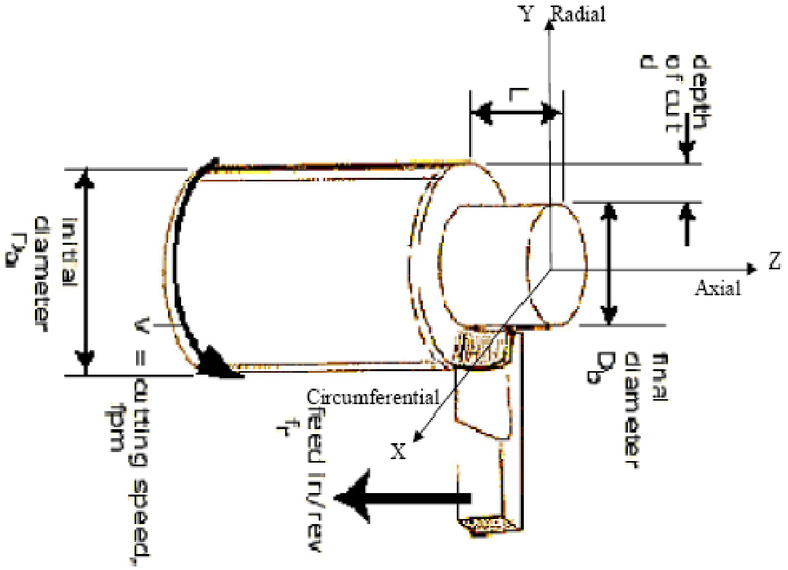

Figure 6.1 Experimental setup

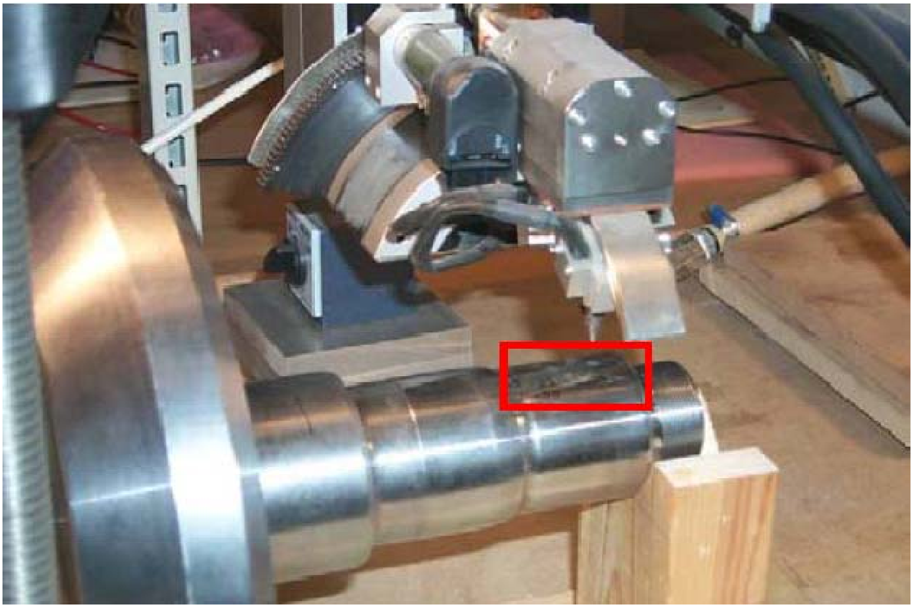

Figure 6.2 Set-up at residual stress measurements.

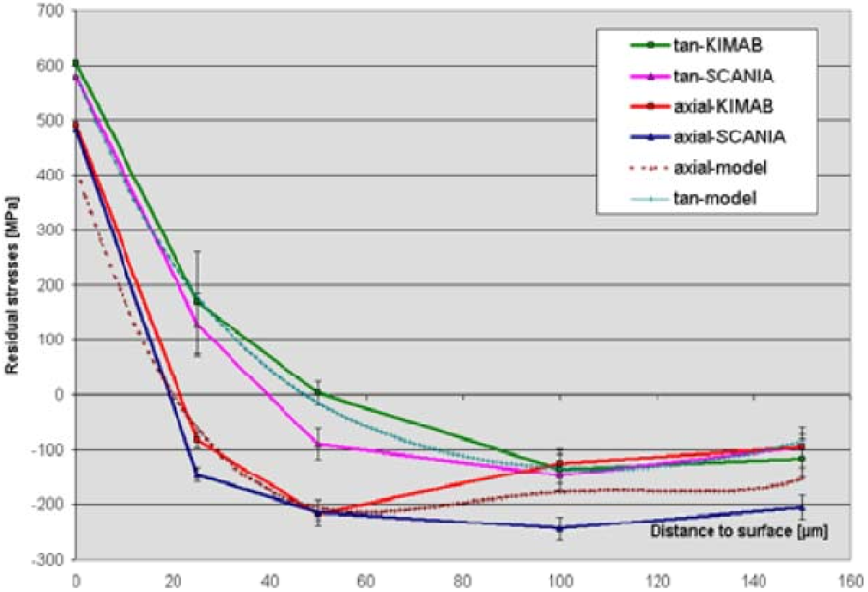

Figure 6.3 Comparison between residual stresses measured on bars in KIMAB lab and on production in SCANIA details.

Table 6.2 Results from orthogonal cutting tests

Vc m/min	f mm/r	t2 µm	Fc N	F_f N	Temp. max. °C	ϕ rad	Strain	Strain rate (Hz),10^5
400	0,2	420	1054	481	-	0,4606	0,6891	2,04
300	0,2	385	1028	522	844	0,5070	0,6425	1,56
200	0,2	510	1106	646	758	0,3898	0,7872	0,99
160	0,2	487	1147	715	745	0,4065	0,7605	0,80
120	0,2	580	1226	853	-	0,3335	0,9004	0,59
80	0,2	636	1193	796	-	0,3128	0,9536	0,39
40	0,2	405	1114	633	-	0,4778	0,6704	0,21
200	0,1	267	650	478	689	0,3738	0,8156	1,98
200	0,3	618	1554	795	>900	0,4664	0,6826	0,68

Rake angle α=6°, w (mm)=3 för alla

Since the main aim of this project work is to verify the residual stress in the finish work piece,The special care has been taken to measure those stress both experimentally and in simulation.

In the table-6.2 experimentally measured value of residual stress in both tangential and axial direction is given.at speed of 260 m/min and at different depth of cut. The Table 6.3 consists of experimental cutting condition performed at Swerea KIMAB lab, on three bars. Each bar is termed with English alphabets and followed by number e.g A1,A3,B2,B4,C1,C4.The numbers following the alphabet stands for the surface number where measurement has been taken off.The residual stresses has been measured upto 150µm depth in axial (sig ax) and circumferential (sig cir) direction for different ‘feed’ (f) rate and ‘ap’.The measured results and corresponding errors are presented in the Table 6.4, 6.5, 6.6, 6.7, 6.8, 6.9 respectively.

Table 6.3 experimental result for three different cutting depth in KIMAB

name	bar	surface no	f mm/rev	ap(t) mm	passes
A1	A	1	0,2	0,5	1
A3	A	3	0,8	0,5	1
B4	B	4	0,45	0,95	1
B2	B	2	0,2	2	1
C1	C	1	0,8	2	1
C3	C	3	0,45	0,95	1

Table 6.4 Bar’A1’ experimental result for three different cutting depth in KIMAB

Depth	sig ax	sig circ	err ax	err circ
0	337	538	23,1	51,5
25	-207	79	30,5	31
50	-254,3	-113,1	9,8	31,9
100	-186,6	-228,5	25,5	50,1
150	-103,5	-101,6	46,6	33,7

Table 6.5 Bar'A3' experimental result for three different cutting depth in KIMAB

Depth	sig ax	sig circ	err ax	err circ
0	451,6	643,1	50,7	63,2
25	62,4	311,1	13,1	19,5
50	-148,3	40,5	20,9	17,1
100	-236,8	-121,7	19,2	29,2
150	-154,6	-79,8	26,7	33,7

Table 6.6 Bar'B4' experimental result for three different cutting depth in KIMAB

Depth	sig ax	sig circ	err ax	err circ
0	491,2	624,1	14,1	81,1
25	-43,5	175,2	12	19
50	-133,4	92	13,6	23,3
100	-159,2	-79,2	26,7	20,1
150	-232	-68,4	35,3	39,6

Table 6.7 Bar'B2' experimental result for three different cutting depth in KIMAB

Depth	sig ax	sig circ	err ax	err circ
0	278,7	492,3	6	58,5
25	-259,3	21,3	26,2	23,6
50	-263,4	-130,9	47,3	44,6
100	-223,9	-200,6	56,3	32,2
150	-155,3	-60	50,5	47,1

Table 6.8 Bar'C1' experimental result for three different cutting depth in KIMAB

Depth	sig ax	sig circ	err ax	err circ
0	313,8	514,4	38,9	105
25	-82,3	172,6	17,5	24,3
50	-213,2	-20,2	3,5	13,7
100	-253,8	-91,9	7,4	33,8
150	-277,4	-77,1	17	24,9

Table 6.9 Bar'C3' experimental result for three different cutting depth in KIMAB

Depth	sig ax	sig circ	err ax	err circ
0	491,3	604	13,7	92,6
25	-82,9	169	24,4	21,8
50	-216,4	3,2	26,2	28
100	-125,5	-135,2	36	34,3
150	-95,9	-116,4	61,1	84,2

7. Simulation Results and Discussion

FEM simulation has been conducted for Test-1 to Test-10 under the orthogonal machining condition Table 6.2, by utilizing the proposed ALE with pure Lagrangian boundaries scheme and

- Residual stress
- Equivalent Plain strain rate
- Shear Angle
- Tool Forces

are measured for the different cutting condition. Then this simulation date is compared with experimental data to validate the proposed FEM model.

7.1 Residual Stress

The machining operation generates large amounts of residual stress, called induced residual stress in the surface layer of the finished work piece component. These unwanted stresses are totally governed by the different cutting parameter during machining process. The residual stress on the machined surface is an important factor in determining the performance and fatigue strength of the work piece. Therefore, it is important to understand and control the residual stress state in the machined part so that undesired failure can be avoided.

In the past few years this has been a very interesting research issue A combined numerical/experimental study of the behavior of different cutting parameters on cutting forces and residual stresses was undertaken by many of the researchers, Kalhori (2001) [8],C.Shet and X.Deng(2002)[9],Özel and Zeren(1998)[16].But all the studies not focusing on the same approaches ′,they differs by lot of different aspect of orthogonal machining and judging the resulting parameters. These studies used ALE-algorithm with predefined chip geometry to simulate the machining operation but this study the concept of predefined chip geometry has been dropped to simulate the model in a more realistic way.

Measurements in the cutting zone are particularly difficult to perform due to the hostile environment. Several laboratory experiments were performed in order to simulate different cutting conditions frequently encountered in practice. The experimental condition and result are given in the Table-6.3, 6.4, 6.5, 6.6, 6.7, 6.8, 6.9.

7.1.1 Comparison between Experimental Measurements and Simulation Result

As evidence of the ability of the simulation procedure to model residual stresses in machined parts, a comparison is made between finite element predictions in this study and experimental results available in the literature (Table 6.4, 6.5, 6.6, 6.7, 6.8, 6.9). In the finite element simulation, the work piece is made of 20NiCrMo5 steel and has an in plane dimension of 5 mm by 2 mm. The tool rake angle is 6°, the velocity of cutting is 260 m/min, and the different depth of cut is 0.2 mm,0.45mm,0.8mm. A mesh containing 41740 nodes and 41503 linear quadrilateral elements of type CPE4RT plane strain elements is used. The simulation the steady state was first reached after a cut of only 2–3 mm. To make sure a full steady state is developed, the simulation is continued until a cut of 4–5 mm is completed.

To collect the data from simulation, residual stresses value in axial(zz) and circumferential (xx) measured at three different points(P-1,P-2,P-3) along the depth from the surface a upto 210μm.further the three measured values are averaged. The main reason to adopt this measurement technique is to co-relate the simulation measurement with experimental measurement. During experimental measurements residual stress values are collected by averaging the measured values at three points for three different cases.

Also residual stress measured at the *integration point* along the path at steady state. The whole scheme is given in the Figure 7.1

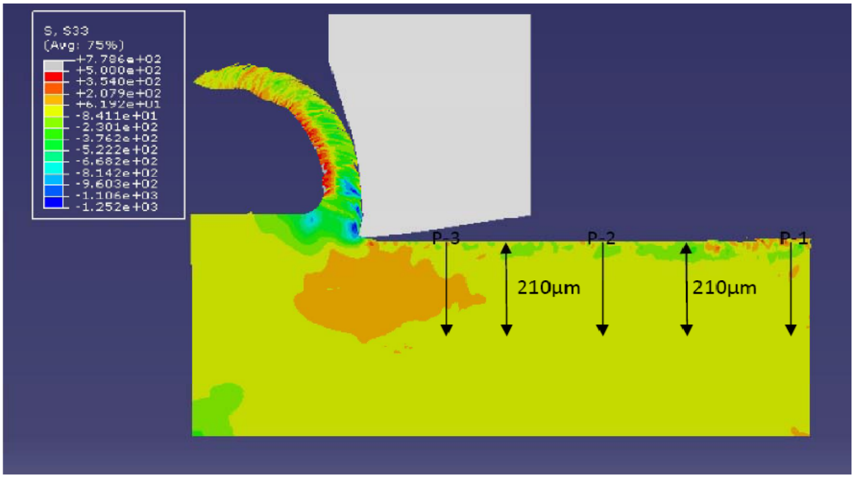

Figure 7.1 The measurement technique of simulated residual stresses

In the Figure 7.2a,Figure 7.3a and Figure 7.4a the measured and simulated residual stress in the axial direction(σ_{zz}) are compared for the depth of cut 0.2mm,0.45mm,0.8mm respectively. Similarly in the Figure 7.5a, Figure 7.6a and Figure 7.6a the measured and simulated residual stress in the circumferential direction(σ_{xx}) are compared for the depth of cut 0.2mm,0.45mm,0.8mm respectively. The *Table7.1* below shows the Cutting parameters used in simulation for 2D case.

Table7.1 Cutting parameters used in experiments and simulation

case	Cutting Speed(m/min)	Rake Angle(degree)	Depth of cut (in mm)
1	260	+6	0.20
2	260	+6	0.45
3	260	+6	0.80

Note:In the 2D case ‘f’ stands for cutting depth or uncut chip thickness,instead of feed rate
As in 3D case, because it not possible to include the feed rate in 2D.

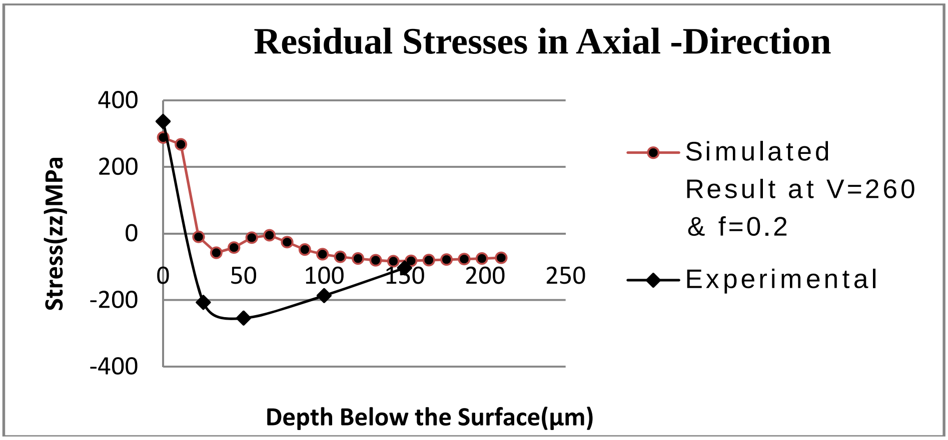

Figure 7.2a The measured and simulated residual stress in axial direction for the depth of cut 0.2mm

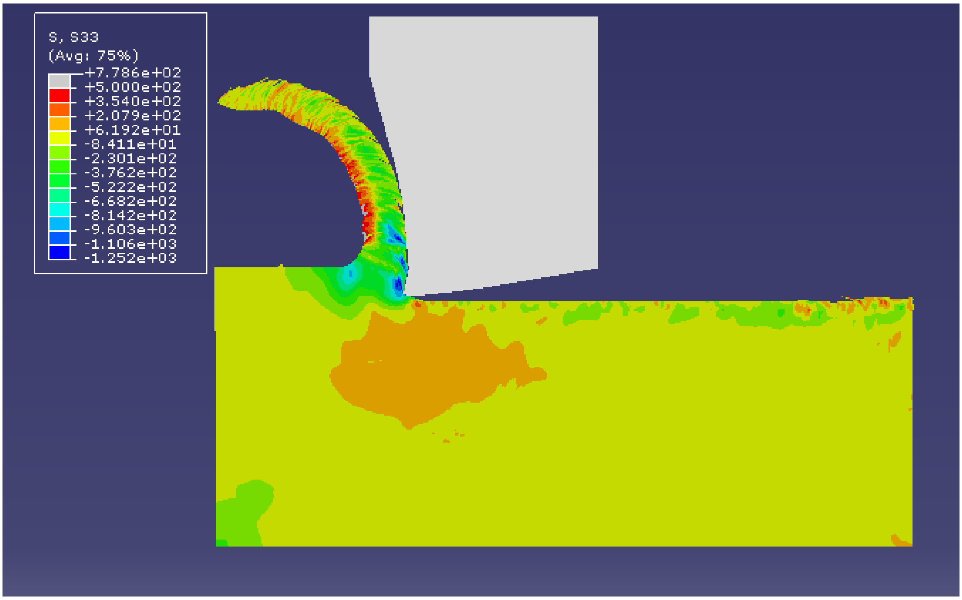

Figure 7.2b Simulated residual stress in axial direction for the depth of cut 0.2mm after steady state condition

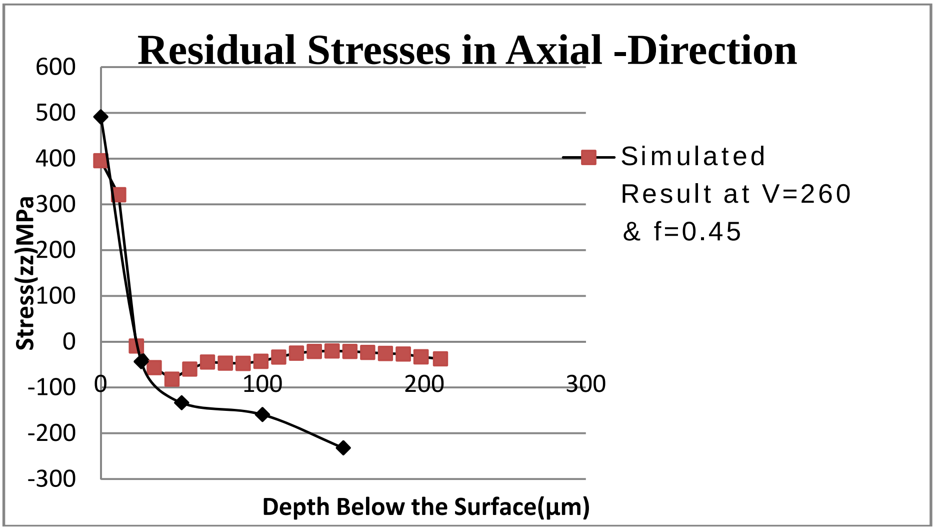

Figure 7.3a The measured and simulated residual stress in axial direction for the depth of cut 0.45mm

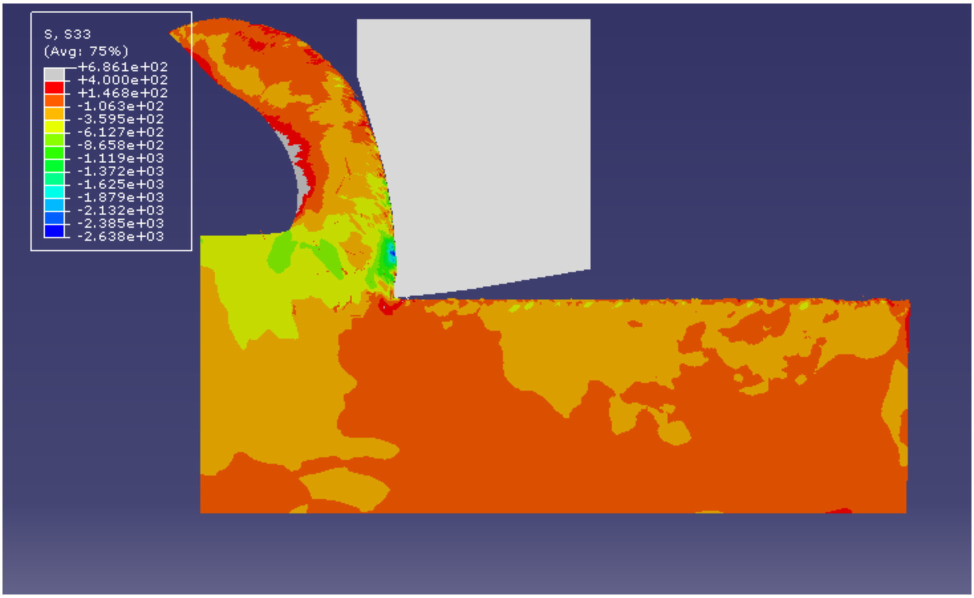

Figure 7.3b Simulated residual stress in axial direction for the depth of cut 0.45mm after steady state condition

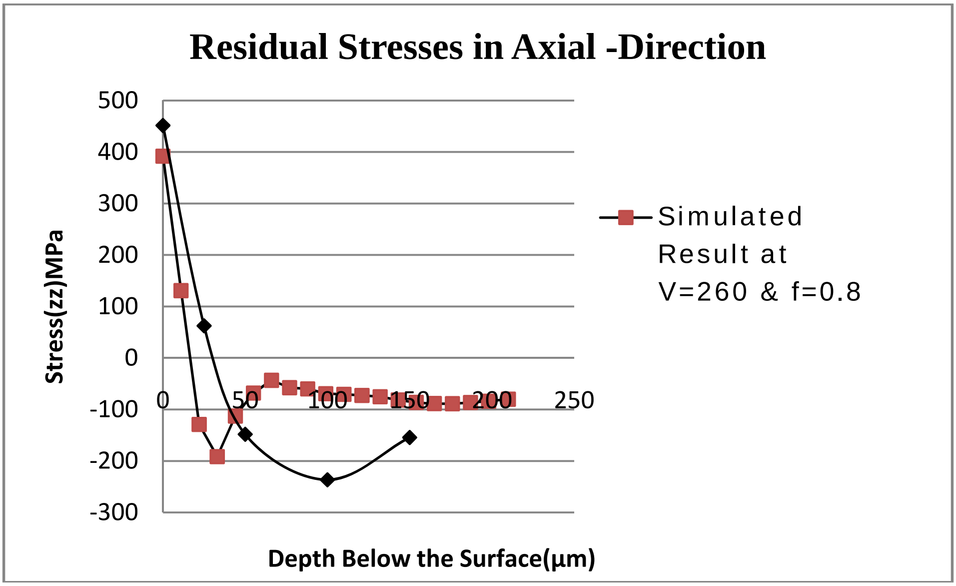

Figure 7.4a The measured and simulated residual stress in axial direction for the depth of cut 0.8mm

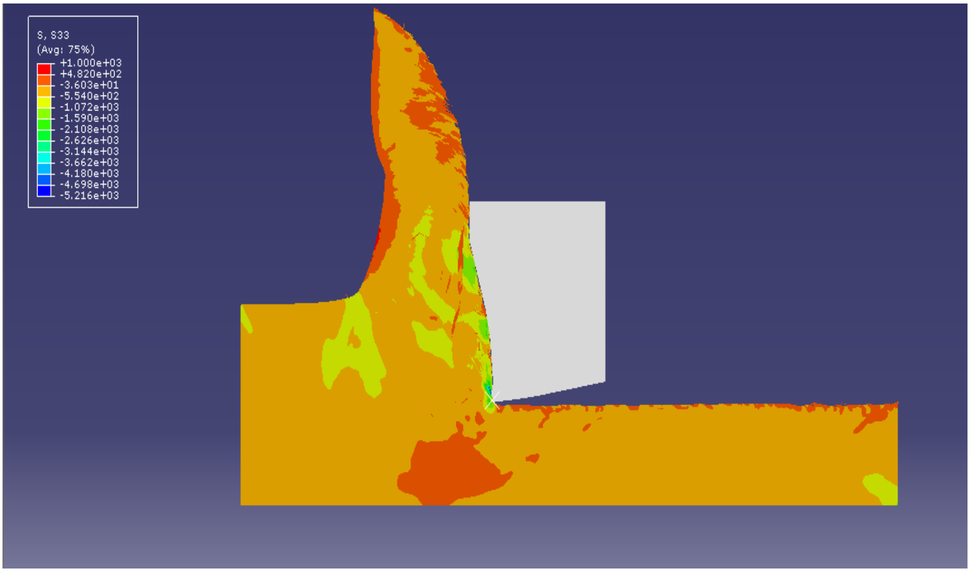

Figure 7.4b Simulated residual stress in axial direction for the depth of cut 0.8mm after steady state condition

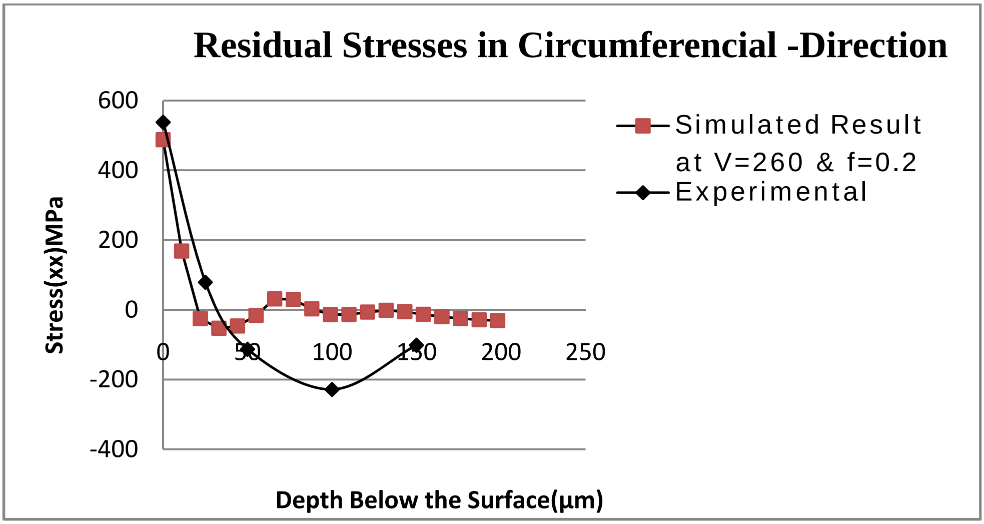

Figure 7.5a The measured and simulated residual stress in circumferential direction for the depth of cut 0.2mm

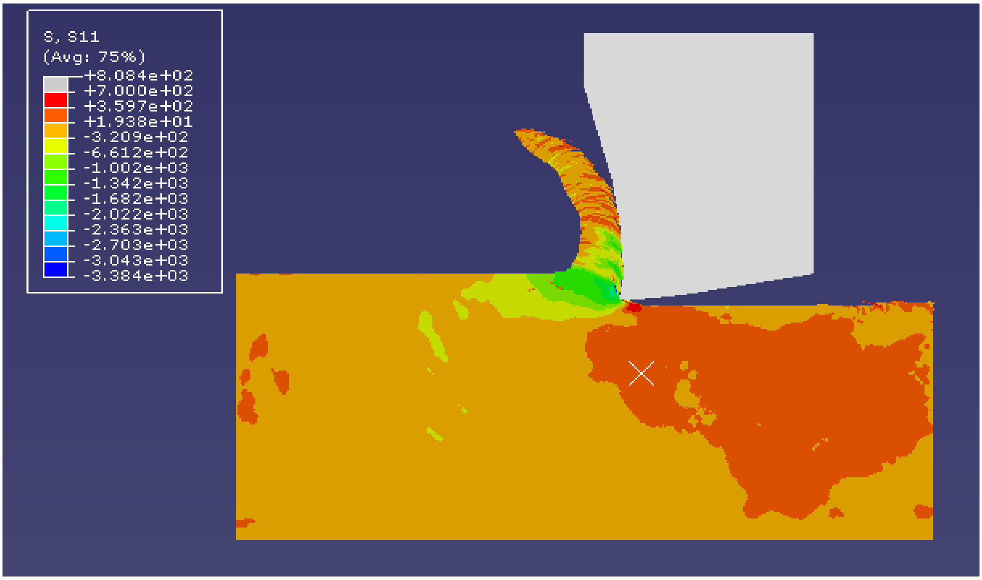

Figure 7.5b Simulated residual stress in circumferential direction for the depth of cut 0.2mm

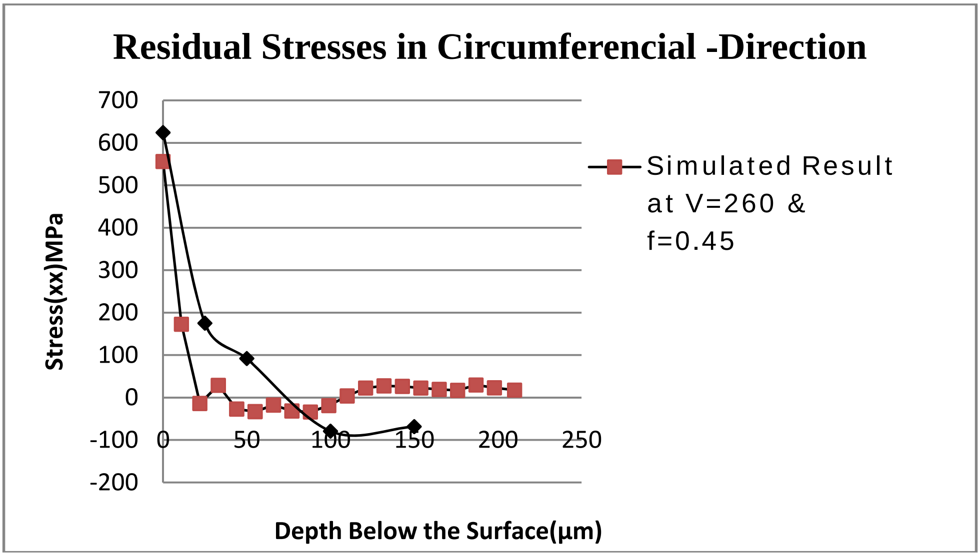

Figure 7.6a The measured and simulated residual stress in circumferential direction for the depth of cut 0.45mm

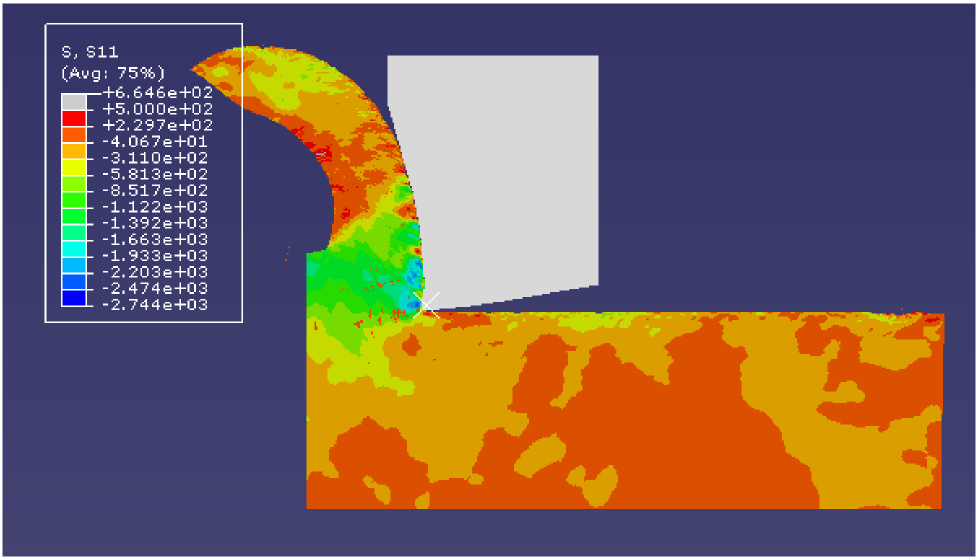

Figure 7.6b Simulated residual stress in circumferential direction for the depth of cut 0.45mm

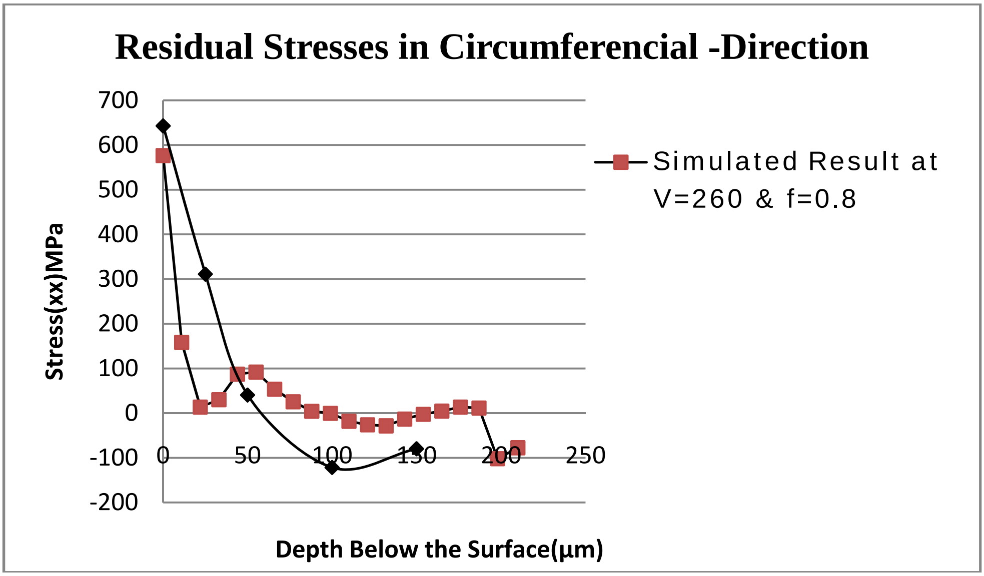

Figure 7.7a The measured and simulated residual stress in circumferential direction for the depth of cut 0.8mm

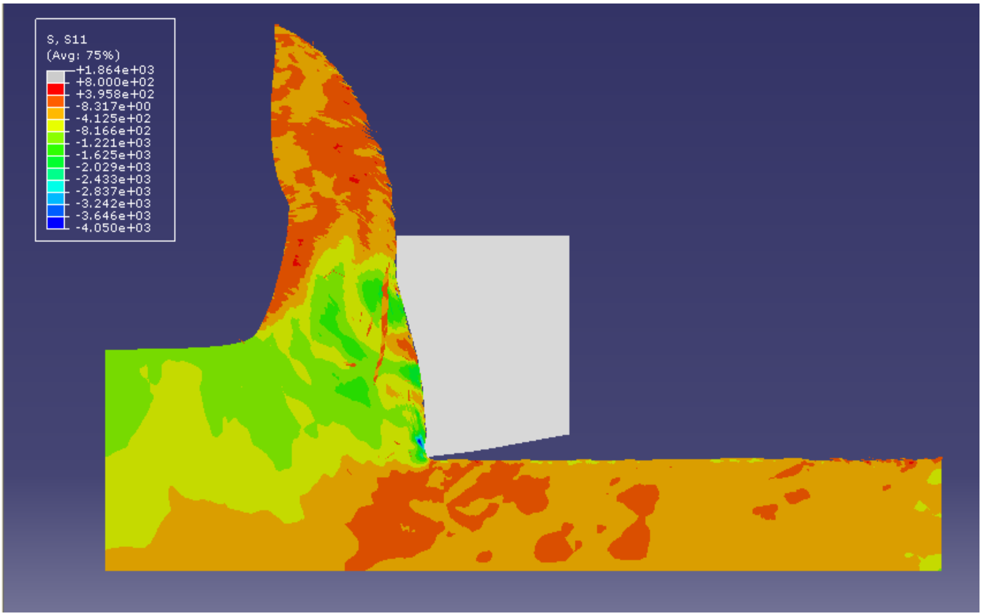

Figure 7.7b Simulated residual stress in circumferential direction for the depth of cut 0.8mm

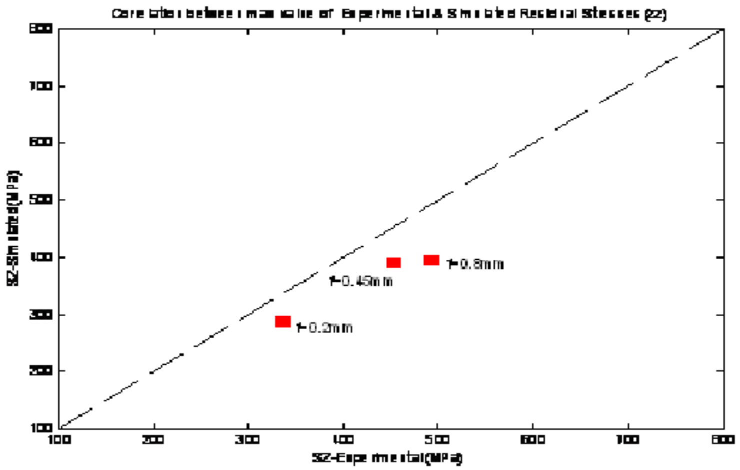

Figure 7.8a Correlation between Experimental and simulated value of max S(zz) at different 'f'

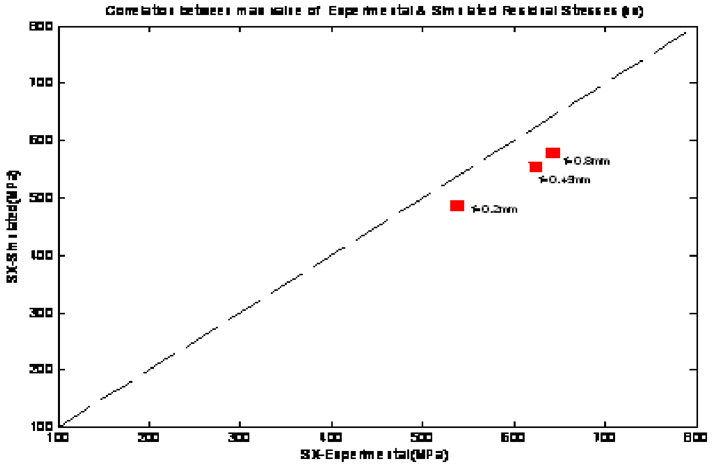

Figure 7.8b Correlation between Experimental and simulated value of max S(xx) at different 'f'

Table 7.2 % error in measured and simulated max-value S(zz) & S(xx) at different depth of cut(f)

Depth of cut (f) in mm	**% error for S(zz) axial**	**% error for S(xx) circumferential**
0.2 mm	14.4214	9.4796
0.45 mm	19.4908	10.8974
0.8 mm	13.3893	10.3421

Note:In the 2D case 'f' stands for the depth of cut.

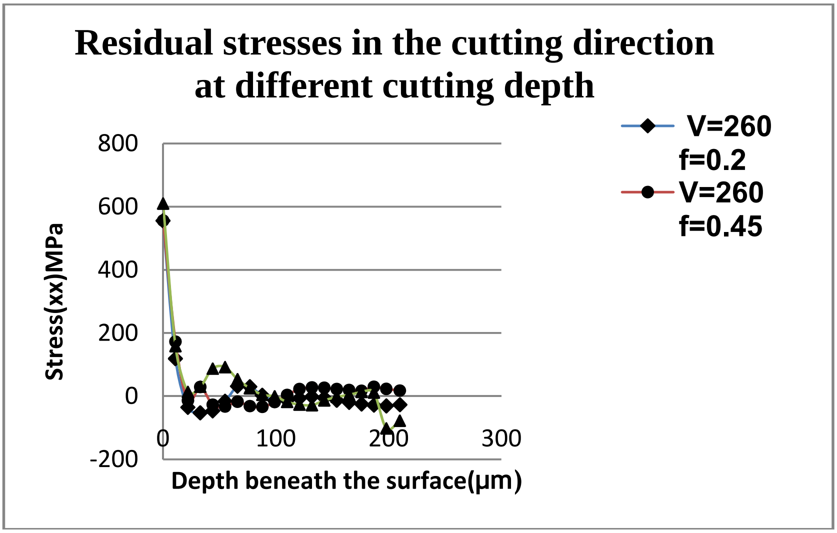

Figure7.9 Simulated residual stress in the circumferential direction at different depth of cut

7.1.2 Comments on the Result

Residual stresses in the work piece are caused by incompatible plastic strains between different layers of materials below the finished surface[8]. Because of the shearing action of the cutting tool in the cutting direction on the material layers below the cut plane, it is expected that plastic incompatibility will be most severe in the cutting direction[7,8,39].
The fields of the predicted von Mises, the stress components σ11 and σ33 represent the residual stress fields on the machined surface given in the Figure 7.2-to-Figure 7.7. From the simulation results it was observed that there exists a region of very high deformation rate as well as very high stress zone around the round edge of the cutting tool. It can also be observed from the simulation and the experimental value of σ11 and σ33 that machined induced residual stress also increases due to increase the cutting depth called feed rate of cutting, but the increments in not very much it’s difference is less than 200 MPa the Figure 7.9 shows the comparative view of the residual stress in the cutting direction, it can be observed in the Figure 7.9 the depth of cut doesn’t affect the residual stress a lot.

In the comparative study between simulated result and the experimental result Figure 7.8a, 7.8b with help of correlation between the max-values of S(zz) and S(xx), we can also observed that the both simulated and experimental result are very close to each other at the surface which is more clear from their percentage error given in the *Table7.2*.

In the Figure 7.2 to Figure 7.7, as we go down in the prescribed path line beneath the machined surface there is significant difference between simulation results and experimental results , the reason for the this corollary situation is that it is very difficult to measure experimentally the accurate von Mises stress components σ11 and σ33 as the depth increase from the surface in the hostile lab environment, another reason it is very complex to consider all the thermo-mechanical physical phenomena in the FEM model with their accurately measured values, also the Software limitation might be a possible reason for that.

More the simulated results are significantly differs from experimental result if we go deep in from the surface, the main reason for this corollary is the measurement error between 40% to 50% [Table 6.4 to 6.9] in the physical experiment because it’s very difficult to measure residual stress accurately for the very deep in the material, that why we can’t say that the simulated results are not correct is this regard.

In summary, these stress field predictions can be combined with the temperature field prediction(is presented in the next section) and fed into surface property models that are highly essential to further predict surface integrity and thermo-mechanical deformation related property alteration on the microstructure of the machined surfaces. Today, most of the surface properties models are empirical and still not sufficient to determine the full surface morphology induced by the machining especially finish machining where most of the machining is done with the edge geometry of the cutting tool.

7.2 Temperature Field Influence

During the orthogonal matching at very high speed large amount of heat is generated due to large deformation and tool-chip friction. The heat generated at the shear zone conducted in the tool, Chip and the work material. The radiation to the ambient is also allowed. The temperature field distribution is measured close to the tool nose in the same prescribed path for three different cutting depths beneath the machined surface presented in the Figure 7.10.But if we measure the temperature far from the tool nose during cutting it will be very less temperature at the surface ranging between 50-70◦c due to radiation of heat from the exposed surface.

7.2.1 Comments on the Result

We can observed from the above Figure 7.10 the surface temperature decrease slightly with increase of the depth of cut, this is due to conduction of generated heat in the different chip thickness means large chip thickness absorbers more heat than small chip thickness which makes less available heat to raise the temperature of the machined surface.

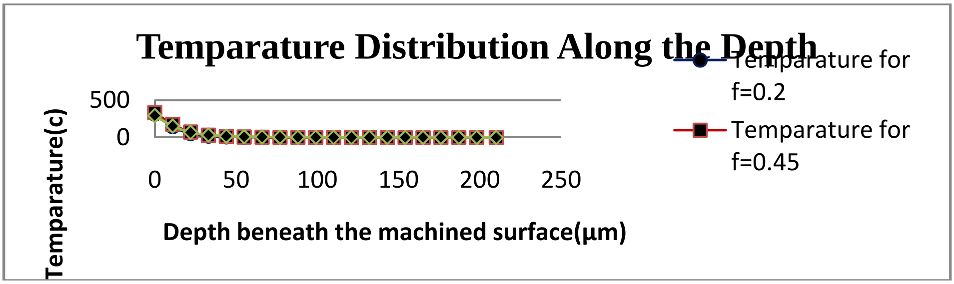

Figure 7.10 Temperature field Distribution beneath the machined surface for three different cutting depths.

7.3 Strain Rate

This is the strain in the unit time, it has a significant impact on the stress field beneath the machined surface, tensile and yield strength of the material increase with increase the strain rate, subsequently material behaves more elastic. The average strain rate in the primary shear zone is measured and presented in the Figure 7.11a for the three different cutting depths,at the cutting speed V=260m/mim.The strain rates are measured and averaged along the path AB in the Figure 7.11b

7.3.1 Comments on the Result

Strain rate in the primary shear zone increase with the increase of depth of cut, and its value is very high for the cutting depth 0.8.Increasing value of strain rate with increase of depth of cut can theoretically understood.The plastic strain ε and shear angle Φ for the continuous and homogeneous chip formation cutting process is related by the equation.(7.1).[40]

$$\varepsilon = \frac{\tan(\emptyset) + \cot(\emptyset)}{\sqrt{3}} \tag{7.1}$$

The strain rate $\dot{\varepsilon}$ can be obtained by integrating the equation (7.1) with respected to *time* and given by equation (7.2).

$$\dot{\varepsilon} = \frac{\sec^2(\emptyset) - \operatorname{cosec}^2(\emptyset)}{\sqrt{3}} \tag{7.2}$$

Now due to increase of depth of cut primary width of primary deformation zone increase and shear angle Φ decreases, consequently numerator of equ (7.2) increase so as the strain rate $\dot{\varepsilon}$ with increase of depth of cut. Also work-hardening in primary deformation zone increase with increase of depth of cut because rise of temperature in this zone is less for larger chip thickness. Temperature generates due to friction is distributed in larger surface area of chip.Increase the strength of material in the primary shear zone which further influences the machined induced stress in work material. In conclusion strain rate us one of the factor for increasing the residual stress field beneath the machined surface due to increase the cutting depth.

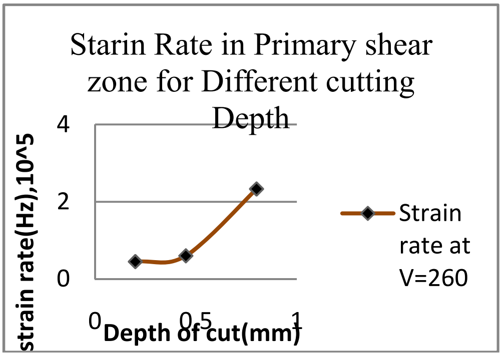

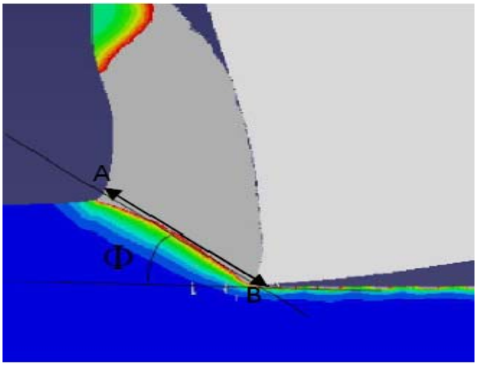

Figure 7.11a Average Strain rate in the primary shear zone for three cutting depths

Figure 7.11b Simulation model of the stain rate measurement.

7.4 Shear Angle

The shear angle of the primary deformation zone has been measured geometrically from the simulation model presented in the Figure 7.12a,b,c,d shows the change of shear angle due to increase the depth of cut.

7.4.1 Comments on the Result

The shear angle in the primary deformation zone decreases proportionally due to increase of cutting depth. Increasing cutting depth we increase the strain rate in this region which in turn reduces the shear angle,trend in change in shera angle is given in the Figure 7.13.

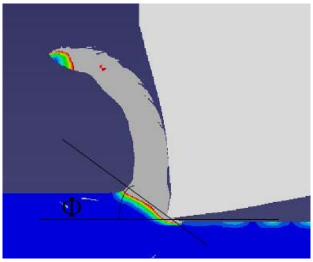

Figure 7.12a f=0.2

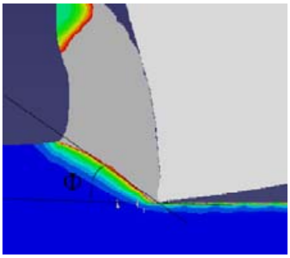

Figure 7.12b f=0.45

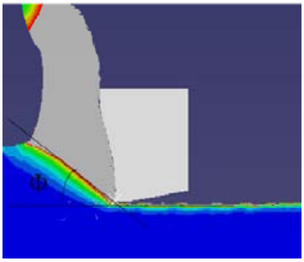

Figure 7.12c f=0.8

Table 7.3 Simulated measured Values of shear Angle

Cutting depth f in mm	Shear Angle Φ(degree)
0.20	41.4
0.45	37.8
0.80	38.2

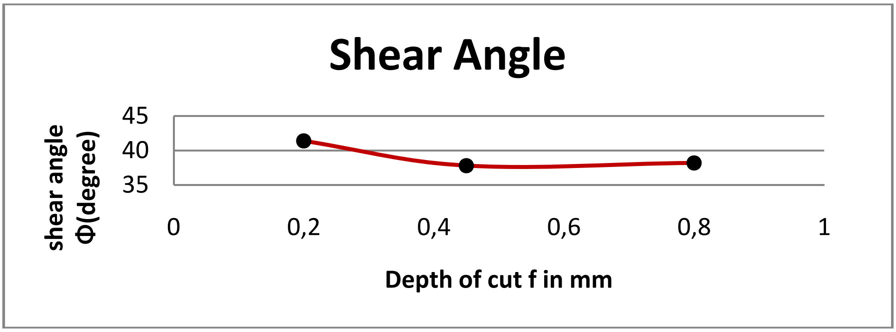

Figure 7.13d Change of Sheare angle at different cutting depth.

7.5 Cutting Forces

The cutting forces on the tool are also calculated from the simulation model for the three different cutting depth has been presented in the Figure 7.14.

7.5.1 Comments on the Result

The magnitude of cutting forces in the cutting direction increases with increase of the depth cut, but if we observed the Figure7.14 the forces in the all depth of cut follows a trend, the oscillation occurs due to remeshing [40] due to continues chip formation the oscillation un the force remains consistence within a certain limits and the mean value remains constant at any time instance, but large fluctuation can be observed in the segmented chip formation process, mean forces value goes very low where chip breaks.

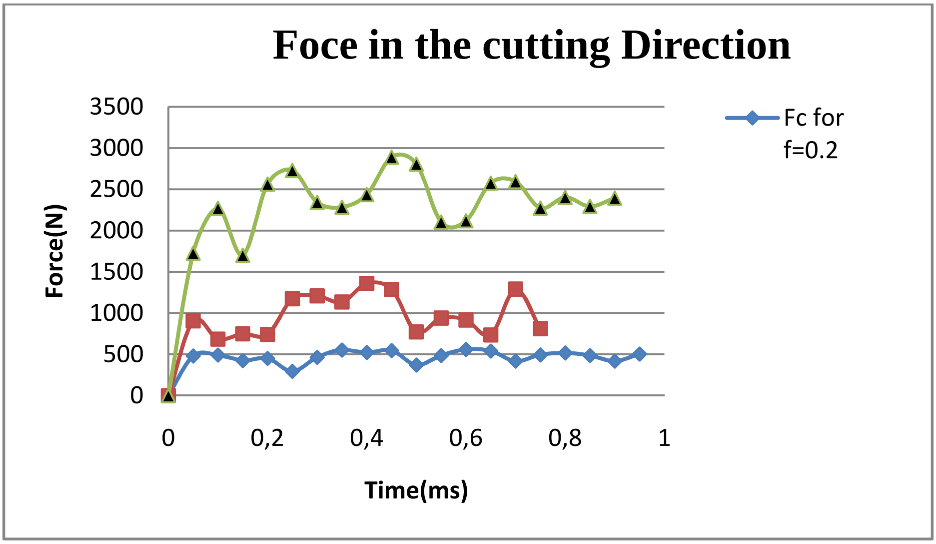

Figure 7.14 Tool magnitudes of the tool forces in the cutting direction for the different depth of cut

7.6 Influence of Mesh Density

From the modeling point of view it very essential to decide suitable mesh density, because it has large impact on the result's accuracy and simulation time. The change of result accuracy with change of mesh density is given in the Figure 7.15 below.Also the mesh density effects the chip thickness of the in the model. Coarse mesh gives very uneven chips. Also the thickness reduces. This can be notice in the Figure 7.16. So it is very important to choose right mesh density to get the reasonable chip thickness. The qualitative description of mesh is given in the Table 7.4.Also percentage error with respect to experimental result of surface residual stresses for each kind of mesh is given in the last column of Table 7.4.

Table 7.4 Meshing description

Mesh Type	Element type	No.of elements	Avg.Element size (mm)	Shortest element(mm)	% error (exp vs Sim)
Coarse	4-node quad(CPE4RT)	6079	0.035	0.017	34.7
Semi-coarse	4-node quad(CPE4RT)	13428	0.023	0.009	23.7
Fine	4-node quad(CPE4RT)	41245	0.012	0.0045	13.2

7.6.1 Comments on the Result

It is cleared from the above comparison that when we proceed from coarse mesh to dense or fine mesh accuracy of the results increase, but during simulation it's also observed that after certain mesh density value accuracy changes very less but due to high mesh density calculation time increase very much so to make the model economical from the calculation point of view I have used the optimal mesh density and meshed the model with fine mesh. Also more coarse mesh have continuous chip formation problem and its geometry is no longer smooth.

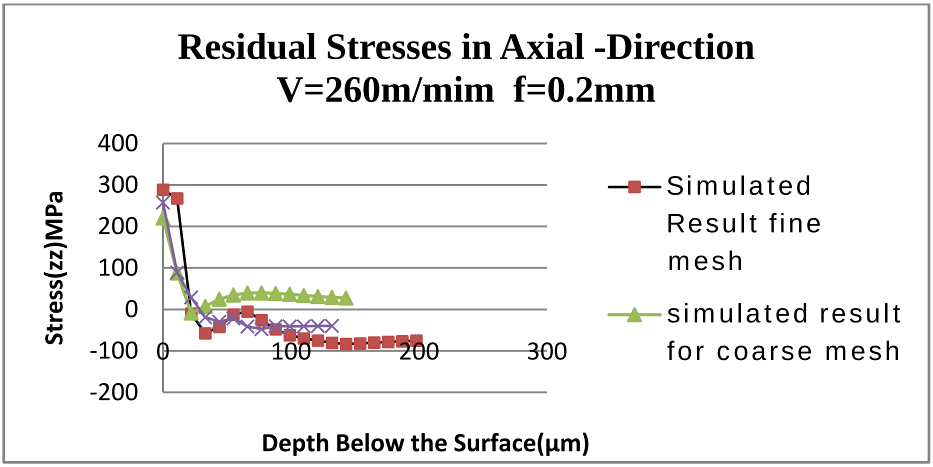

Figure 7.15 Change of result Accuracy due to change of mesh density for the residual stress in Axial-direction for V=260m/min and f=0.2.

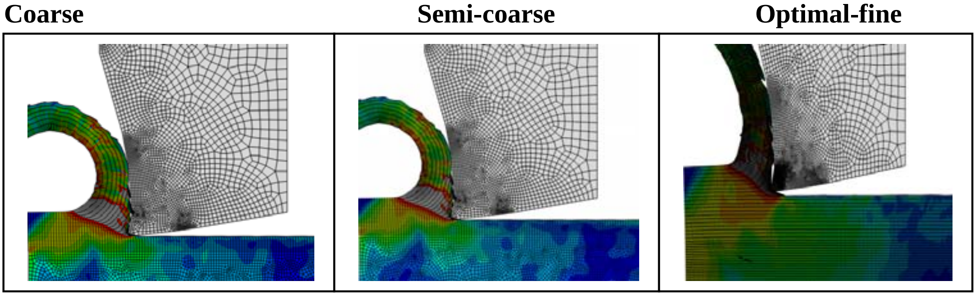

Figure 7.16 change in chip thickness due to change in mesh density

7.7 Chip Thickness

The simulated and the experimental measured value of chip thickness has been presented in this section. The dimension (thickness) of the actual chip is measured and the dimension of the simulated chip is measured in the deformed co-ordinate Figure 7.17

7.7.1 Comment on the Result

The measured value of chip thickness and the simulated chip thickness value are given the table 7.5, due to uneven shape of the chip for the depth 0.80 mm average value is taken in that case.

Table-7.5 Measured and simulated chip thickness

Comparison of Chip thickness for V=260 for different feed ‘f’		
Feed in mm	Feed in mm	Feed in mm
f = 0.2	f = 0.2	f = 0.2
f = 0.45	f = 0.45	f = 0.45
f = 0.8	f = 0.8	f = 0.8

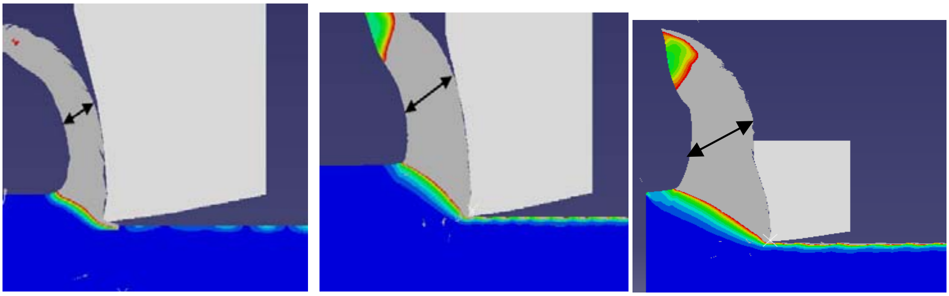

Chip thickness for f=0.2 Chip thickness for f=0.45 Chip thickness for f=0.8

Figure 7.17 Measurement of chip thickness in simulation

7.8 Influence of Cutting Speed (V)

The simulated value of the residual stress in beneath the machined surface in the circumferential direction σ_{xx} for the different cutting speed is presented in the Figure 7.18 below.

7.8.1 Comments on the Result

As we can see in the Figure 7.18 with increase in velocity machined induced residual stress in the circumferential direction increases. But due to the change in velocity don’t have any effects deeper in the finished material. The above trend of in change of residual stress due to change cutting velocity agrees with result obtain by J.C Outeiro,D.Umbrello R. M’Saoubi (2006) [41].

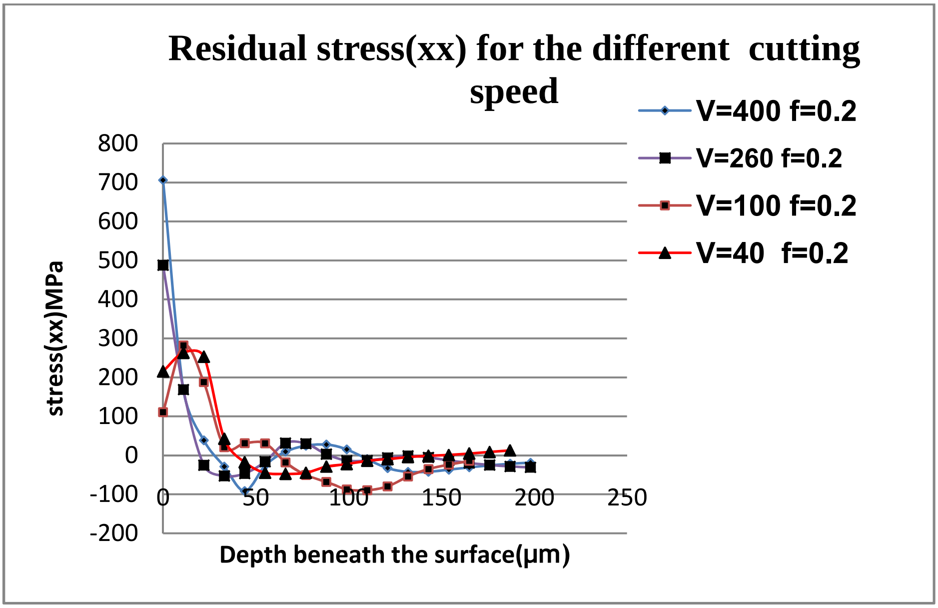

Figure 7.18 Residual stresses for the different cutting speed

7.9 Influence of Rake Angle

The simulated value for the residual stress in the cutting direction for the three rake angle -6, 0, +6 degree is presented in the Figure 7.19a,b .In all case cutting velocity was 260m/min and depth of cut was 0.2mm.

7.9.1 Comments on the result

If we change the value of rake angle from -6 degree to +6 degree the residual stresses value inside the material changes. when rake angle value approaches to –ve value compressive residual stresses dominate the stress domain [42].If we absorbed the Figure 7.19a we can see the change of residual stress within the 50µm region very significant and they varies form -20MPa to -390MPa.As a conclusion we can say a lager rake angle gives higher compressive stress as well as a deeper affected zone below the surface. With increased rake angles, the maximum stress position is moved further in to the material.

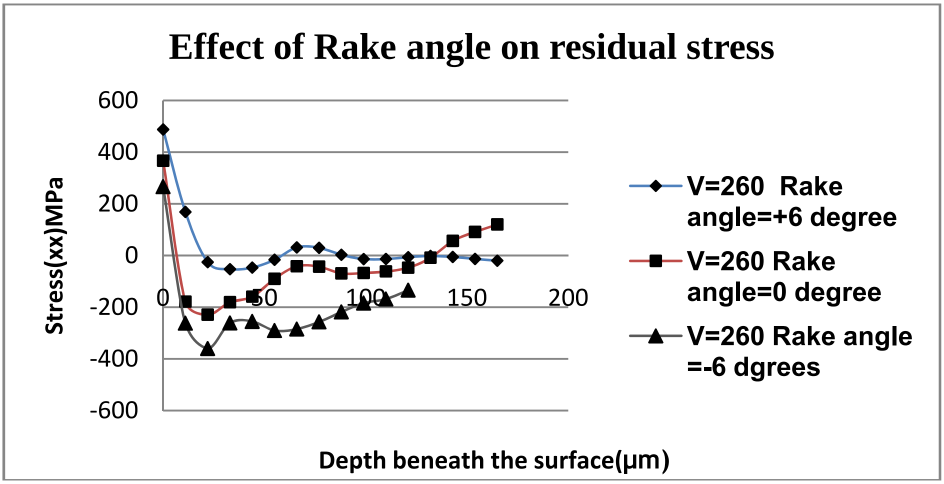

Figure 7.19a Influence of rake angle on the residual stress

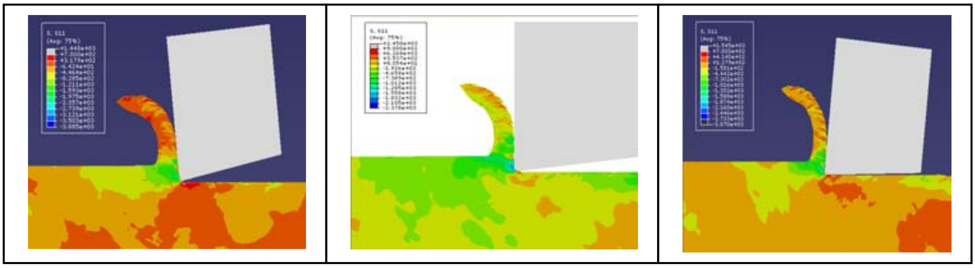

α= -6 degree α= 0 degree α= +6 degree

Figure 7.19b Influence of rake angle on the residual stress

7.10 Influence of Material Physical Property and Cutting Condition on Chip Geometry

It has been shown and proved experimentally and theoretically that not only cutting condition but material properties have large impact on the chip geometry. Using this 2D model it can be verify as well. Simulations are run for different cutting condition with changing the material physical property and resulting chip morphology is checked. The results are presented in the Figure 7.20a, b, c, d, e, and f, below and different effecting parameters in Table 7.6

7.10.1 Comments on the result

Fig 40a show the chip formation of the brittle material having ductile damage value 0.6 and very low cutting speed 24m/min, Figure 7.20b,c,d shows the chip formation of the ductile materials having ductile damage value 1.5 and cutting speed 260m/min,300m/min,400m/min respectively. The fig40e shows the chip formation of high conductive, ductile material with thermal conductivity value 47.7 W/m°C,sp-heat 556.8 J/kg/°C and cutting speed 260m/min.The Figure 7.20f shows the chip formation of high conductive ductile material with thermal conductivity 47.7 W/m°C,low sp-heat 55.6 J/kg/°C and cutting speed 300m/min. It is verified experimentally in lab.

Table-7.6

Figure	Cutting speed m/min	thermal conductivity J/kg/°C /m°C,	sp-heat J/kg/°C	ductile damage value
Figure-7.20a	24	47.7	556.8	0.6
Figure-7.20b	260	47.7	556.8	1.5
Figure-7.20c	300	47.7	556.8	1.5
Figure-7.20d	400	47.7	556.8	1.5
Figure-7.20e	260	47.7	556.8	1.5
Figure-7.20f	300	4.77	55.6	1.5

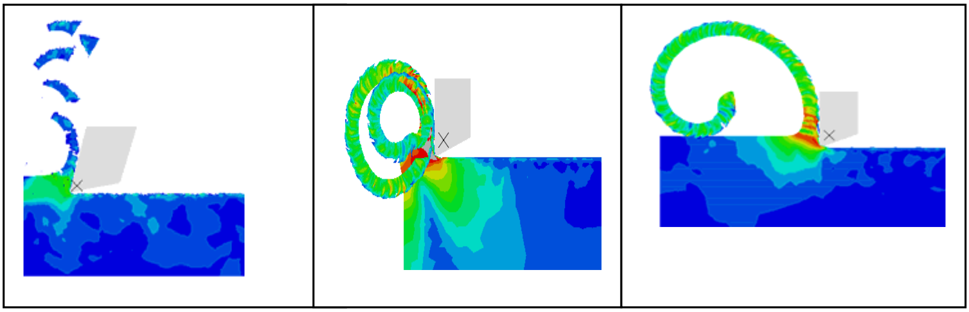

Fig7.20a Discontinuous chip   Fig7.20b Continuous curly chip
Fig7.20c Continuous semicircular chip

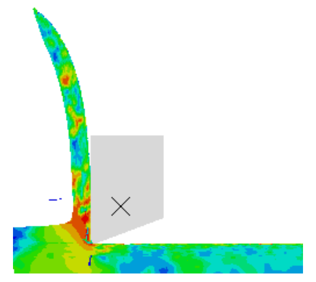

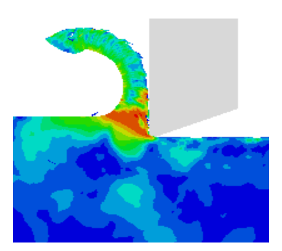

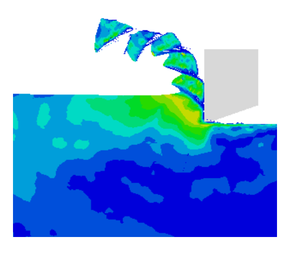

Fig7.20d Continuous straight Fig7.20e Continuous circular Fig7.20f Shear Localized Segmented chip

8. 3D Numerical model of Orthogonal cutting

So far we have been dealing with the 2D numerical model to simulate the residual stresses. But in reality most of the orthogonal cutting is done by the leading edge of tool. As show in the Figure 2.1.In orthogonal cutting motion of the moving material is perpendicular with the tool motion, so these two mutually perpendicular motions can't be implemented in the 2D model. In 2D model it is assumed that either tool is moving or work material is moving, but in orthogonal cutting both move relative to each other in the perpendicular direction. The detailed schematic orthogonal cutting give in the Figure 8.1 below

8.1 3D FE-Model and Boundary Condition of Orthogonal Cutting with Abaqus/Explicit

In this thesis work Abaqus/explicit a general-porpus FEM code have been used to create a 3D model to simulate the residual stresses the finite element model is given in the Figure 8.1

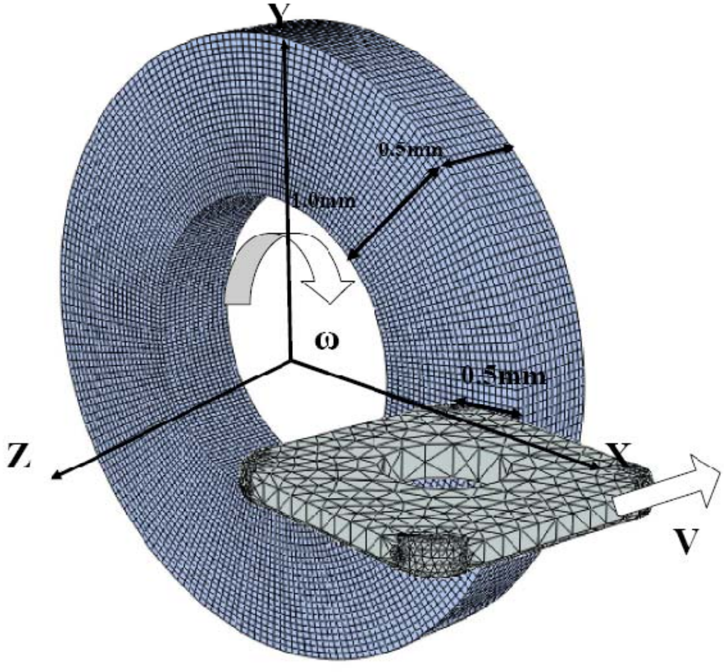

Figure 8.1 3D Finite element model of orthogonal cutting with ALE formulation and Pure Lagrangian boundary conditions

In the Figure 8.1 the dimension of work material in the y-direction is 1mm and in the z-direction is 0.5mm.Feed rate is V= 0.2mm/rev and the cutting depth is 0.5mm, angular velocity is ω=2167 rad/sec. Rounded edge tool is used for the cutting with edge radius R_{edge}=0.02mm and R_{nose} =1.2 mm.The tool is positioned with of clearance angle α=+6 degree and Rake angle γ=+6 degree. Tabulated data given in Table 8.1
The work piece is modeled with purely Lagrangian boundary condition

Table 8.1

Model	Cutting speed rad/sec	Feed mm/rev	Ap mm	Cutting depth mm	Tool R_{edge} mm	Tool R_{nose} mm	clearance angle α	Rake angle γ
3D-Fig8.1	2167	0.2	0.5	0.5	0.02	1.2	+6	+6

8.2 Element Type and Finite Element Meshing

The work material is discredited with 8 node hexahedron temperature-displacement coupled plain strain reduced integration type element. Whereas tool is descriptive with 6-node tetrahedron elements, just to improve the computational efficiency of the solver.

ALE adaptive meshing combined with pure Langrangian boundary condition is implemented to mesh the work material domain with 93251 finite elements.

8.3 Simulation and Result

Explicit dynamic temperature-displacement time integration scheme is used to simulate the model. Simulation is preformed for 1.2 ms.

The results from simulation are given in the Figure 8.2a to Fig 8.2d at different time intervals.

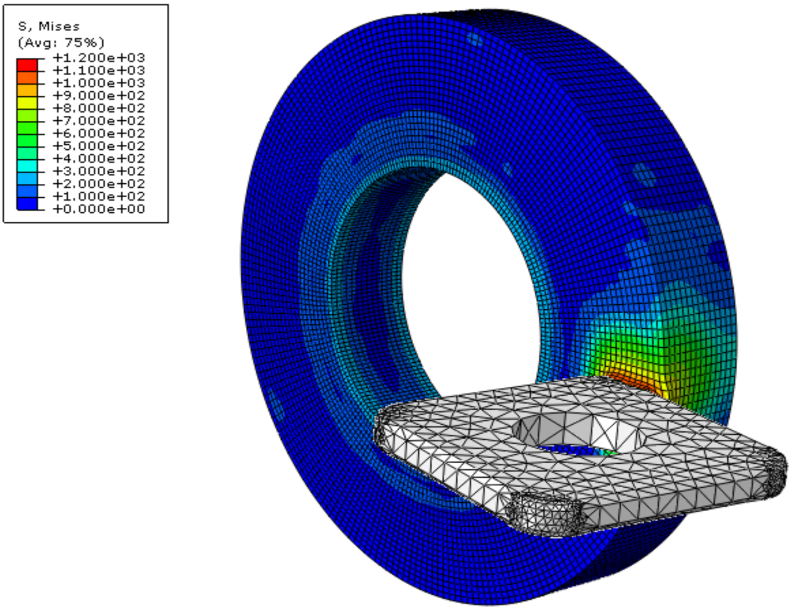

Figure 8.2a Simulation result after 0.2ms

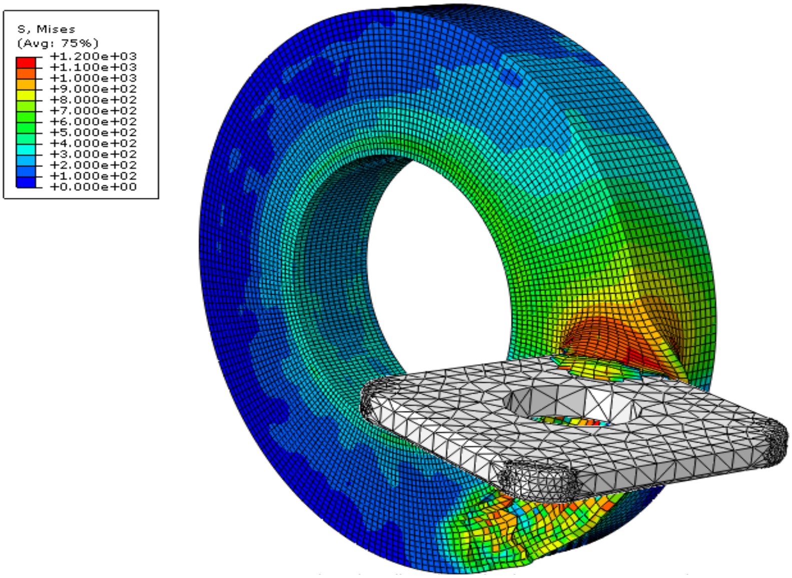

Figure 8.3b Simulation after 0.5 ms

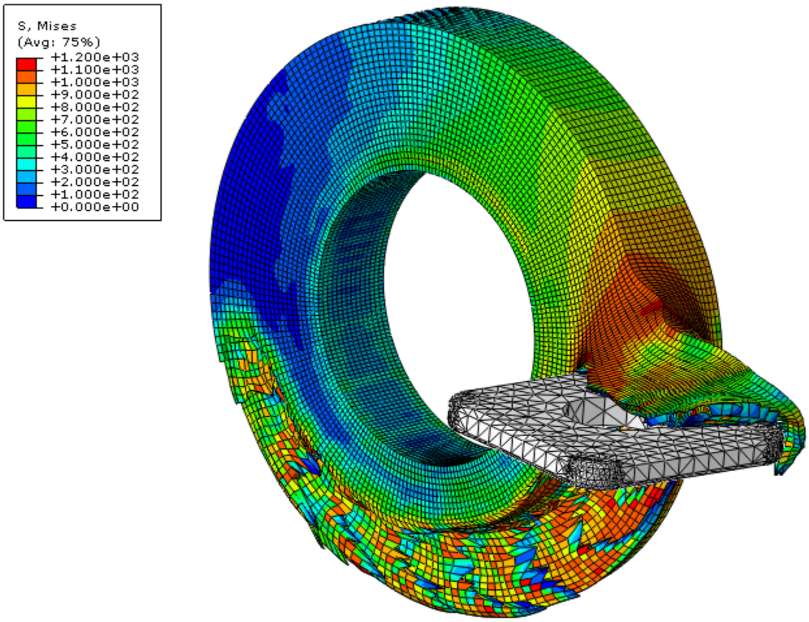

Figure 8.2c Simulation after 0.8 ms

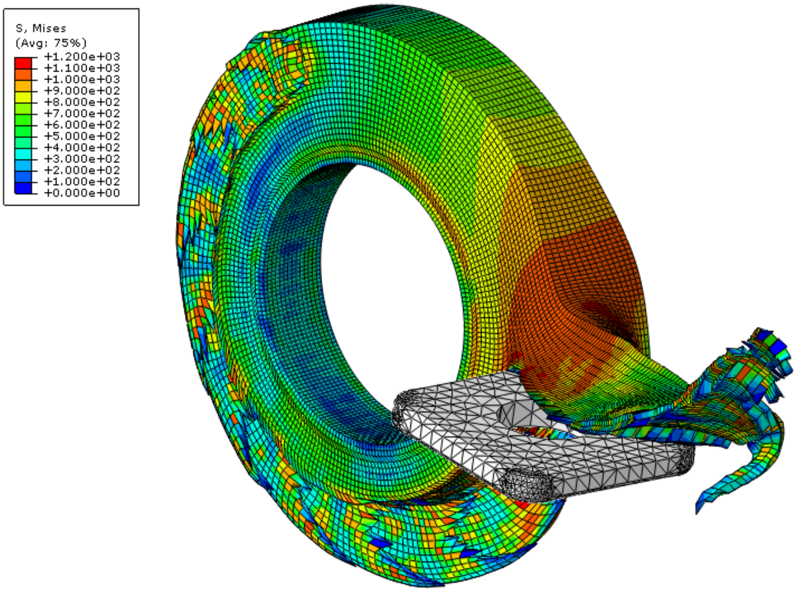

Figure 8.2d Simulation after 1.2 ms

To measure the residual stresses in the machined work piece, it is sectioned and then measurements are taken in the three different points according to the path shown in the Figure 8.3. The experimental result and the result form 3D-simulation are presented in the Figure 8.4a and Figure 8.4b for the stresses in the both axial and circumferential direction. The residual stress values have been collected along the path shown in the Figure 8.3 with arrow mark for each *integration* point. The measurements at three points along the machined surface (axially) have been averaged and presented in the Figure 8.4a and Figure 8.4b.

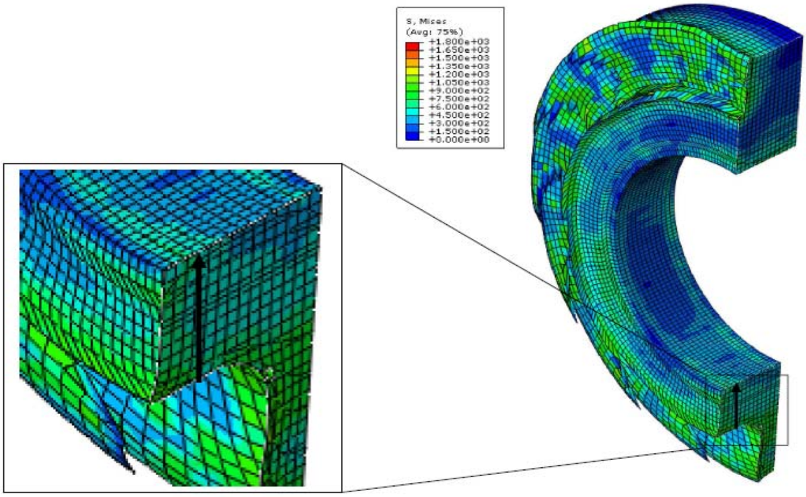

Figure 8.3 Measurements path in the machined work material.

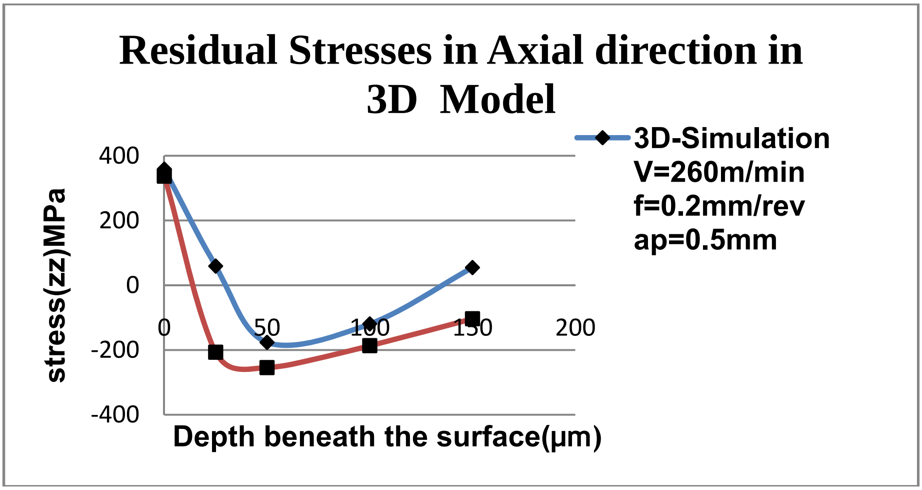

Figure 8.4a Residual stress in the axial direction

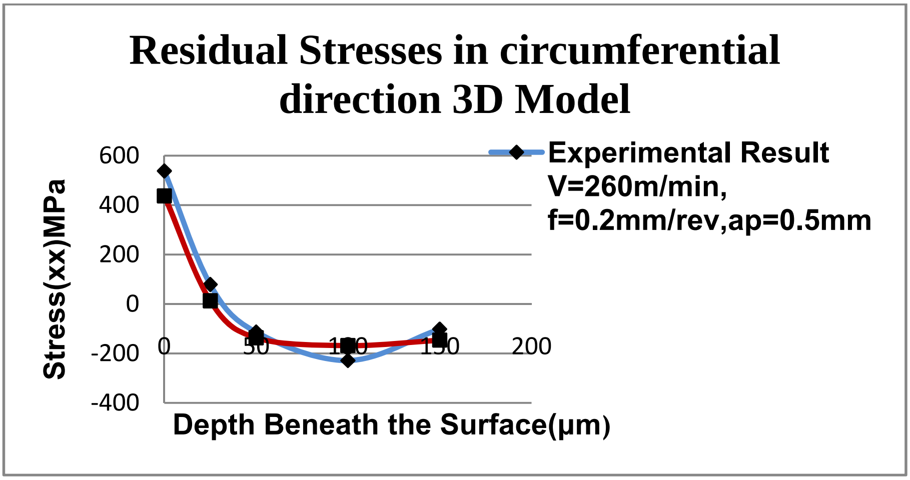

Figure 8.4b Residual stresses in the circumferential direction

8.4 Comments on Result

The 3D simulation include all parameter of real time orthogonal cutting, like feed rate (f), depth of cut (a_p) and cutting velocity (V), So 3D is more realistic in compare to 2D-model.The results which are presented in the Figure 8.4a and Figure 8.4b measured in the unsteady state because due to high complexity and very long computational time (more than one week) it is difficult to achieve the desire steady state condition in this 3D model.
But it can be observed that the results form 3D-model is very close to the experimental value and more accurate than 2D model result, because in 2D it is not possible to include *feed rate (f)* for the orthogonal cutting. Since in the 3D simulation case the results are taken in the unsteady state condition, so some point they are not agreeing with the experimental results. This disagreement is more visible in the axial direction stress case as seen the Figure 8.4a.More the error in the measured value are also significant to define that difference and it’s very difficult to say that how accurate the simulation result are because in some case error in experimental measurement is 40to 45%. See in the Table 6.4.

As summary of the 3D simulation it can be concluded that is possible to accurately simulate and model the real time stress flow in the material for orthogonal machining including all cutting parameters as used in reality.eg feed rate, cutting depth, and cutting speed.

9 Conclusions

In this research, the explicit dynamic Arbitrary Lagrangian Eulerian (ALE) method with adaptive meshing capability has been used to develop FEM simulation model. The Commercial finite element code Abaqus/ExplicitV6.8 is used for modeling for orthogonal cutting of 20NiCrMo5 steel using round edge carbide cutting tools. No remeshing scheme is employed in the model. The extended Johnson-Cook work material model and a detailed friction model are also employed and work material flow around the round edge of the cutting tool is simulated in conjunction with an adaptive meshing scheme.

The Prediction of the machining induced residual stresses in the Axial and Tangential direction is the main focus point of this research and it's effectively carried out, afterwards the predicted values are compared with the experimental values in the table-6, to validate the model. The development of temperature fields during the cutting process, Forces on the tool, strain rate in primary shear zone, shear angle changes and the chip thickness for the different cutting depth is also captured.

Also the effects of changing of different cutting parameters on residual stresses are studied in this work. Process induced stress profiles depict that there exist both compressive and tensile stress regions beneath the surface. Finite Element modeling of stresses and resultant surface properties induced by round edge cutting tools is performed for high speed machining of 20NiCrMo5 steel for different depth of cuts. The results indicate that the round edge design tools influence the stress and temperature fields greatly.

These predictions combined with the temperature field predictions are highly essential to further predict surface integrity and thermo-mechanical deformation related property alteration on the microstructure of the machined surfaces. It has been demonstrated that the ALE simulation approach presented in this work without remeshing definitely results the better predictions for machining induced stresses.

As a remark I would like to say Numerical simulation of machining has proved to be a challenge to existing algorithms and computational tools. Large and localized plastic deformation and complex contact conditions are some of the difficulties associated with this class of problems. The intent of this research is to illustrate different approaches used and the advancements in this field. In spite of the current progress, there is still a need for more research before a modeling practice is established that can predict residual stresses with an acceptable degree of accuracy. The modeling of the material behavior and friction in the process zone is particularly uncertain.

10 References

[1] Shih, A. J., 1995, “Finite element simulation of orthogonal metal cutting,” *ASME Journal of Engineering for Industry*, **117**, 84-93.

[2] Strenkowski, J.S. and Carroll, J.T., 1985, “A finite element model of orthogonal Metal cutting,” *ASME Journal of Engineering for Industry*, **107**, 346-354.

[3] Strenkowski, J.S. and Carroll, J.T., 1986, “Finite element models of orthogonal cutting with application to single point diamond turning,” *Int. Journal of Mechanical Science*, **30**, 899-920.

[4] Black, J. T. and Huang, J. M., 1996, “An evaluation of chip separation criteria for the fem simulation of machining”, *ASME Journal of Manufacturing Science and Engineering*, **118**, 545 – 553.

[5] Madhavan, V., Chandrasekar, S. and Farris, T.N., 2000, “Machining as a wedge indentation,” *Journal of Applied Mechanics*, **67**, 128-139.

[6] Olovsson, L., Nilsson, L., and Simonsson, K., 1999, ‘‘An ALE Formulation for the Solution of Two-Dimensional Metal Cutting Problems,’’ *Computers and Structures*, **72**, 497–507.

[7] Özel, T. and Zeren, E., 2005, “Finite Element Modeling of Stresses Induced by High Speed Machining with Round Edge Cutting Tools,” *Proc. of IMECE’05,* Paper No. 81046, November 5-11, 2005, Orlando, Florida, USA.

[8] M. Vaz Jr. · D.R.J. Owen ,V. Kalhori · M. Lundblad · L.-E. Lindgren, Modelling and Simulation of Machining Processes.

[9] C.Shet, X.Deng , Residual stresses and strains in orthogonal metal cutting, International Journal of Machine Tools & Manufacture *43 (2003) 573–587.*

[10] C Wisner Residual stresses after orthogonal machining of AlSl 304: numerical calculation of the thermal component and comparison with experimental results Journal Metallurgical and Materials Transactions A (2007) 989-996

[11] Marusich, T.D. and Ortiz, M., 1995, "Modeling and simulation of high-speed
machining," *Int. Journal for Numerical Methods in Engineering*, **38**, 3675-3694.

[12] Ceretti, E., Fallböhmer, P., Wu, W.T. and Altan, T., 1996, "Application of 2-D FEM
to chip formation in orthogonal cutting," *Journal of Materials Processing Technology*, **59**, 169-181.

[13] Liu and Guo Finite element modeling the influence of edge roundness on the stress and temperature fields induced by high-speed machining, The International Journal of Advanced Manufacturing Technology March (2006) 255-267.

[14] Liu, C.R. and Guo, Y.B., 2000, "Finite element analysis of the effect of sequential
cuts and tool-chip friction on residual stresses in a machined layer," *Int. Journal of*
Mechanical Sciences, **42**, 1069–1086.

[15] Yang, X. and Liu, C. R., 2002, "A new stress-based model of friction behavior in
machining and its significant impact on residual stresses computed by finite element
method," *Int. Journal of Mechanical Sciences*, **44/4**, 703-723.

[16] Özel, T., 2003, "Modeling of Hard Part Machining: Effect of Insert Edge
Preparation for CBN Cutting Tools," *Journal of Materials Processing Technology*,

141, 284-293

[17] Özel, T. and Altan, T., 2000, “Determination of workpiece flow stress and friction at the chip-tool contact for high-speed cutting,” *Int. Journal of Machine Tools and Manufacture*, **40/1**, 133-152.

[18] Özel, T. and Altan, T., 2000, “Determination of workpiece flow stress and friction at the chip-tool contact for high-speed cutting,” *Int. Journal of Machine Tools and Manufacture*, **40/1**, 133-152.

[19] Adibi-Sedeh, A.H., and Madhavan, V., 2003, “Understanding of finite element analysis results under the framework of Oxley’s machining model,” *Proc. of the 6th CIRP Int. Workshop on Modeling of Machining Operations*, Hamilton, Canada

[20] *Fundamentals of Machining* and *Machine* Tools by CHAPMAN & HALL

[21] Johnson, G.R. and W.H. Cook, 1983, “A constitutive model and data for metals subjected to large strains, high strain rates and high temperatures,” *Proc. of the 7th Int. Symposium on Ballistics*, The Hague, The Netherlands, 541-547.

[22] ABAQUS/CAE V6.8 User manual.

[23] Zorev NN (1966) Metal cutting mechanics. Pergamon, New York

[24] Shaw MC (1984) Metal cutting principles. Clarendon, Oxford

[25] Usui, E., Shirakashi, T. and Kitagawa, T., 1978, "Analytical Prediction of Three Dimensional Cutting Process: Part 3. Cutting Temperature and Crater Wear of Carbide Tool", J. Engng. Ind., Trans. ASME, Vol. 100, pp. 237-243

[26] Klamecki BE (1973) Incipient chip formation in metal cutting—a three-dimensional finite element analysis. Ph.D. thesis, University of Illinois at Urbana-Champaign, Urbana

[27] Ehmann KF, Kpoor SG, DeVor RE, Lazoglu I (1997) Machining processes modeling: a review. J Manuf Sci Eng Trans ASME 119:655–663

[28] Movahhedy, M. R., Gadala, M. S., and Altintas, Y., 2000, ''FE Modeling of Chip
Formation in Orthogonal Metal Cutting Process: An ALE Approach,'' *Machining*
Science and Technology, **4**, 15–47.

[29] Barge M, Hamdi H, Rech J, Bergheau J-M (2005) Numerical modelling of orthogonal cutting: influence of numerical parameters.J Mater Process Technol 164–165:1148–1153

[30] Joshi VS, Dixit PM, Jain VK (1994) Viscoplastic analysis of metal cutting by finite element method. Int J Mach Tools Manuf 34:553–571.

[31] McClain B, Batzer SA, Maldonado GI (2002) A numeric investigation of the rake face stress distribution in orthogonal machining.J Mater Process Technol 123:114–119

[32] Eldridge KF, Dillon OW, Lu WY (1991) Thermo-viscoplastic finite element modeling of machining under various cutting conditions.Trans NAMRI/SME XIX:162–169

[33] Lin Z-C, Lin SY (1992) A coupled finite element model of thermo-elastic-plastic large deformation for orthogonal cutting.J Eng Mater Technol Trans ASME 114:218–226

[34] Marusich TD, Ortiz M (1995) Modeling and simulation of high speed machining. Int J Numer Methods Eng 38:3675–3694.

[35] Guo, Y. B. and Liu, C. R., 2002, " 3D FEA Modeling of Hard Turning," *ASME*
Journal of Manufacturing Science and Engineering, **124**, 189-199.

[36] Guo, Y.B. and Wen, Q, 2005, “A Hybrid Modeling Approach to Investigate Chip
Morphology Transition with The Stagnation Effect by Cutting Edge Geometry,”
Transactions of NAMRI/SME, **33**, 469-476.

[37] Mohamed N.A. Nasr, E.-G. Ng, M.A. Elbestawi, Modelling the effects of tool-edge radius on residual stresses when orthogonal cutting AISI 316L, Received 27 January 2006; received in revised form 2 March 2006; accepted 6 March 2006 Available online 22 May 2006.

[38] Mittal and Liu “Single-step superfinishing using hard machining resulting in superior surface integrity” Purdue University, West Lafayette, Indiana, USA

[39] Mechanics of Machining by Oxley 2nd edition.

[40] Martin Bäker , Finite element simulation of high-speed cutting forces, Journal of Materials Processing Technology 176 (2006) 117–126, Received 13 May 2004; accepted 22 February 2006

[41] J.C Outeiro,D.Umbrello R. M’Saoubi ,Experimental and numerical modeling of the residual stresses induced in orthogonal cutting of AISI 316 L steel
International Journal of Machine Tools & Manufacture *46 (2006) 1786-1794.*

[42] Patrik Dahlman , Fredrik Gunnberg and Michael Jacobson**,**The influence of rake angle, cutting feed and cutting depth on residual stresses in hard turning,*Department of Product and Production Development, Chalmers University of Technology, Gothenburg 412-96, Sweden* Received 27 January 2003; accepted 10 December 2003

11 Appendixes

11.1 Appendix-A

ABAQUS/CAE

2D-model with depth of cut 0.2mm and angle of clearance +6.for the different combination of parameters the basic code will be remain same. Due to unavaibility of space it's not possible to include all those codes.

```
*Heading
** Job name: 2D-fine-Job2 Model name: 2D-fine
** Generated by: Abaqus/CAE Version 6.8-1
*Preprint, echo=NO, model=NO, history=NO, contact=NO
**
** PARTS
**
*Part, name=TOOL-1
*Node
      1,   2.0914433,  0.476500988
      2,  2.15388823,  0.463497341
    3,  2.18651128,  0.430013835
    4,  2.18057036,  0.376343161
    5,  2.47268605,  0.407566637
    6,  2.47268605,  0.507566631
    7,  2.47268605,  0.995044231
    8,  2.07346487,  0.995044231
    9,  2.07346487,  0.795044243
   10,   2.10838389,  0.584341884
   ..,    ……………,……………
  ……………………………….
  …………………………………
  1067,  2.11573386,  0.435255885
  1068,  2.12824202,  0.405946374
  1069,  2.15199614,  0.411748916
  1070,  2.14630198,  0.426587939
  1071,  2.14615631,  0.417093724
*Element, type=CPE4RT
   1,  156,   14,  15,    164
   2,  109,   11,  229,   230
   3,    2,   25,  157,    237
   4,  231,  232,  106,  107
   5,   25,   26,  159,   157
   6,  163,   36,   37,   183
   7,  240,  665,  333,  306
```

```
   8,  98,  222,  223,   97
   9,  101,  102,  234,  162
  10,   90,  218,  217,   89
……………………………….
…………………………….
…………………………….
1000, 1041, 1035,  756,  795
1001, 1038, 1039,  787,  730
1002, 1040,  850,  755,  785
1003,  843, 1035, 1041, 1044
1004, 1042,  813,  729, 1034
1005, 1044, 1045,  939, 1046
1006, 1048, 1047,  844,  943
1007, 1058, 1059, 1056,  912
1008, 1066, 1008, 1005, 1019
1009, 1025, 1020, 1015, 1070
1010, 1070, 1010, 1028, 1025
*Nset, nset=_PICKEDSET2, internal, generate
   1,  1071,     1
*Elset, elset=_PICKEDSET2, internal, generate
   1,  1010,     1
** Section: Section-1-_PICKEDSET2
*Solid Section, elset=_PICKEDSET2, material=TOOL-MAT

*End Part
**
*Part, name=WP-1
*Node
      1,          -3.,           0.
      2,           2.,           0.
      3,           2.,  0.600000024
      4,          -3.,  0.600000024
      5,          -3.,  -1.39999998
      6,           2.,  -1.39999998
      7,  -2.99000001,           0.
      8,  -2.98000002,           0.
      9,  -2.97000003,           0.
     10,  -2.96000004,           0.
  41736, -0.834625185, -0.243661389
  41737,  -1.29558933, -0.206965894
  41738,  -1.31896794, -0.218787268
  41739,  -1.71272695, -0.215938672
  41740,  -1.33865535,  -0.22489804
*Element, type=CPE4RT
   1,    1,     7,  1230,  1102
   2,    7,     8,  1231,  1230
   3,    8,     9,  1232,  1231
   4,    9,    10,  1233,  1232
```

```
    5,    10,    11,  1234,  1233
    6,    11,    12,  1235,  1234
    7,    12,    13,  1236,  1235
    8,    13,    14,  1237,  1236
    9,    14,    15,  1238,  1237
   10,    15,    16,  1239,  1238
  ……………………………..
 ………………………………
  ……………………………..
  41498, 41670, 37764, 37449, 37119
41499, 41712, 37298, 36937, 41700
41500, 37125, 37128, 37772, 37770
41501, 41706, 41720, 41735, 37930
41502, 36985, 37048, 37333, 41739
41503, 41717, 37315, 37652, 37651
*Element, type=CPE3T
25001, 40725, 28379, 35579
25002, 40905, 37171, 37273
25003, 33223, 40826, 32805
25004, 36772, 36396, 36529
25005, 34185, 33221, 34184
25006,   505, 27234,     2
25007, 27234,  1229,     2
25008, 40630, 26678, 27335
……………………………........
……………………………….
……………………………….
25251, 37713, 38023, 37971
25252, 41699, 37587, 37739
25253, 41704, 37023, 37364
25254, 41704, 36942, 41663
25255, 37442, 37112, 37111
25256, 41731, 36936, 37296
25257, 41697, 38204, 38512
25258, 41724, 37311, 36939
*Nset, nset=_PICKEDSET2, internal, generate
     1,  41740,      1
*Elset, elset=_PICKEDSET2, internal, generate
     1,  41503,      1
** Section: Section-2-_PICKEDSET2
*Solid Section, elset=_PICKEDSET2, material=WP-MAT

*End Part
**
**
** ASSEMBLY
**
*Assembly, name=Assembly
```

```
**
*Instance, name=TOOL-1, part=TOOL-1
*End Instance
**
*Instance, name=WP-1, part=WP-1
*End Instance
**
*Node
      1,    2.0999999,  0.400000006
*Nset, nset=_PickedSet47, internal
 1,
*Nset, nset=TOOL-SET, instance=TOOL-1, generate
    1,  1071,     1
*Elset, elset=TOOL-SET, instance=TOOL-1, generate
    1,  1010,     1
*Nset, nset=_PICKEDSET13, internal
 1,
*Nset, nset=_PICKEDSET14, internal
 1,
*Nset, nset=_PICKEDSET15, internal, instance=TOOL-1, generate
    1,  1071,     1
*Elset, elset=_PICKEDSET15, internal, instance=TOOL-1, generate
    1,  1010,     1
*Nset, nset=_PICKEDSET16, internal, instance=WP-1
    5,    6, 1132, 1133, 1134, 1135, 1136, 1137, 1138, 1139, 1140, 1141, 1142, 1143, 1144,
1145
 1146, 1147, 1148, 1149, 1150, 1151, 1152, 1153, 1154, 1155, 1156, 1157, 1158, 1159,
1160, 1161
 1162, 1163, 1164, 1165, 1166, 1167, 1168, 1169, 1170, 1171, 1172, 1173, 1174, 1175,
1176, 1177
 1178, 1179, 1180, 1181, 1182, 1183, 1184, 1185, 1186, 1187, 1188, 1189, 1190, 1191,
1192, 1193
 1194, 1195, 1196, 1197, 1198, 1199, 1200
*Elset, elset=_PICKEDSET16, internal, instance=WP-1
 25306, 25307, 25309, 25383, 25384, 25385, 25398, 25404, 25405, 25407, 25435, 25438,
25451, 25452, 25455, 25459
 25473, 25475, 25508, 25511, 25515, 25531, 25922, 25936, 25943, 25944, 25956, 25964,
26002, 26009, 26010, 26402
 26403, 26405, 26406, 26408, 26410, 26411, 26412, 26413, 26414, 26416, 26417, 26420,
26421, 26422, 26423, 26425
 26426, 26427, 26449, 26501, 26503, 26506, 26507, 26512, 26515, 26533, 26534, 26536,
26538, 26540, 27000, 27004
 27007, 27010, 27011, 27012, 27014, 27015
*Nset, nset=_PICKEDSET30, internal, instance=TOOL-1
  7,  8, 74, 75, 76, 77, 78, 79, 80, 81, 82
*Elset, elset=_PICKEDSET30, internal, instance=TOOL-1
  56,  57,  65,  69,  71,  72, 153, 158, 162, 165
*Nset, nset=_PICKEDSET36, internal
```

```
 1,
*Nset, nset=SET-BACK, instance=WP-1
   1,    4,    5, 1054, 1055, 1056, 1057, 1058, 1059, 1060, 1061, 1062, 1063, 1064, 1065,
1066
 1067, 1068, 1069, 1070, 1071, 1072, 1073, 1074, 1075, 1076, 1077, 1078, 1079, 1080,
1081, 1082
 1083, 1084, 1085, 1086, 1087, 1088, 1089, 1090, 1091, 1092, 1093, 1094, 1095, 1096,
1097, 1098
 1099, 1100, 1101, 1102, 1103, 1104, 1105, 1106, 1107, 1108, 1109, 1110, 1111, 1112,
1113, 1114
 1115, 1116, 1117, 1118, 1119, 1120, 1121, 1122, 1123, 1124, 1125, 1126, 1127, 1128,
1129, 1130
 1131,
*Elset, elset=SET-BACK, instance=WP-1
    1,  501,  1001,  1501,  2001,  2501,  3001,  3501,  4001,  4501,  5001,  5501,  6001,
6501,  7001,  7501
  8001,  8501,  9001,  9501, 10001, 10501, 11001, 11501, 12001, 12501, 13001, 13501,
14001, 14501, 15001, 15501
 16001, 16501, 17001, 17501, 18001, 18501, 19001, 19501, 20001, 20501, 21001, 21501,
22001, 22501, 23001, 23501
 24001, 24501, 25296, 25298, 25299, 25375, 25389, 25392, 26385, 26387, 26388, 26389,
26392, 26393, 26396, 26397
 26398, 26399, 26400, 26401, 26402, 26446, 26495, 26497, 26500, 26543, 26980, 26986,
26988, 26992, 26995, 26997
*Nset, nset=SET-FRONT, instance=WP-1
   2,    3,    6,  506,  507,  508,  509,  510,  511,  512,  513,  514,  515,  516,  517,  518
  519,  520,  521,  522,  523,  524,  525,  526,  527,  528,  529,  530,  531,  532,  533,  534
  535,  536,  537,  538,  539,  540,  541,  542,  543,  544,  545,  546,  547,  548,  549,  550
  551,  552,  553,  554, 1201, 1202, 1203, 1204, 1205, 1206, 1207, 1208, 1209, 1210, 1211,
1212
 1213, 1214, 1215, 1216, 1217, 1218, 1219, 1220, 1221, 1222, 1223, 1224, 1225, 1226,
1227, 1228
 1229,
*Elset, elset=SET-FRONT, instance=WP-1
  500,  1000,  1500,  2000,  2500,  3000,  3500,  4000,  4500,  5000,  5500,  6000,  6500,
7000,  7500,  8000
  8500,  9000,  9500, 10000, 10500, 11000, 11500, 12000, 12500, 13000, 13500, 14000,
14500, 15000, 15500, 16000
 16500, 17000, 17500, 18000, 18500, 19000, 19500, 20000, 20500, 21000, 21500, 22000,
22500, 23000, 23500, 24000
 24500, 25000, 25007, 25495, 25532, 25541, 25549, 25557, 25558, 25562, 26020, 26427,
26428, 26429, 26430, 26432
 26433, 26434, 26435, 26437, 26438, 26439, 26440, 26441, 26513, 26519, 26522, 26544,
26548, 26549, 27021, 27026
*Nset, nset=SET-TOP, instance=WP-1
   3,    4,  555,  556,  557,  558,  559,  560,  561,  562,  563,  564,  565,  566,  567,  568
  569,  570,  571,  572,  573,  574,  575,  576,  577,  578,  579,  580,  581,  582,  583,  584
  585,  586,  587,  588,  589,  590,  591,  592,  593,  594,  595,  596,  597,  598,  599,  600
```

```
 601, 602, 603, 604, 605, 606, 607, 608, 609, 610, 611, 612, 613, 614, 615, 616
 617, 618, 619, 620, 621, 622, 623, 624, 625, 626, 627, 628, 629, 630, 631, 632
 633, 634, 635, 636, 637, 638, 639, 640, 641, 642, 643, 644, 645, 646, 647, 648
 649, 650, 651, 652, 653, 654, 655, 656, 657, 658, 659, 660, 661, 662, 663, 664
 665, 666, 667, 668, 669, 670, 671, 672, 673, 674, 675, 676, 677, 678, 679, 680
 681, 682, 683, 684, 685, 686, 687, 688, 689, 690, 691, 692, 693, 694, 695, 696
 697, 698, 699, 700, 701, 702, 703, 704, 705, 706, 707, 708, 709, 710, 711, 712
 713, 714, 715, 716, 717, 718, 719, 720, 721, 722, 723, 724, 725, 726, 727, 728
 729, 730, 731, 732, 733, 734, 735, 736, 737, 738, 739, 740, 741, 742, 743, 744
 745, 746, 747, 748, 749, 750, 751, 752, 753, 754, 755, 756, 757, 758, 759, 760
 761, 762, 763, 764, 765, 766, 767, 768, 769, 770, 771, 772, 773, 774, 775, 776
 777, 778, 779, 780, 781, 782, 783, 784, 785, 786, 787, 788, 789, 790, 791, 792
 793, 794, 795, 796, 797, 798, 799, 800, 801, 802, 803, 804, 805, 806, 807, 808
 809, 810, 811, 812, 813, 814, 815, 816, 817, 818, 819, 820, 821, 822, 823, 824
 825, 826, 827, 828, 829, 830, 831, 832, 833, 834, 835, 836, 837, 838, 839, 840
 841, 842, 843, 844, 845, 846, 847, 848, 849, 850, 851, 852, 853, 854, 855, 856
 857, 858, 859, 860, 861, 862, 863, 864, 865, 866, 867, 868, 869, 870, 871, 872
 873, 874, 875, 876, 877, 878, 879, 880, 881, 882, 883, 884, 885, 886, 887, 888
 889, 890, 891, 892, 893, 894, 895, 896, 897, 898, 899, 900, 901, 902, 903, 904
 905, 906, 907, 908, 909, 910, 911, 912, 913, 914, 915, 916, 917, 918, 919, 920
 921, 922, 923, 924, 925, 926, 927, 928, 929, 930, 931, 932, 933, 934, 935, 936
 937, 938, 939, 940, 941, 942, 943, 944, 945, 946, 947, 948, 949, 950, 951, 952
 953, 954, 955, 956, 957, 958, 959, 960, 961, 962, 963, 964, 965, 966, 967, 968
 969, 970, 971, 972, 973, 974, 975, 976, 977, 978, 979, 980, 981, 982, 983, 984
 985, 986, 987, 988, 989, 990, 991, 992, 993, 994, 995, 996, 997, 998, 999, 1000
 1001, 1002, 1003, 1004, 1005, 1006, 1007, 1008, 1009, 1010, 1011, 1012, 1013, 1014,
1015, 1016
 1017, 1018, 1019, 1020, 1021, 1022, 1023, 1024, 1025, 1026, 1027, 1028, 1029, 1030,
1031, 1032
 1033, 1034, 1035, 1036, 1037, 1038, 1039, 1040, 1041, 1042, 1043, 1044, 1045, 1046,
1047, 1048
 1049, 1050, 1051, 1052, 1053
*Elset, elset=SET-TOP, instance=WP-1, generate
 24501, 25000,     1
*Nset, nset=SET-BOTTOM, instance=WP-1
   5,   6, 1132, 1133, 1134, 1135, 1136, 1137, 1138, 1139, 1140, 1141, 1142, 1143, 1144,
1145
 1146, 1147, 1148, 1149, 1150, 1151, 1152, 1153, 1154, 1155, 1156, 1157, 1158, 1159,
1160, 1161
 1162, 1163, 1164, 1165, 1166, 1167, 1168, 1169, 1170, 1171, 1172, 1173, 1174, 1175,
1176, 1177
 1178, 1179, 1180, 1181, 1182, 1183, 1184, 1185, 1186, 1187, 1188, 1189, 1190, 1191,
1192, 1193
 1194, 1195, 1196, 1197, 1198, 1199, 1200
*Elset, elset=SET-BOTTOM, instance=WP-1
 25306, 25307, 25309, 25383, 25384, 25385, 25398, 25404, 25405, 25407, 25435, 25438,
25451, 25452, 25455, 25459
```

```
 25473, 25475, 25508, 25511, 25515, 25531, 25922, 25936, 25943, 25944, 25956, 25964,
26002, 26009, 26010, 26402
 26403, 26405, 26406, 26408, 26410, 26411, 26412, 26413, 26414, 26416, 26417, 26420,
26421, 26422, 26423, 26425
 26426, 26427, 26449, 26501, 26503, 26506, 26507, 26512, 26515, 26533, 26534, 26536,
26538, 26540, 27000, 27004
 27007, 27010, 27011, 27012, 27014, 27015
*Nset, nset=SET-RF
 1,
*Nset, nset=WP-SET, instance=WP-1, generate
    1,  41740,      1
*Elset, elset=WP-SET, instance=WP-1, generate
    1,  41503,      1
*Nset, nset=_PICKEDSET71, internal, instance=TOOL-1
  7,  8, 74, 75, 76, 77, 78, 79, 80, 81, 82
*Elset, elset=_PICKEDSET71, internal, instance=TOOL-1
  56,  57,  65,  69,  71,  72, 153, 158, 162, 165
*Nset, nset=_PICKEDSET73, internal
 1,
*Elset, elset=_WP-FRONT-SURF_S2, internal, instance=WP-1
   500,  1000,  1500,  2000,  2500,  3000,  3500,  4000,  4500,  5000,  5500,  6000,  6500,
7000,  7500,  8000
  8500,  9000,  9500, 10000, 10500, 11000, 11500, 12000, 12500, 13000, 13500, 14000,
14500, 15000, 15500, 16000
 16500, 17000, 17500, 18000, 18500, 19000, 19500, 20000, 20500, 21000, 21500, 22000,
22500, 23000, 23500, 24000
 24500, 25000, 25007, 25495, 25532, 25541, 25549, 25557, 25558, 25562, 26020, 26427,
26513, 26519, 26522, 26544
 26548, 26549, 27021, 27026
*Elset, elset=_WP-FRONT-SURF_S4, internal, instance=WP-1
 26428, 26429, 26430, 26432, 26433, 26434, 26435, 26437, 26438, 26439, 26440, 26441
*Elset, elset=_WP-TOP_S3, internal, instance=WP-1, generate
 24501,  25000,      1
*Elset, elset=_WP-SUFR-TOT_S2, internal, instance=WP-1
   500,  1000,  1500,  2000,  2500,  3000,  3500,  4000,  4500,  5000,  5500,  6000,  6500,
7000,  7500,  8000
  8500,  9000,  9500, 10000, 10500, 11000, 11500, 12000, 12500, 13000, 13500, 14000,
14500, 15000, 15500, 16000
 16500, 17000, 17500, 18000, 18500, 19000, 19500, 20000, 20500, 21000, 21500, 22000,
22500, 23000, 23500, 24000
 24500, 25000, 25007, 25495, 25532, 25541, 25549, 25557, 25558, 25562, 26020, 26402,
26427, 26513, 26519, 26522
 26544, 26548, 26549, 27021, 27026
*Elset, elset=_WP-SUFR-TOT_S3, internal, instance=WP-1
 24501, 24502, 24503, 24504, 24505, 24506, 24507, 24508, 24509, 24510, 24511, 24512,
24513, 24514, 24515, 24516
 24517, 24518, 24519, 24520, 24521, 24522, 24523, 24524, 24525, 24526, 24527, 24528,
24529, 24530, 24531, 24532
```

24533, 24534, 24535, 24536, 24537, 24538, 24539, 24540, 24541, 24542, 24543, 24544, 24545, 24546, 24547, 24548

24549, 24550, 24551, 24552, 24553, 24554, 24555, 24556, 24557, 24558, 24559, 24560, 24561, 24562, 24563, 24564

24565, 24566, 24567, 24568, 24569, 24570, 24571, 24572, 24573, 24574, 24575, 24576, 24577, 24578, 24579, 24580

24581, 24582, 24583, 24584, 24585, 24586, 24587, 24588, 24589, 24590, 24591, 24592, 24593, 24594, 24595, 24596

24597, 24598, 24599, 24600, 24601, 24602, 24603, 24604, 24605, 24606, 24607, 24608, 24609, 24610, 24611, 24612

24613, 24614, 24615, 24616, 24617, 24618, 24619, 24620, 24621, 24622, 24623, 24624, 24625, 24626, 24627, 24628

24629, 24630, 24631, 24632, 24633, 24634, 24635, 24636, 24637, 24638, 24639, 24640, 24641, 24642, 24643, 24644

24645, 24646, 24647, 24648, 24649, 24650, 24651, 24652, 24653, 24654, 24655, 24656, 24657, 24658, 24659, 24660

24661, 24662, 24663, 24664, 24665, 24666, 24667, 24668, 24669, 24670, 24671, 24672, 24673, 24674, 24675, 24676

24677, 24678, 24679, 24680, 24681, 24682, 24683, 24684, 24685, 24686, 24687, 24688, 24689, 24690, 24691, 24692

24693, 24694, 24695, 24696, 24697, 24698, 24699, 24700, 24701, 24702, 24703, 24704, 24705, 24706, 24707, 24708

24709, 24710, 24711, 24712, 24713, 24714, 24715, 24716, 24717, 24718, 24719, 24720, 24721, 24722, 24723, 24724

24725, 24726, 24727, 24728, 24729, 24730, 24731, 24732, 24733, 24734, 24735, 24736, 24737, 24738, 24739, 24740

24741, 24742, 24743, 24744, 24745, 24746, 24747, 24748, 24749, 24750, 24751, 24752, 24753, 24754, 24755, 24756

24757, 24758, 24759, 24760, 24761, 24762, 24763, 24764, 24765, 24766, 24767, 24768, 24769, 24770, 24771, 24772

24773, 24774, 24775, 24776, 24777, 24778, 24779, 24780, 24781, 24782, 24783, 24784, 24785, 24786, 24787, 24788

24789, 24790, 24791, 24792, 24793, 24794, 24795, 24796, 24797, 24798, 24799, 24800, 24801, 24802, 24803, 24804

24805, 24806, 24807, 24808, 24809, 24810, 24811, 24812, 24813, 24814, 24815, 24816, 24817, 24818, 24819, 24820

24821, 24822, 24823, 24824, 24825, 24826, 24827, 24828, 24829, 24830, 24831, 24832, 24833, 24834, 24835, 24836

24837, 24838, 24839, 24840, 24841, 24842, 24843, 24844, 24845, 24846, 24847, 24848, 24849, 24850, 24851, 24852

24853, 24854, 24855, 24856, 24857, 24858, 24859, 24860, 24861, 24862, 24863, 24864, 24865, 24866, 24867, 24868

24869, 24870, 24871, 24872, 24873, 24874, 24875, 24876, 24877, 24878, 24879, 24880, 24881, 24882, 24883, 24884

24885, 24886, 24887, 24888, 24889, 24890, 24891, 24892, 24893, 24894, 24895, 24896, 24897, 24898, 24899, 24900

24901, 24902, 24903, 24904, 24905, 24906, 24907, 24908, 24909, 24910, 24911, 24912, 24913, 24914, 24915, 24916

```
 24917, 24918, 24919, 24920, 24921, 24922, 24923, 24924, 24925, 24926, 24927, 24928,
24929, 24930, 24931, 24932
 24933, 24934, 24935, 24936, 24937, 24938, 24939, 24940, 24941, 24942, 24943, 24944,
24945, 24946, 24947, 24948
 24949, 24950, 24951, 24952, 24953, 24954, 24955, 24956, 24957, 24958, 24959, 24960,
24961, 24962, 24963, 24964
 24965, 24966, 24967, 24968, 24969, 24970, 24971, 24972, 24973, 24974, 24975, 24976,
24977, 24978, 24979, 24980
 24981, 24982, 24983, 24984, 24985, 24986, 24987, 24988, 24989, 24990, 24991, 24992,
24993, 24994, 24995, 24996
 24997, 24998, 24999, 25000, 25299, 25307, 25405, 25435, 25452, 25459, 25473, 25508,
25515, 25922, 25936, 25944
 25964, 26387, 26388, 26389, 26392, 26393, 26396, 26397, 26398, 26399, 26400, 26401,
26403, 26411, 26412, 26414
 26417, 26421, 26422, 26423, 26543, 26986, 26988, 26992, 26995, 26997, 27000, 27004,
27007, 27010, 27011, 27012
 27014, 27015
*Elset, elset=_WP-SUFR-TOT_S4, internal, instance=WP-1
    1,   501,  1001,  1501,  2001,  2501,  3001,  3501,  4001,  4501,  5001,  5501,  6001,
6501,  7001,  7501
  8001,  8501,  9001,  9501, 10001, 10501, 11001, 11501, 12001, 12501, 13001, 13501,
14001, 14501, 15001, 15501
 16001, 16501, 17001, 17501, 18001, 18501, 19001, 19501, 20001, 20501, 21001, 21501,
22001, 22501, 23001, 23501
 24001, 24501, 26426, 26428, 26429, 26430, 26432, 26433, 26434, 26435, 26437, 26438,
26439, 26440, 26441, 26980
*Elset, elset=_WP-SUFR-TOT_S1, internal, instance=WP-1
 25296, 25298, 25306, 25309, 25375, 25383, 25384, 25385, 25389, 25392, 25398, 25404,
25407, 25438, 25451, 25455
 25475, 25511, 25531, 25943, 25956, 26002, 26009, 26010, 26385, 26402, 26405, 26406,
26408, 26410, 26413, 26416
 26420, 26425, 26427, 26446, 26449, 26495, 26497, 26500, 26501, 26503, 26506, 26507,
26512, 26515, 26533, 26534
 26536, 26538, 26540
*Elset, elset=_TOOL-SURF_S3, internal, instance=TOOL-1
   4,  41,  45,  61,  62,  66,  93, 105, 130, 135, 140, 148, 180, 630, 640, 646
 648, 701, 755
*Elset, elset=_TOOL-SURF_S1, internal, instance=TOOL-1
   2,   9,  43,  44,  48,  56,  58,  59,  63,  65,  80,  82,  90,  92,  94, 101
 103, 106, 129, 139, 182, 655, 662, 692, 697, 698, 699, 715, 750
*Elset, elset=_TOOL-SURF_S4, internal, instance=TOOL-1
   8,  10,  12,  48,  52,  65,  67,  71,  72,  73,  78,  84,  85,  99, 117, 145
 152, 153, 167, 171, 178, 187, 209, 635, 637, 647, 650, 659, 660, 668, 669, 670
 705,
*Elset, elset=_TOOL-SURF_S2, internal, instance=TOOL-1
  20,  47,  49,  53,  56,  57,  68,  69,  75,  79,  83,  89,  97, 142, 143, 144
 146, 158, 162, 163, 165, 166, 169, 631, 633, 634, 636, 639, 656, 658, 661, 663
 665, 695, 717, 718, 723, 727, 770
```

```
*Nset, nset=CLOUD, instance=WP-1, generate
     1,  41740,      1
*Elset, elset=_WP-FRONT-SURF_S2_1, internal, instance=WP-1
   500,  1000,  1500,  2000,  2500,  3000,  3500,  4000,  4500,  5000,  5500,  6000,  6500,  7000,  7500,  8000
  8500,  9000,  9500, 10000, 10500, 11000, 11500, 12000, 12500, 13000, 13500, 14000, 14500, 15000, 15500, 16000
 16500, 17000, 17500, 18000, 18500, 19000, 19500, 20000, 20500, 21000, 21500, 22000, 22500, 23000, 23500, 24000
 24500, 25000, 25007, 25495, 25532, 25541, 25549, 25557, 25558, 25562, 26020, 26427, 26513, 26519, 26522, 26544
 26548, 26549, 27021, 27026
*Elset, elset=_WP-FRONT-SURF_S4_1, internal, instance=WP-1
 26428, 26429, 26430, 26432, 26433, 26434, 26435, 26437, 26438, 26439, 26440, 26441
*Surface, type=ELEMENT, name=WP-FRONT-SURF
_WP-FRONT-SURF_S2_1, S2
_WP-FRONT-SURF_S4_1, S4
*Elset, elset=_WP-TOP_S3_1, internal, instance=WP-1, generate
 24501,  25000,      1
*Surface, type=ELEMENT, name=WP-TOP
_WP-TOP_S3_1, S3
*Elset, elset=_WP-SUFR-TOT_S2_1, internal, instance=WP-1
   500,  1000,  1500,  2000,  2500,  3000,  3500,  4000,  4500,  5000,  5500,  6000,  6500,  7000,  7500,  8000
  8500,  9000,  9500, 10000, 10500, 11000, 11500, 12000, 12500, 13000, 13500, 14000, 14500, 15000, 15500, 16000
 16500, 17000, 17500, 18000, 18500, 19000, 19500, 20000, 20500, 21000, 21500, 22000, 22500, 23000, 23500, 24000
 24500, 25000, 25007, 25495, 25532, 25541, 25549, 25557, 25558, 25562, 26020, 26402, 26427, 26513, 26519, 26522
 26544, 26548, 26549, 27021, 27026
*Elset, elset=_WP-SUFR-TOT_S3_1, internal, instance=WP-1
 24501, 24502, 24503, 24504, 24505, 24506, 24507, 24508, 24509, 24510, 24511, 24512, 24513, 24514, 24515, 24516
 24517, 24518, 24519, 24520, 24521, 24522, 24523, 24524, 24525, 24526, 24527, 24528, 24529, 24530, 24531, 24532
 24533, 24534, 24535, 24536, 24537, 24538, 24539, 24540, 24541, 24542, 24543, 24544, 24545, 24546, 24547, 24548
 24549, 24550, 24551, 24552, 24553, 24554, 24555, 24556, 24557, 24558, 24559, 24560, 24561, 24562, 24563, 24564
 24565, 24566, 24567, 24568, 24569, 24570, 24571, 24572, 24573, 24574, 24575, 24576, 24577, 24578, 24579, 24580
 24581, 24582, 24583, 24584, 24585, 24586, 24587, 24588, 24589, 24590, 24591, 24592, 24593, 24594, 24595, 24596
 24597, 24598, 24599, 24600, 24601, 24602, 24603, 24604, 24605, 24606, 24607, 24608, 24609, 24610, 24611, 24612
 24613, 24614, 24615, 24616, 24617, 24618, 24619, 24620, 24621, 24622, 24623, 24624, 24625, 24626, 24627, 24628
```

24629, 24630, 24631, 24632, 24633, 24634, 24635, 24636, 24637, 24638, 24639, 24640, 24641, 24642, 24643, 24644

24645, 24646, 24647, 24648, 24649, 24650, 24651, 24652, 24653, 24654, 24655, 24656, 24657, 24658, 24659, 24660

24661, 24662, 24663, 24664, 24665, 24666, 24667, 24668, 24669, 24670, 24671, 24672, 24673, 24674, 24675, 24676

24677, 24678, 24679, 24680, 24681, 24682, 24683, 24684, 24685, 24686, 24687, 24688, 24689, 24690, 24691, 24692

24693, 24694, 24695, 24696, 24697, 24698, 24699, 24700, 24701, 24702, 24703, 24704, 24705, 24706, 24707, 24708

24709, 24710, 24711, 24712, 24713, 24714, 24715, 24716, 24717, 24718, 24719, 24720, 24721, 24722, 24723, 24724

24725, 24726, 24727, 24728, 24729, 24730, 24731, 24732, 24733, 24734, 24735, 24736, 24737, 24738, 24739, 24740

24741, 24742, 24743, 24744, 24745, 24746, 24747, 24748, 24749, 24750, 24751, 24752, 24753, 24754, 24755, 24756

24757, 24758, 24759, 24760, 24761, 24762, 24763, 24764, 24765, 24766, 24767, 24768, 24769, 24770, 24771, 24772

24773, 24774, 24775, 24776, 24777, 24778, 24779, 24780, 24781, 24782, 24783, 24784, 24785, 24786, 24787, 24788

24789, 24790, 24791, 24792, 24793, 24794, 24795, 24796, 24797, 24798, 24799, 24800, 24801, 24802, 24803, 24804

24805, 24806, 24807, 24808, 24809, 24810, 24811, 24812, 24813, 24814, 24815, 24816, 24817, 24818, 24819, 24820

24821, 24822, 24823, 24824, 24825, 24826, 24827, 24828, 24829, 24830, 24831, 24832, 24833, 24834, 24835, 24836

24837, 24838, 24839, 24840, 24841, 24842, 24843, 24844, 24845, 24846, 24847, 24848, 24849, 24850, 24851, 24852

24853, 24854, 24855, 24856, 24857, 24858, 24859, 24860, 24861, 24862, 24863, 24864, 24865, 24866, 24867, 24868

24869, 24870, 24871, 24872, 24873, 24874, 24875, 24876, 24877, 24878, 24879, 24880, 24881, 24882, 24883, 24884

24885, 24886, 24887, 24888, 24889, 24890, 24891, 24892, 24893, 24894, 24895, 24896, 24897, 24898, 24899, 24900

24901, 24902, 24903, 24904, 24905, 24906, 24907, 24908, 24909, 24910, 24911, 24912, 24913, 24914, 24915, 24916

24917, 24918, 24919, 24920, 24921, 24922, 24923, 24924, 24925, 24926, 24927, 24928, 24929, 24930, 24931, 24932

24933, 24934, 24935, 24936, 24937, 24938, 24939, 24940, 24941, 24942, 24943, 24944, 24945, 24946, 24947, 24948

24949, 24950, 24951, 24952, 24953, 24954, 24955, 24956, 24957, 24958, 24959, 24960, 24961, 24962, 24963, 24964

24965, 24966, 24967, 24968, 24969, 24970, 24971, 24972, 24973, 24974, 24975, 24976, 24977, 24978, 24979, 24980

24981, 24982, 24983, 24984, 24985, 24986, 24987, 24988, 24989, 24990, 24991, 24992, 24993, 24994, 24995, 24996

24997, 24998, 24999, 25000, 25299, 25307, 25405, 25435, 25452, 25459, 25473, 25508, 25515, 25922, 25936, 25944

```
 25964, 26387, 26388, 26389, 26392, 26393, 26396, 26397, 26398, 26399, 26400, 26401,
26403, 26411, 26412, 26414
 26417, 26421, 26422, 26423, 26543, 26986, 26988, 26992, 26995, 26997, 27000, 27004,
27007, 27010, 27011, 27012
 27014, 27015
*Elset, elset=_WP-SUFR-TOT_S4_1, internal, instance=WP-1
    1,  501,  1001,  1501,  2001,  2501,  3001,  3501,  4001,  4501,  5001,  5501,  6001,
6501,  7001,  7501
  8001,  8501,  9001,  9501, 10001, 10501, 11001, 11501, 12001, 12501, 13001, 13501,
14001, 14501, 15001, 15501
 16001, 16501, 17001, 17501, 18001, 18501, 19001, 19501, 20001, 20501, 21001, 21501,
22001, 22501, 23001, 23501
 24001, 24501, 26426, 26428, 26429, 26430, 26432, 26433, 26434, 26435, 26437, 26438,
26439, 26440, 26441, 26980
*Elset, elset=_WP-SUFR-TOT_S1_1, internal, instance=WP-1
 25296, 25298, 25306, 25309, 25375, 25383, 25384, 25385, 25389, 25392, 25398, 25404,
25407, 25438, 25451, 25455
 25475, 25511, 25531, 25943, 25956, 26002, 26009, 26010, 26385, 26402, 26405, 26406,
26408, 26410, 26413, 26416
 26420, 26425, 26427, 26446, 26449, 26495, 26497, 26500, 26501, 26503, 26506, 26507,
26512, 26515, 26533, 26534
 26536, 26538, 26540
*Surface, type=ELEMENT, name=WP-SUFR-TOT
_WP-SUFR-TOT_S2_1, S2
_WP-SUFR-TOT_S3_1, S3
_WP-SUFR-TOT_S4_1, S4
_WP-SUFR-TOT_S1_1, S1
*Elset, elset=_TOOL-SURF_S3_1, internal, instance=TOOL-1
   4,  41,  45,  61,  62,  66,  93, 105, 130, 135, 140, 148, 180, 630, 640, 646
 648, 701, 755
*Elset, elset=_TOOL-SURF_S1_1, internal, instance=TOOL-1
   2,   9,  43,  44,  48,  56,  58,  59,  63,  65,  80,  82,  90,  92,  94, 101
 103, 106, 129, 139, 182, 655, 662, 692, 697, 698, 699, 715, 750
*Elset, elset=_TOOL-SURF_S4_1, internal, instance=TOOL-1
   8,  10,  12,  48,  52,  65,  67,  71,  72,  73,  78,  84,  85,  99, 117, 145
 152, 153, 167, 171, 178, 187, 209, 635, 637, 647, 650, 659, 660, 668, 669, 670
 705,
*Elset, elset=_TOOL-SURF_S2_1, internal, instance=TOOL-1
  20,  47,  49,  53,  56,  57,  68,  69,  75,  79,  83,  89,  97, 142, 143, 144
 146, 158, 162, 163, 165, 166, 169, 631, 633, 634, 636, 639, 656, 658, 661, 663
 665, 695, 717, 718, 723, 727, 770
*Surface, type=ELEMENT, name=TOOL-SURF
_TOOL-SURF_S3_1, S3
_TOOL-SURF_S1_1, S1
_TOOL-SURF_S4_1, S4
_TOOL-SURF_S2_1, S2
*Surface, type=NODE, name=CLOUD_CNS_, internal
CLOUD, 1.
```

```
** Constraint: COUPLING
*Coupling, constraint name=COUPLING, ref node=_PICKEDSET13, surface=TOOL-SURF
*Kinematic
** Constraint: RigidBody-1
*Rigid Body, ref node=_PickedSet47, elset=_PICKEDSET15
*End Assembly
**
** MATERIALS
**
*Material, name=TOOL-MAT
*Conductivity
 0.046,
*Density
 1.5e-08,
*Elastic
800000., 0.3
*Expansion
 4.7e-08,
*Inelastic Heat Fraction
        0.9,
*Specific Heat
 2.03e+08,
*Material, name=WP-MAT
*Conductivity
 0.0477,
*Damage Initiation, criterion=DUCTILE
 1.5, 0.2,500.
*Damage Evolution, type=ENERGY
10.,
*Damage Initiation, criterion=SHEAR
 1.5,  1.,500.
*Density
 7.8e-09,
*Elastic
210000., 0.3
*Expansion
 1.2e-08,
*Inelastic Heat Fraction
        0.9,
*Plastic, hardening=JOHNSON COOK
490., 600., 0.21,  0.6,1900., 300.
*Specific Heat
 5.56e+08,
**
** INTERACTION PROPERTIES
**
*Surface Interaction, name=CON
```

```
*Friction, shear traction slope=200000., taumax=2.1e+06
 0.4,
*Surface Behavior, pressure-overclosure=LINEAR
2.1e+06,
** ----------------------------------------------------------------
**
** STEP: cutting
**
*Step, name=cutting
*Dynamic Temperature-displacement, Explicit
, 0.001
*Bulk Viscosity
0.06, 1.2
** Mass Scaling: Semi-Automatic
**              Whole Model
*Fixed Mass Scaling, factor=10.
**
** BOUNDARY CONDITIONS
**
** Name: Disp-BC-1 Type: Displacement/Rotation
*Boundary
_PICKEDSET71, 1, 1
** Name: Disp-BC-2 Type: Displacement/Rotation
*Boundary
_PICKEDSET71, 2, 2
** Name: Disp-BC-3 Type: Displacement/Rotation
*Boundary
_PICKEDSET71, 6, 6
** Name: Disp-BC-4 Type: Displacement/Rotation
*Boundary
SET-BOTTOM, 2, 2
** Name: Vel-BC-1 Type: Velocity/Angular velocity
*Boundary, type=VELOCITY
_PICKEDSET73, 1, 1
** Name: Vel-BC-2 Type: Velocity/Angular velocity
*Boundary, type=VELOCITY
_PICKEDSET73, 2, 2
** Name: Vel-BC-3 Type: Velocity/Angular velocity
*Boundary, type=VELOCITY
_PICKEDSET73, 6, 6
** Name: Vel-BC-4 Type: Velocity/Angular velocity
*Boundary, type=VELOCITY
SET-BACK, 1, 1, 5000.
*Adaptive Mesh Controls, name=ALE-CON, geometric enhancement=YES, curvature
refinement=2.
0.8, 0.1, 0.1
*Adaptive Mesh, elset=WP-SET, controls=ALE-CON, frequency=100, initial mesh
sweeps=5, mesh sweeps=5, op=NEW
```

```
**
** ADAPTIVE MESH CONSTRAINTS
**
** Name: AdMeshCnstr-1 Type: Velocity/Angular velocity
*Adaptive Mesh Constraint, constraint type=LAGRANGIAN, type=VELOCITY
WP-SET
**
** INTERACTIONS
**
** Interaction: tool-chip
*Contact Pair, interaction=CON, mechanical constraint=KINEMATIC, cpset=tool-chip
TOOL-SURF, CLOUD_CNS_
**
** OUTPUT REQUESTS
**
*Restart, write, number interval=1, time marks=NO
**
** FIELD OUTPUT: F-Output-1
**
*Output, field
*Node Output
A, NT, RF, RFL, U, V
*Element Output, directions=YES
TEMP,
**
** FIELD OUTPUT: F-Output-2
**
*Element Output, directions=YES
BF, ER, HFL, LE, PE, PEEQ, S, STATUS, VS
**
** FIELD OUTPUT: F-Output-3
**
*Contact Output
CSTRESS,
**
** FIELD OUTPUT: F-Output-4
**
*Node Output, nset=SET-RF
CF, RF, RM, RT
**
** HISTORY OUTPUT: H-Output-1
**
*Output, history, variable=PRESELECT
*End Step
```

3D-Model –ABAQUS/CAE input code,

```
*Heading
** Job name: 3DM-circular-Job Model name: 3DM-circular
** Generated by: Abaqus/CAE Version 6.8-1
*Preprint, echo=NO, model=NO, history=NO, contact=NO
**
** PARTS
**
*Part, name=TOOL-1
*Node
      1,  0.514054239, -0.830450952,  0.396607786
      2,  0.608424306, -0.927439332,  0.294199079
      3,  0.565424323, -0.969284356,  0.294204652
      4,  0.471054256, -0.872295976,  0.396613359
      5,    1.0288173,  -1.35942459,  0.377655745
      6,  0.985817373,  -1.40126956,  0.377661288
      7,  0.549179375, -0.981265664,  0.314017534
      8,  0.969572365,   -1.4132508,   0.39747417
      9,  0.470537663, -0.900442004,  0.399358124
     10,  0.412373632, -0.840592504,   1.00213623
      …………………………………….............
     ………………………………………………..
    ……………………………………………………
   2037,  0.607059062, -0.967405558,  0.722901881
   2038,   0.80324465,  -1.17136776,  0.383321077
   2039,   1.08134985,  -1.42341471,  0.455263108
   2040,  0.878625453,  -1.26017702,  0.909815252
   2041,  0.938565135,  -1.31130934,  0.623456955
   2042,   1.03271139,  -1.37972498,  0.392293334
   2043,  0.562153995, -0.926429391,  0.872905314
   2044,  0.479278564,  -0.87830621,    1.1253885
   2045,  0.697423398,  -1.06308961,   1.00654316
   2046,  0.585796058,  -0.94052583,  0.826654017
   2047,  0.969223678,  -1.33966923,  0.837234855
   2048,  0.894427001,  -1.26263011,  0.655344188
*Element, type=C3D4T
  1, 1415, 1416, 1417, 1418
  2, 1415,  573, 1419,  608
  3, 1420, 1421, 1422, 1423
  4, 1420, 1424, 1425, 1426
  5, 1427, 1420, 1423, 1428
  6, 1420, 1423, 1428, 1421
  7, 1420, 1429, 1430, 1431
  8, 1420, 1429, 1425, 1424
  9, 1432, 1433, 1434, 1435
 10, 1432, 1436, 1437, 1438
 …………………………….
 …………………………….
 …………………………….
```

```
7382, 1919, 1176, 1177,  327
7383, 1330, 1329, 1446, 1335
7384, 1631, 1627, 1624, 1629
7385,  559,  558, 1346, 1920
7386, 1571,  568,  567,  569
7387, 1898, 1393, 1389,  556
7388, 1738,  601,  603,  574
7389, 1900, 1578, 1919, 1891
7390, 1895, 1358, 1362,   32
7391,   31, 1329,  494, 1940
*Nset, nset=_PICKEDSET3, internal, generate
    1,  2048,     1
*Elset, elset=_PICKEDSET3, internal, generate
    1,  7391,     1
*Nset, nset=TOOL-SET, generate
    1,  2048,     1
*Elset, elset=TOOL-SET, generate
    1,  7391,     1
*Elset, elset=_TOOL-SURF_S3, internal
   28,   42,   54,   69,   80,  113,  130,  206,  217,  226,  238,  259,  262,  288,  379,  418
  438,  460,  607,  634,  638,  650,  661,  706,  723,  725,  829,  833,  931,  942,  958,  973
  981, 1010, 1014, 1036, 1061, 1073, 1086, 1088, 1098, 1113, 1125, 1150, 1164, 1168,
1179, 1199
 1212, 1214, 1215, 1231, 1241, 1254, 1255, 1257, 1263, 1268, 1278, 1303, 1328, 1343,
1385, 1393
 1394, 1443, 1445, 1446, 1449, 1462, 1463, 1468, 1483, 1494, 1503, 1524, 1532, 1533,
1542, 1557
 1561, 1564, 1567, 1571, 1572, 1573, 1574, 1575, 1580, 1582, 1583, 1585, 1591, 1592,
1600, 1621
 1622, 1624, 1635, 1640, 1647, 1648, 1649, 1650, 1660, 1665, 1667, 1678, 1679, 1680,
1681, 1685
 1686, 1688, 1690, 1691, 1692, 1697, 1699, 1700, 1701, 1702, 1703, 1707, 1713, 1722,
1724, 1733
 1737, 1740, 1741, 1742, 1743, 1745, 1746, 1748, 1750, 1751, 1755, 1757, 1760, 1761,
1768, 1772
 1775, 1780, 1784, 1786, 1789, 1792, 1796, 1797, 1798, 1800, 1801, 1803, 1804, 1806,
1807, 1808
 1810, 1811, 1816, 1817, 1825, 1827, 1834, 1839, 1840, 1841, 1844, 1850, 1855, 1866,
1869, 1874
…………………………………………………………………………………………
…………
…………………………………………………………………………………………
…………
…………………………………………………………………………………………
…………
7122, 7124, 7125, 7126, 7130, 7135, 7136, 7138, 7140, 7141, 7147, 7149, 7150, 7152,
7156, 7157
```

```
 7158, 7165, 7169, 7171, 7172, 7176, 7177, 7181, 7182, 7185, 7189, 7190, 7191, 7193,
7195, 7196
 7197, 7200, 7204, 7206, 7209, 7214, 7217, 7221, 7222, 7230, 7231, 7233, 7234, 7236,
7238, 7242
 7245, 7246, 7247, 7248, 7256, 7258, 7260, 7264, 7265, 7266, 7268, 7269, 7272, 7275,
7276, 7277
 7280, 7281, 7283, 7284, 7285, 7286, 7289, 7290, 7291, 7292, 7293, 7298, 7301, 7302,
7303, 7305
 7307, 7309, 7312, 7313, 7318, 7321, 7322, 7323, 7327, 7329, 7330, 7332, 7333, 7335,
7336, 7337
 7339, 7340, 7341, 7347, 7349, 7355, 7356, 7357, 7358, 7359, 7360, 7361, 7362, 7363,
7364, 7365
 7366, 7367, 7368, 7370, 7374, 7376, 7382, 7386, 7387, 7388, 7390
*Elset, elset=_TOOL-SURF_S1, internal
  219,  224,  355,  512,  584,  592,  637,  671,  717,  795,  838,  923, 1135, 1162, 1365, 1408
 1482, 1487, 1521, 1527, 1540, 1785, 1907, 1921, 2003, 2146, 2226, 2248, 2287, 2301,
2342, 2585
 2591, 2611, 2663, 2762, 2771, 2798, 2848, 2938, 2941, 2992, 3024, 3033, 3147, 3198,
3217, 3247
 3252, 3266, 3300, 3357, 3487, 3509, 3553, 3637, 3643, 3674, 3689, 3786, 3870, 3968,
3983, 4037
 4055, 4100, 4115, 4306, 4328, 4332, 4344, 4368, 4404, 4444, 4491, 4526, 4614, 4648,
4721, 4882
 4916, 4943, 4969, 5014, 5037, 5093, 5306, 5445, 5532, 5560, 5765, 5814, 5851, 5983,
6078, 6083
 6206, 6227, 6230, 6274, 6279, 6376, 6377, 6405, 6412, 6446, 6502, 6523, 6557, 6573,
6574, 6589
 6708, 6724, 6808, 6857, 6887, 6895, 6940, 7023, 7037, 7091, 7170, 7192, 7212, 7297,
7344, 7380
 7385, 7391
*Elset, elset=_TOOL-SURF_S4, internal
   38,   67,  211,  260,  347,  377,  388,  391,  405,  505,  506,  507,  518,  537,  593,  597
  598,  600,  609,  621,  622,  651,  748,  776,  777,  781,  800,  808,  828,  837,  992, 1027
 1038, 1054, 1147, 1170, 1226, 1353, 1391, 1549, 1581, 1593, 1642, 1717, 1738, 1769,
1774, 1794
 1814, 1847, 1848, 1861, 1873, 1886, 1974, 1983, 2001, 2052, 2067, 2116, 2130, 2189,
2199, 2201
 2242, 2250, 2327, 2375, 2384, 2450, 2462, 2477, 2487, 2515, 2571, 2602, 2613, 2652,
2740, 2764
 2810, 2833, 2872, 2889, 2929, 2935, 2977, 2994, 3001, 3101, 3106, 3140, 3146, 3189,
3226, 3284
 3336, 3381, 3382, 3393, 3409, 3420, 3467, 3496, 3598, 3778, 3821, 3847, 3865, 3902,
3928, 4044
 4107, 4142, 4202, 4223, 4285, 4295, 4303, 4415, 4505, 4587, 4637, 4681, 4769, 4825,
4863, 4975
 4985, 4992, 4993, 5012, 5017, 5039, 5044, 5069, 5135, 5176, 5300, 5321, 5332, 5354,
5390, 5418
```

```
 5443, 5462, 5463, 5470, 5519, 5563, 5591, 5623, 5667, 5673, 5733, 5758, 5763, 5765,
5831, 5876
 5897, 5924, 5928, 5934, 5938, 6036, 6101, 6106, 6155, 6172, 6181, 6256, 6329, 6363,
6367, 6372
 6403, 6418, 6455, 6477, 6494, 6522, 6568, 6637, 6652, 6687, 6754, 6800, 6878, 6881,
6921, 6941
 6970, 7179, 7194, 7225, 7239, 7252, 7271, 7308, 7377, 7379
*Elset, elset=_TOOL-SURF_S2, internal
   81,   83,  106,  116,  166,  170,  221,  334,  352,  492,  517,  663,  780,  878,  902,  945
 1124, 1289, 1454, 1458, 1638, 1689, 1799, 1833, 1975, 2051, 2123, 2140, 2150, 2200,
2202, 2337
 2391, 2427, 2458, 2576, 2578, 2646, 2877, 3044, 3084, 3125, 3181, 3254, 3279, 3304,
3305, 3308
 3375, 3379, 3396, 3440, 3447, 3485, 3546, 3587, 3763, 3802, 3814, 3984, 3990, 4094,
4151, 4187
 4191, 4198, 4239, 4251, 4256, 4261, 4304, 4330, 4333, 4453, 4589, 4669, 4763, 4866,
4912, 4958
 4960, 5007, 5035, 5043, 5048, 5049, 5162, 5209, 5246, 5304, 5305, 5373, 5437, 5442,
5452, 5527
 5546, 5581, 5611, 5639, 5670, 5682, 5686, 5729, 5739, 5755, 5815, 5868, 5898, 5936,
6067, 6117
 6122, 6124, 6144, 6167, 6221, 6276, 6323, 6330, 6335, 6342, 6388, 6394, 6410, 6425,
6445, 6451
 6505, 6550, 6561, 6641, 6642, 6654, 6668, 6731, 6735, 6748, 6780, 6824, 6844, 6858,
6886, 6933
 7035, 7045, 7048, 7055, 7062, 7117, 7161, 7164, 7173, 7175, 7184, 7187, 7210, 7220,
7235, 7267
 7278, 7319, 7342, 7373, 7383
*Elset, elset=_TOOL-SURF_S3_1, internal
   28,   42,   54,   69,   80,  113,  130,  206,  217,  226,  238,  259,  262,  288,  379,  418
  438,  460,  607,  634,  638,  650,  661,  706,  723,  725,  829,  833,  931,  942,  958,  973
  981, 1010, 1014, 1036, 1061, 1073, 1086, 1088, 1098, 1113, 1125, 1150, 1164, 1168,
1179, 1199
 1212, 1214, 1215, 1231, 1241, 1254, 1255, 1257, 1263, 1268, 1278, 1303, 1328, 1343,
1385, 1393
 1394, 1443, 1445, 1446, 1449, 1462, 1463, 1468, 1483, 1494, 1503, 1524, 1532, 1533,
1542, 1557
 1561, 1564, 1567, 1571, 1572, 1573, 1574, 1575, 1580, 1582, 1583, 1585, 1591, 1592,
1600, 1621
 1622, 1624, 1635, 1640, 1647, 1648, 1649, 1650, 1660, 1665, 1667, 1678, 1679, 1680,
1681, 1685
 1686, 1688, 1690, 1691, 1692, 1697, 1699, 1700, 1701, 1702, 1703, 1707, 1713, 1722,
1724, 1733
 1737, 1740, 1741, 1742, 1743, 1745, 1746, 1748, 1750, 1751, 1755, 1757, 1760, 1761,
1768, 1772
 1775, 1780, 1784, 1786, 1789, 1792, 1796, 1797, 1798, 1800, 1801, 1803, 1804, 1806,
1807, 1808
```

```
………………………………………………………………………………………………
………..
………………………………………………………………………………………………
…………
………………………………………………………………………………………………
…………
7158, 7165, 7169, 7171, 7172, 7176, 7177, 7181, 7182, 7185, 7189, 7190, 7191, 7193,
7195, 7196
 7197, 7200, 7204, 7206, 7209, 7214, 7217, 7221, 7222, 7230, 7231, 7233, 7234, 7236,
7238, 7242
 7245, 7246, 7247, 7248, 7256, 7258, 7260, 7264, 7265, 7266, 7268, 7269, 7272, 7275,
7276, 7277
 7280, 7281, 7283, 7284, 7285, 7286, 7289, 7290, 7291, 7292, 7293, 7298, 7301, 7302,
7303, 7305
 7307, 7309, 7312, 7313, 7318, 7321, 7322, 7323, 7327, 7329, 7330, 7332, 7333, 7335,
7336, 7337
 7339, 7340, 7341, 7347, 7349, 7355, 7356, 7357, 7358, 7359, 7360, 7361, 7362, 7363,
7364, 7365
 7366, 7367, 7368, 7370, 7374, 7376, 7382, 7386, 7387, 7388, 7390
*Elset, elset=_TOOL-SURF_S1_1, internal
  219,  224,  355,  512,  584,  592,  637,  671,  717,  795,  838,  923, 1135, 1162, 1365, 1408
 1482, 1487, 1521, 1527, 1540, 1785, 1907, 1921, 2003, 2146, 2226, 2248, 2287, 2301,
2342, 2585
 2591, 2611, 2663, 2762, 2771, 2798, 2848, 2938, 2941, 2992, 3024, 3033, 3147, 3198,
3217, 3247
 3252, 3266, 3300, 3357, 3487, 3509, 3553, 3637, 3643, 3674, 3689, 3786, 3870, 3968,
3983, 4037
 4055, 4100, 4115, 4306, 4328, 4332, 4344, 4368, 4404, 4444, 4491, 4526, 4614, 4648,
4721, 4882
 4916, 4943, 4969, 5014, 5037, 5093, 5306, 5445, 5532, 5560, 5765, 5814, 5851, 5983,
6078, 6083
 6206, 6227, 6230, 6274, 6279, 6376, 6377, 6405, 6412, 6446, 6502, 6523, 6557, 6573,
6574, 6589
 6708, 6724, 6808, 6857, 6887, 6895, 6940, 7023, 7037, 7091, 7170, 7192, 7212, 7297,
7344, 7380
 7385, 7391
*Elset, elset=_TOOL-SURF_S4_1, internal
   38,   67,  211,  260,  347,  377,  388,  391,  405,  505,  506,  507,  518,  537,  593,  597
  598,  600,  609,  621,  622,  651,  748,  776,  777,  781,  800,  808,  828,  837,  992, 1027
 1038, 1054, 1147, 1170, 1226, 1353, 1391, 1549, 1581, 1593, 1642, 1717, 1738, 1769,
1774, 1794
 1814, 1847, 1848, 1861, 1873, 1886, 1974, 1983, 2001, 2052, 2067, 2116, 2130, 2189,
2199, 2201
 2242, 2250, 2327, 2375, 2384, 2450, 2462, 2477, 2487, 2515, 2571, 2602, 2613, 2652,
2740, 2764
 2810, 2833, 2872, 2889, 2929, 2935, 2977, 2994, 3001, 3101, 3106, 3140, 3146, 3189,
3226, 3284
```

```
 3336, 3381, 3382, 3393, 3409, 3420, 3467, 3496, 3598, 3778, 3821, 3847, 3865, 3902,
3928, 4044
 4107, 4142, 4202, 4223, 4285, 4295, 4303, 4415, 4505, 4587, 4637, 4681, 4769, 4825,
4863, 4975
 4985, 4992, 4993, 5012, 5017, 5039, 5044, 5069, 5135, 5176, 5300, 5321, 5332, 5354,
5390, 5418
 5443, 5462, 5463, 5470, 5519, 5563, 5591, 5623, 5667, 5673, 5733, 5758, 5763, 5765,
5831, 5876
 5897, 5924, 5928, 5934, 5938, 6036, 6101, 6106, 6155, 6172, 6181, 6256, 6329, 6363,
6367, 6372
 6403, 6418, 6455, 6477, 6494, 6522, 6568, 6637, 6652, 6687, 6754, 6800, 6878, 6881,
6921, 6941
 6970, 7179, 7194, 7225, 7239, 7252, 7271, 7308, 7377, 7379
*Elset, elset=_TOOL-SURF_S2_1, internal
   81,   83,  106,  116,  166,  170,  221,  334,  352,  492,  517,  663,  780,  878,  902,  945
 1124, 1289, 1454, 1458, 1638, 1689, 1799, 1833, 1975, 2051, 2123, 2140, 2150, 2200,
2202, 2337
 2391, 2427, 2458, 2576, 2578, 2646, 2877, 3044, 3084, 3125, 3181, 3254, 3279, 3304,
3305, 3308
 3375, 3379, 3396, 3440, 3447, 3485, 3546, 3587, 3763, 3802, 3814, 3984, 3990, 4094,
4151, 4187
 4191, 4198, 4239, 4251, 4256, 4261, 4304, 4330, 4333, 4453, 4589, 4669, 4763, 4866,
4912, 4958
 4960, 5007, 5035, 5043, 5048, 5049, 5162, 5209, 5246, 5304, 5305, 5373, 5437, 5442,
5452, 5527
 5546, 5581, 5611, 5639, 5670, 5682, 5686, 5729, 5739, 5755, 5815, 5868, 5898, 5936,
6067, 6117
 6122, 6124, 6144, 6167, 6221, 6276, 6323, 6330, 6335, 6342, 6388, 6394, 6410, 6425,
6445, 6451
 6505, 6550, 6561, 6641, 6642, 6654, 6668, 6731, 6735, 6748, 6780, 6824, 6844, 6858,
6886, 6933
 7035, 7045, 7048, 7055, 7062, 7117, 7161, 7164, 7173, 7175, 7184, 7187, 7210, 7220,
7235, 7267
 7278, 7319, 7342, 7373, 7383
*Surface, type=ELEMENT, name=TOOL-SURF
_TOOL-SURF_S3_1, S3
_TOOL-SURF_S1_1, S1
_TOOL-SURF_S4_1, S4
_TOOL-SURF_S2_1, S2
** Section: Section-1-_PICKEDSET3
*Solid Section, elset=_PICKEDSET3, material=TOOL-MAT
1.,
*End Part
**
*Part, name=WP-1
*Node
      1, -0.475410461,    -0.145129398,        0.
      2,  -0.94522965,     0.0264061317,       0.
```

```
     3, -0.00333115668,     0.699994445,        0.
     4, -0.000121085533,   0.199999988,        0.
     5,          0.,                 -0.800000012,      0.
     6, -0.0517315418,     -1.29866099,         0.
     7,  0.951402843,      - 0.607949078,       0.
     8,  0.475616187,      -0.45423761,         0.
     9,  0.707106769,     -1.00710678,          0.
    10, -0.495113879,     -0.138327986,       0.
   ……………………………………………
   ……………………………………………
  ……………………………………………..
 81365, -0.00653537456,  -1.06978643,  0.300000012
  81366, -0.00807730481,  -1.09059381,  0.300000012
  81367, -0.00961923786,   -1.1114012,  0.300000012
  81368, -0.0111611718,   -1.1322087,  0.300000012
  81369, -0.0127031095,  -1.15301621,  0.300000012
  81370, -0.0142450482,  -1.17382407,  0.300000012
  81371, -0.0157869998,  -1.19463253,  0.300000012
  81372, -0.0173289999,  -1.21544313,  0.300000012
  81373, -0.0188711546,  -1.23626018,  0.300000012
  81374, -0.0203566104,  -1.25709653,  0.300000012
  81375, -0.021609297,  -1.27812934,  0.300000012
*Element, type=C3D8RT
   1,  5426,  5435,  5952,  5564,    1,    10,   527,   139
   2,  5435,  5436,  5953,  5952,   10,    11,   528,   527
   3,  5436,  5437,  5954,  5953,   11,    12,   529,   528
   4,  5437,  5438,  5955,  5954,   12,    13,   530,   529
   5,  5438,  5439,  5956,  5955,   13,    14,   531,   530
   6,  5439,  5440,  5957,  5956,   14,    15,   532,   531
   7,  5440,  5441,  5958,  5957,   15,    16,   533,   532
   8,  5441,  5442,  5959,  5958,   16,    17,   534,   533
   9,  5442,  5443,  5960,  5959,   17,    18,   535,   534
  10,  5443,  5444,  5961,  5960,   18,    19,   536,   535
……………………………………………………..
…………………………………………………….
…………………………………………………….
72902, 81365, 81366, 76165, 76164, 75940, 75941, 70740, 70739
72903, 81366, 81367, 76166, 76165, 75941, 75942, 70741, 70740
72904, 81367, 81368, 76167, 76166, 75942, 75943, 70742, 70741
72905, 81368, 81369, 76168, 76167, 75943, 75944, 70743, 70742
72906, 81369, 81370, 76169, 76168, 75944, 75945, 70744, 70743
72907, 81370, 81371, 76170, 76169, 75945, 75946, 70745, 70744
72908, 81371, 81372, 76171, 76170, 75946, 75947, 70746, 70745
72909, 81372, 81373, 76172, 76171, 75947, 75948, 70747, 70746
72910, 81373, 81374, 76173, 76172, 75948, 75949, 70748, 70747
72911, 81374, 81375, 76174, 76173, 75949, 75950, 70749, 70748
72912, 81375, 76431, 75956, 76174, 75950, 71006, 70531, 70749
*Nset, nset=_PICKEDSET2, internal, generate
```

```
    1,  81375,      1
*Elset, elset=_PICKEDSET2, internal, generate
    1,  72912,      1
*Nset, nset=WP-SET, generate
    1,  81375,      1
*Elset, elset=WP-SET, generate
    1,  72912,      1
*Elset, elset=_WP-SURF_S4, internal, generate
   24,  72912,     24
*Elset, elset=_WP-SURF_S6, internal, generate
    1,  72889,     24
*Elset, elset=_WP-SURF_S1, internal, generate
 67705,  72912,      1
*Elset, elset=_WP-SURF_S2, internal, generate
   1,  5208,     1
*Elset, elset=_WP-SURF_S4_1, internal, generate
   24,  72912,     24
*Elset, elset=_WP-SURF_S6_1, internal, generate
    1,  72889,     24
*Elset, elset=_WP-SURF_S2_1, internal, generate
   1,  5208,     1
*Elset, elset=_WP-SURF_S1_1, internal, generate
 67705,  72912,      1
*Surface, type=ELEMENT, name=WP-SURF
_WP-SURF_S4_1, S4
_WP-SURF_S6_1, S6
_WP-SURF_S2_1, S2
_WP-SURF_S1_1, S1
** Section: Section-2-_PICKEDSET2
*Solid Section, elset=_PICKEDSET2, material=WP-MAT
1.,
*End Part
**
**
** ASSEMBLY
**
*Assembly, name=Assembly
**
*Instance, name=TOOL-1, part=TOOL-1
*End Instance
**
*Instance, name=WP-1, part=WP-1
*End Instance
**
*Node
      1,           0., -0.300000012,  0.150000006
      2,  0.800000012,  -1.20000005,          0.5
*Nset, nset=_PickedSet28, internal
```

```
 2,
*Nset, nset=SET-RF2
 2,
*Nset, nset=_PICKEDSET15, internal
 1,
*Nset, nset=_PICKEDSET16, internal
 2,
*Nset, nset=_PICKEDSET17, internal
 2,
*Nset, nset=_PICKEDSET18, internal, instance=TOOL-1, generate
    1,  2048,     1
*Elset, elset=_PICKEDSET18, internal, instance=TOOL-1, generate
    1,  7391,     1
*Nset, nset=_PICKEDSET19, internal, instance=TOOL-1
   17,   18,   20,   21,   22,   24,   25,   32,   33,  260,  261,  262,  263,  264,  265,  266
  267,  268,  278,  279,  280,  281,  282,  283,  284,  285,  286,  305,  306,  307,  308,  309
  310,  311,  312,  313,  323,  324,  325,  326,  327,  328,  329,  330,  331,  346,  347,  348
  349,  350,  351,  352,  353,  354,  355,  356,  357,  358,  359,  378,  379,  380,  381,  382
  383,  384,  385,  386,  477,  478,  479,  480,  481,  482,  483,  484,  485,  495,  496,  497
  498,  499,  500,  501,  502,  503,  504,  505,  506,  507,  508,  509,  510,  511,  512, 1124
 1125, 1126, 1127, 1128, 1129, 1130, 1131, 1132, 1133, 1134, 1135, 1136, 1137, 1138,
1139, 1140
 1141, 1142, 1143, 1144, 1145, 1146, 1147, 1148, 1149, 1150, 1151, 1152, 1153, 1154,
1155, 1156
 1157, 1158, 1159, 1160, 1161, 1162, 1163, 1164, 1165, 1166, 1167, 1168, 1169, 1170,
1171, 1172
 1173, 1174, 1175, 1176, 1177, 1178, 1179, 1180, 1181, 1182, 1183, 1184, 1185, 1186,
1187, 1188
 1189, 1190, 1191, 1192, 1193, 1194, 1195, 1196, 1197, 1198, 1199, 1200, 1201, 1202,
1203, 1204
 1205, 1206, 1207, 1208, 1209, 1210, 1211, 1212, 1213, 1214, 1215, 1216, 1217, 1218,
1219, 1220
 1221, 1222, 1223, 1224, 1225, 1226, 1227, 1228, 1229, 1230, 1231, 1232, 1233, 1234,
1235, 1236
 1237, 1238, 1239, 1240, 1241, 1242, 1243, 1244, 1245, 1246, 1247, 1248, 1249, 1250,
1251, 1252
 1253, 1254, 1255, 1256, 1257, 1258, 1259, 1260, 1261, 1262, 1263, 1264, 1265, 1266
*Elset, elset=_PICKEDSET19, internal, instance=TOOL-1
   80,  377,  391,  661,  829,  931, 1038, 1214, 1226, 1231, 1257, 1268, 1328, 1353, 1468,
1503
 1521, 1527, 1532, 1533, 1567, 1571, 1649, 1691, 1697, 1701, 1702, 1741, 1748, 1757,
1768, 1772
 1780, 1792, 1794, 1833, 1847, 1901, 1908, 1928, 1946, 1949, 1961, 1962, 1967, 1969,
1977, 2022
 2045, 2129, 2130, 2140, 2146, 2159, 2176, 2187, 2189, 2192, 2200, 2201, 2202, 2203,
2211, 2249
 2257, 2315, 2336, 2375, 2377, 2379, 2381, 2383, 2391, 2424, 2433, 2487, 2555, 2607,
2613, 2614
```

```
 2626, 2638, 2647, 2648, 2666, 2673, 2681, 2714, 2725, 2738, 2743, 2765, 2770, 2808,
2826, 2848
 2858, 2870, 2877, 2883, 2891, 2910, 2926, 2927, 2955, 2967, 2971, 2980, 2984, 3014,
3015, 3181
 3200, 3205, 3223, 3254, 3266, 3273, 3280, 3288, 3299, 3344, 3472, 3474, 3492, 3496,
3524, 3537
 3579, 3598, 3600, 3621, 3648, 3671, 3674, 3678, 3709, 3712, 3726, 3729, 3732, 3745,
3752, 3753
 3763, 3767, 3785, 3793, 3794, 3795, 3807, 3811, 3815, 3848, 3911, 3920, 3936, 3938,
3963, 3965
 3981, 4006, 4020, 4054, 4067, 4073, 4080, 4114, 4118, 4131, 4132, 4177, 4186, 4201,
4247, 4267
 4278, 4303, 4497, 4511, 4512, 4525, 4526, 4564, 4605, 4618, 4653, 4658, 4659, 4665,
4667, 4697
 4701, 4763, 4771, 4791, 4792, 4807, 4809, 4815, 4825, 4827, 4833, 4836, 4846, 4850,
4868, 4872
 4882, 4894, 4930, 4986, 5002, 5032, 5042, 5118, 5120, 5203, 5207, 5221, 5236, 5241,
5247, 5249
 5250, 5312, 5326, 5347, 5364, 5381, 5383, 5386, 5390, 5402, 5463, 5469, 5482, 5483,
5501, 5505
 5509, 5513, 5519, 5534, 5548, 5561, 5565, 5575, 5583, 5587, 5614, 5642, 5668, 5683,
5726, 5756
 5769, 5772, 5775, 5779, 5788, 5793, 5796, 5859, 5865, 5879, 5881, 5884, 5887, 5901,
5910, 5914
 5927, 5928, 5943, 5946, 5951, 5956, 5960, 5962, 5967, 5970, 5977, 5995, 6021, 6041,
6046, 6049
 6052, 6054, 6055, 6068, 6072, 6079, 6091, 6092, 6102, 6122, 6126, 6145, 6157, 6172,
6179, 6181
 6183, 6185, 6214, 6215, 6223, 6242, 6245, 6282, 6301, 6304, 6337, 6339, 6431, 6443,
6449, 6451
 6454, 6462, 6509, 6515, 6519, 6565, 6589, 6598, 6625, 6649, 6670, 6674, 6675, 6703,
6708, 6716
 6730, 6757, 6799, 6804, 6806, 6825, 6828, 6830, 6835, 6855, 6864, 6870, 6873, 6897,
6955, 6966
 6976, 6978, 7000, 7008, 7135, 7149, 7150, 7169, 7170, 7177, 7182, 7217, 7221, 7222,
7248, 7272
 7281, 7286, 7303, 7305, 7313, 7319, 7327, 7330, 7337, 7344, 7358, 7370, 7382
*Nset, nset=_PICKEDSET20, internal
 2,
*Nset, nset=_PICKEDSET21, internal
 1,
*Nset, nset=TOOL-SET, instance=TOOL-1, generate
   1,  2048,    1
*Nset, nset=TOOL-SET
 2,
*Elset, elset=TOOL-SET, instance=TOOL-1, generate
   1,  7391,    1
*Nset, nset=WP-SET, instance=WP-1, generate
```

```
    1,  81375,      1
*Nset, nset=WP-SET
 1,
*Elset, elset=WP-SET, instance=WP-1, generate
    1,  72912,      1
*Nset, nset=SET-BACK, instance=WP-1, generate
   1,  5425,     1
*Elset, elset=SET-BACK, instance=WP-1, generate
   1,  5208,     1
*Elset, elset=_WP-BAC-SRUF_S2, internal, instance=WP-1, generate
   1,  5208,     1
*Nset, nset=CLOUD, instance=WP-1, generate
    1,  81375,      1
*Nset, nset=CLOUD
 1,
*Elset, elset=_WP-BAC-SRUF_S2_1, internal, instance=WP-1, generate
   1,  5208,     1
*Surface, type=ELEMENT, name=WP-BAC-SRUF
_WP-BAC-SRUF_S2_1, S2
*Surface, type=NODE, name=CLOUD_CNS_, internal
CLOUD, 1.
** Constraint: RigidBody-1
*Rigid Body, ref node=_PickedSet28, elset=_PICKEDSET18
** Constraint: TOOL-COUPLING
*Coupling, constraint name=TOOL-COUPLING, ref node=_PICKEDSET16,
surface=TOOL-1.TOOL-SURF
*Kinematic
** Constraint: WP-COUPLING
*Coupling, constraint name=WP-COUPLING, ref node=_PICKEDSET15, surface=WP-
1.WP-SURF, influence radius=0.55
*Kinematic
*End Assembly
**
** MATERIALS
**
*Material, name=TOOL-MAT
*Conductivity
 0.0208,
*Density
 1.5e-08,
*Elastic
800000., 0.3
*Expansion
 4.7e-08,
*Inelastic Heat Fraction
        0.9,
*Specific Heat
 4.45e+08,
```

```
*Material, name=WP-MAT
*Conductivity
 0.0477,
*Damage Initiation, criterion=DUCTILE
 1.5,0.,0.
*Damage Evolution, type=ENERGY
10.,
*Density
 7.8e-09,
*Elastic
210000., 0.3
*Expansion
 1.2e-08,
*Inelastic Heat Fraction
        0.9,
*Plastic, hardening=JOHNSON COOK
490., 600., 0.21,  0.8,1900., 500.
*Specific Heat
 5.56e+08,
**
** INTERACTION PROPERTIES
**
*Surface Interaction, name=CON
*Friction
 0.5,
*Surface Behavior, pressure-overclosure=LINEAR
2.1e+06,
** ----------------------------------------------------------------
**
** STEP: cutting
**
*Step, name=cutting
*Dynamic Temperature-displacement, Explicit
, 0.003
*Bulk Viscosity
0.06, 1.2
** Mass Scaling: Semi-Automatic
**              Whole Model
*Fixed Mass Scaling, factor=100.
**
** BOUNDARY CONDITIONS
**
** Name: Disp-BC-1 Type: Displacement/Rotation
*Boundary
_PICKEDSET19, 1, 1
** Name: Disp-BC-2 Type: Displacement/Rotation
*Boundary
_PICKEDSET19, 2, 2
```

```
** Name: Disp-BC-3 Type: Displacement/Rotation
*Boundary
_PICKEDSET19, 4, 4
** Name: Disp-BC-4 Type: Displacement/Rotation
*Boundary
_PICKEDSET19, 5, 5
** Name: Disp-BC-5 Type: Displacement/Rotation
*Boundary
_PICKEDSET19, 6, 6
** Name: Disp-BC-6 Type: Displacement/Rotation
*Boundary
SET-BACK, 3, 3
** Name: Vel-BC-1 Type: Velocity/Angular velocity
*Boundary, type=VELOCITY
_PICKEDSET20, 1, 1
** Name: Vel-BC-2 Type: Velocity/Angular velocity
*Boundary, type=VELOCITY
_PICKEDSET20, 2, 2
** Name: Vel-BC-3 Type: Velocity/Angular velocity
*Boundary, type=VELOCITY
_PICKEDSET20, 3, 3, -247.
** Name: Vel-BC-4 Type: Velocity/Angular velocity
*Boundary, type=VELOCITY
_PICKEDSET20, 4, 4
** Name: Vel-BC-5 Type: Velocity/Angular velocity
*Boundary, type=VELOCITY
_PICKEDSET20, 5, 5
** Name: Vel-BC-6 Type: Velocity/Angular velocity
*Boundary, type=VELOCITY
_PICKEDSET20, 6, 6
** Name: Vel-BC-7 Type: Velocity/Angular velocity
*Boundary, type=VELOCITY
_PICKEDSET21, 1, 1
** Name: Vel-BC-8 Type: Velocity/Angular velocity
*Boundary, type=VELOCITY
_PICKEDSET21, 2, 2
** Name: Vel-BC-9 Type: Velocity/Angular velocity
*Boundary, type=VELOCITY
_PICKEDSET21, 3, 3
** Name: Vel-BC-10 Type: Velocity/Angular velocity
*Boundary, type=VELOCITY
_PICKEDSET21, 4, 4
** Name: Vel-BC-11 Type: Velocity/Angular velocity
*Boundary, type=VELOCITY
_PICKEDSET21, 5, 5
** Name: Vel-BC-12 Type: Velocity/Angular velocity
*Boundary, type=VELOCITY
_PICKEDSET21, 6, 6, -3111.
```

```
*Adaptive Mesh Controls, name=ALE, geometric enhancement=YES, curvature
refinement=5.
1., 0., 0.
*Adaptive Mesh, elset=WP-SET, controls=ALE, frequency=1000, mesh sweeps=5,
op=NEW
**
** ADAPTIVE MESH CONSTRAINTS
**
** Name: AdMeshCnstr-1 Type: Velocity/Angular velocity
*Adaptive Mesh Constraint, constraint type=LAGRANGIAN, type=VELOCITY
WP-SET
**
** INTERACTIONS
**
** Interaction: tool-chip
*Contact Pair, interaction=CON, mechanical constraint=KINEMATIC, cpset=tool-chip
TOOL-1.TOOL-SURF, CLOUD_CNS_
**
** OUTPUT REQUESTS
**
*Restart, write, number interval=1, time marks=NO
**
** FIELD OUTPUT: F-Output-1
**
*Output, field
*Node Output
A, NT, RF, RFL, RT, U, V
**
** FIELD OUTPUT: F-Output-3
**
*Contact Output
CSTRESS,
**
** FIELD OUTPUT: F-Output-2
**
*Element Output, directions=YES
ER, HFL, LE, PE, PEEQ, S, STATUS, TEMP
**
** HISTORY OUTPUT: H-Output-1
**
*Output, history, variable=PRESELECT
*End Step
```

Department of Mechanical Engineering, Master’s Degree Programme
Blekinge Institute of Technology, Campus Gräsvik
SE-371 79 Karlskrona, SWEDEN

Telephone: +46 455-38 55 10
Fax: +46 455-38 55 07
E-mail: ansel.berghuvud@bth.se